UNIVERSITÀ DEGLI STUDI DI SALERNO
Facoltà di Scienze Matematiche Fisiche e Naturali

Dottorato di Ricerca in Fisica (IX Ciclo II Serie)

IMPROVEMENTS IN THE ACOUSTICAL MODELLING OF TRAFFIC NOISE PREDICTION: THEORETICAL AND EXPERIMENTAL RESULTS

Coordinatore del dottorato:
Prof. Giuseppe Grella

Candidato:
Dott. Gerardo Iannone

Relatore:
Prof. Joseph Quartieri

ANNO ACCADEMICO 2010/2011

Contents

Introduction

Traffic acoustical noise is one of the most important component of the urban environmental pollution in densely populated areas all over the world. A very recent ACI-Censis study [1] on Italian urban areas shows that car is the favorite mean of transportation for 90% of population. In particular, this study shows that during years ranging from 2000 to 2007, the number of circulating vehicles is grown of 14.5%. To this growth did not always correspond an improvement of national street network. This problem can be evidenced by the high growth of the traffic charge on urban, sub-urban and extra-urban roads, with a clear impact on costs, security and environment, even in term of acoustical noise. A similar tendency can be observed in the framework of many european countries. Traffic noise affects areas surrounding roads especially when high traffic load and high speed conditions occur and can lead to a degradation of the quality of life in residential areas. The impact of noise on mental and physical health and on daily activities has been widely documented in the scientific literature [2, 3, 4]. In particular a continuous exposure to acoustical noise may affect sleep and/or conversation, may lead to perception of annoyance, may cause hearing loss, cardiovascular problems etc. As a consequence, during last years, a large number of anti-noise laws, ordinances and regulations were decreed by many national governments and international institutions. Looking to Italy, it is the D.P.C.M. 01.03.1991 [5] which regulates noise pollution matters, giving the main acoustical elements definitions such as maximum limit of noise exposure in inner and external environment, acoustic zoning criteria, etc. Then the Framework Law n. 447/1995 has defined a general policy on the noise pollution that has been implemented in different decrees and regulations. Among these, one of the most interesting is the D.M.A. 16.03.1998 "Noise pollution detection and measurement method" (*Tecniche di rilevamento e di misurazione dell'inquinamento acustico*) which deals with the vehicular and

railway noise detection procedure. Moreover the D.Lgs 194/2005 (*Attuazione della direttiva 2002/49/CE relativa alla determinazione e alla gestione del rumore ambientale*) establishes the method to set the acoustic indicator for the different kind of noise sources such as vehicular traffic.
In this Ph.D. thesis our aim is to improve the current prediction tools for traffic noise prediction in non trivial situations such as traffic lights, traffic jam, intersections etc., accounting some aspects of traffic dynamics by the use of traffic models (TM), i.e. following the leader model and Cellular Automata.
This thesis is organized as follows. In the first chapter we briefly discuss the main features of sound and noise propagation. In the second chapter we focus our attention on vehicle noise emission and existing traffic noise models (TNM) while in the third we present a new noise prediction procedure: GERIAN2009. In chapter four some general features of physics of road traffic and transportation are discussed. In the last three chapters we propose an integration of traffic noise model and traffic dynamic model in the "following the leader" and Cellular Automata (CA) framework, with a particular attention on road's intersection issue.

Chapter 1

Fundamentals about Sound

As a prelude to the analytical expositions presented in the following one, this chapter presents a brief descriptive introduction to the nature of sound, describing a range of phenomena exhibited by wave fields. In addition a section is devoted to the ear and the perception of sound and sound propagation.

1.1 Nature of sound and some sound wave features

Perception of sound requires the presence of some simple physical phenomena, in contrast to the very deep physiological and psychological effects.. A sound source oscillates and brings the surrounding air into motion. The compressability and mass of the air cause these oscillations to be transmitted to the listener's ear. As every body knows, generally, in this phenomenon one has momentum transportation without a corresponding mass transportation. Pressure fluctuations, referred to as sound pressure p, occur in air (or other fluid) and are superimposed to the constant atmospheric pressure p_0. A spatially distributed sound field radiates from the source with different instantaneous sound pressures at each moment. The sound pressure is the most important quantity to describe sound fields and is space- and time-dependent.
If an air particle is displaced from its original position, elastic forces of the air tend to restore it to its original position. Because of the inertia of the particle, it overshoots the resting position, bringing into play elastic forces in the opposite direction, and so on. Sound is readily conducted in gases,

liquids, and solids such as air, water, steel, concrete, etc., which are all elastic media. Without a medium, sound cannot be propagated. In figure 1.1 the value of speed of sound in different medium is reported.

The little dots of figure 1.2 represent air molecules. The molecules crowded

Speed of Sound in Selected Materials [m/s]					
Air @ 20°C	343	Copper	5000	Steel	6100
Aluminum	6300	Glass (pyrex)	5600	Water, fresh 20°C	1481
Brass	4700	Ice	3200	Water, sea 13°C	1500
Concrete	3100	Steam @ 100°C	404.8	Wood, oak	4000

Figure 1.1: Speed of sound in different medium.

together represent areas of compression (C) in which the air pressure is slightly greater than the prevailing atmospheric pressure. The sparse areas represent rarefactions (R) in which the pressure is slightly less than atmospheric. The small arrows indicate that, on the average, the molecules are moving to the right of the compression crests and to the left in the rarefaction troughs between the crests. Any given molecule will move a certain distance to the right and then the same distance to the left of its undisplaced position as the sound wave progresses uniformly to the right. As a consequence a sound wave is a longitudinal wave, not a transverse wave (as the E.M.s, for example). Because of the particular nature of the physical phenomenon we name it "sound". So important in humane relations and in higher manifestations of man creativity (let us think of Bach, Mozart, Beethoven, etc), it is not surprising that this phenomenon can be approached from two different, but at the end, equivalent disciplines: physics and music. As a consequence of that, also terms describing sound properties have, at least, double nature. If, in addition, we think of the psychological aspects involved, we have a taste of the complexity we can find in the "sound universe". From a physics-mathematical point of view (but, at the beginning, using musical terms) we can say that the observed sound incident at a point has two main distinguishing attributes: "timbre" and "loudness". The physical quantity for loudness is sound pressure intensity and the quantity for timbre is frequency f, measured in cycles per second, or Hertz (Hz). The frequency range audible by the human ear, which is referred to as hearing range, starts at about 16 Hz and ranges up to 16000 Hz (or 16 kHz). The infrasound, which is located below that frequency range, is less important for air-borne sound problems, but be-

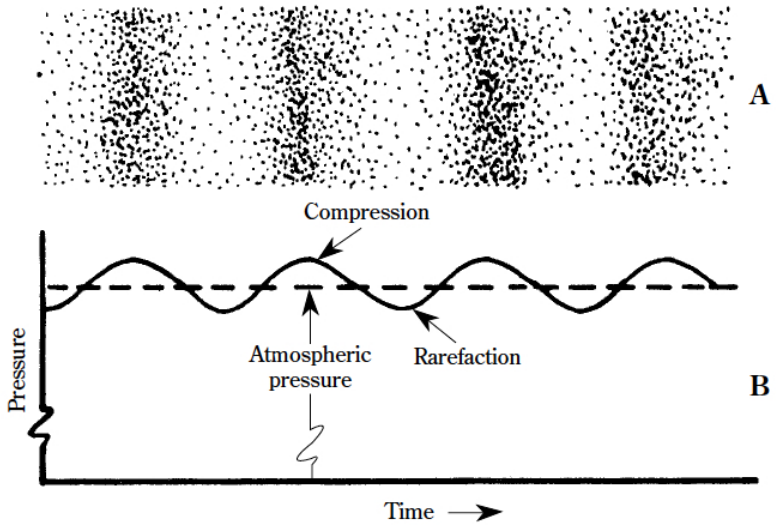

Figure 1.2: (A) An instantaneous view of the compressed and rarefied regions of a sound wave in air. (B) The compressed regions are very slightly above and the rarefied regions very slightly below atmospheric pressure p_0. Pressure variations of sound waves are thus superimposed on prevailing barometric pressure.

comes relevant when dealing with vibrations of structures (e.g. in vibration control of machinery). Ultrasound begins above the audible frequency range. It is used in applications ranging from acoustic modelling techniques to medical diagnosis and non-destructive material testing. Clearly the boundaries of the audible frequency cannot be defined precisely. The upper limit varies individually, depending on factors like age, and also in cases of extensive workplace noise exposure or the misuse of musical devices. The value of 16 kHz refers to a healthy, human being who is about 20 years old. With increasing age, the upper limit decreases by about 1 kHz per decade.The lower limit is likewise not easy to define and corresponds to flickering. The term 'frequency' in acoustics is bound to pure tones, meaning a sinusoidal wave form in the time-domain. A simple sine wave is illustrated in figure 1.3. The wavelength is the distance a wave travels in the time it takes to complete one cycle. A wavelength can be measured between successive peaks or between any two corresponding points on the cycle. This holds for periodic waves other than the sine wave as well. The frequency is the number of cycles per

second (or hertz). Frequency and wavelength are related as follows:

$$\text{Wavelength (m)} = \frac{\text{Speed of sound (m/s)}}{\text{Frequency (hertz)}} \tag{1.1}$$

where speed of sound is $331,5$ m/s at $T = 0$ Celsius and 343 m/s at $T = 20$ Celsius (in general we have $331,4 + 0,62T$). Speech and music waveshapes

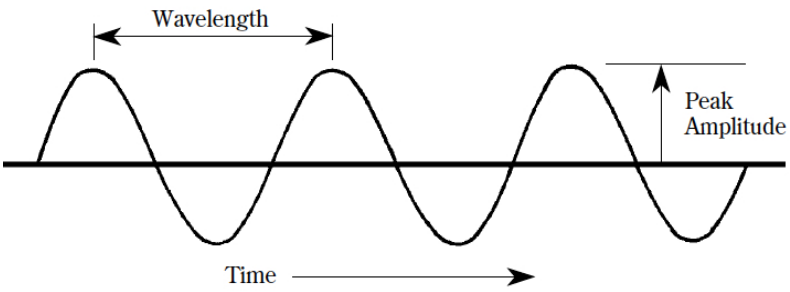

Figure 1.3: Wavelength is the distance a wave travels in the time it takes to complete one cycle. It can also be expressed as the distance from one point on a periodic wave to the corresponding point on the next cycle of the wave.

depart radically from the simple sine form. In particular a periodic function can be composed by a numerable infinity of harmonics whereas a not periodic (i.e. with an infinite period) admits a continuous infinite of harmonics. The obverse of this is that, theoretically, any complex periodic wave can be synthesized from sine waves of different frequencies, different amplitudes, and different time relationships (phase). A friend of Napoleon, named Joseph Fourier, was the first to develop this surprising idea. To pictorially illustrate this concept we look at figure 1.5 where a simple sine wave of a given amplitude and frequency f_1 and another sine wave half the amplitude and twice the frequency (f_2) are reported. Combining A and B at each point in time the waveshape of figure 1.5 C is obtained. In figure 1.5, another sine wave half the amplitude of A and three times its frequency (f_3) is shown. Adding this to the f_1 plus f_2 wave of C, figure 1.5 E is obtained. The simple sine wave of figure 1.5 A has been progressively distorted as other sine waves have been added to it. Whether these are acoustic waves or electronic signals, the process can be reversed. The distorted wave can be disassembled, as it were, to the simple f_1, f_2, and f_3 sine components by either acoustical or electronic filters. Applying names, the sine wave with the lowest frequency (f_1) of figure 1.5 A is called the fundamental, the one with twice the frequency (f_2)

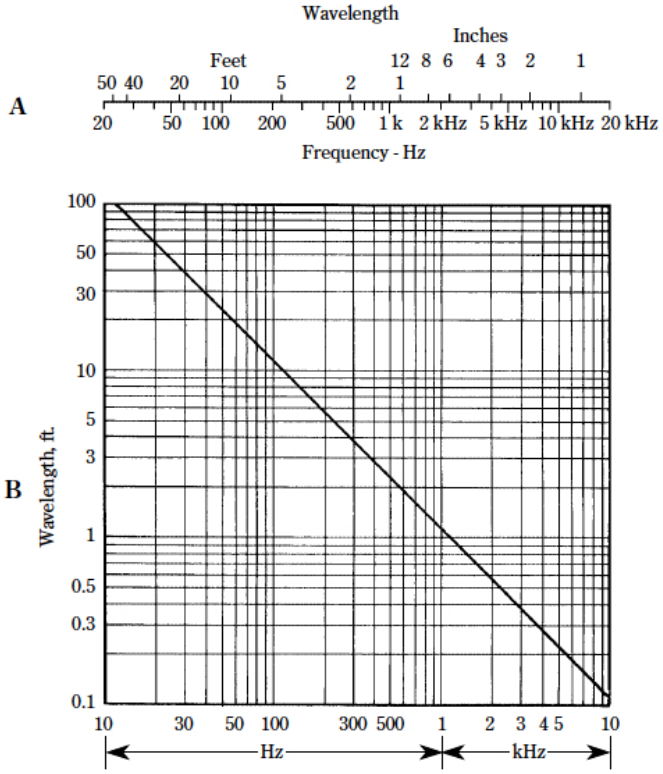

Figure 1.4: (A) Convenient scales for rough determination of wavelength of sound in air from known frequency, or vice versa. (B) A chart for easy determination of the wavelength in air of sound waves of different frequencies. (Both based on speed of sound of 1,139 ft per second.). Note that 1 ft = 0.357 m.

is called the second harmonic, and the one three times the frequency (f_3) is the third harmonic. The fourth harmonic, the fifth harmonic, etc., are four and five times the frequency of the fundamental, and so on. In figure 1.5, all

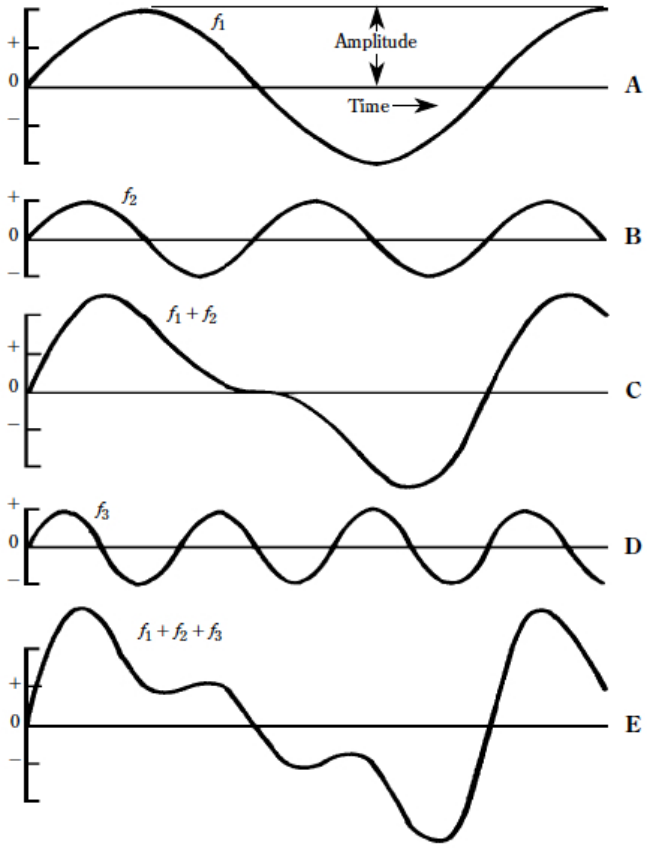

Figure 1.5: A study in the combination of sine waves. (A) The fundamental of frequency f_1. (B) A second harmonic of frequency $f_2 = 2f_1$ and half the amplitude of f_1. (C) The sum of f_1 and f_2 obtained by adding ordinates point by point. (D) A third harmonic of frequency $f_3 = 3f_1$ and half the amplitude of f_1. (E) The waveshape resulting from the addition of f_1, f_2, and f_3. All three components are "in phase" that is, they all start from zero at the same instant.

three components, f_1, f_2, and f_3, start from zero together: this is called an in-phase condition. In some cases, the time relationships between harmonics or between harmonics and the fundamental are quite different from this and an angular delay is possible (out-phase condition). This situation is reported

in figure 1.6
Audio and electronics engineers and acousticians frequently use the integral multiple concept of harmonics, closely allied as it is to the physical aspect of sound. The musician often refers to the octave, a logarithmic concept that is firmly embedded in musical scales and terminology because of its relationship to the ear's characteristics.
An octave is defined as a 2:1 ratio of two frequencies. For example, middle DO (C4) on the piano has a frequency close to 261 Hz. The next highest DO (C5) has a frequency of about 522 Hz. Ratios of frequencies are very much a part of the musical scale. The frequency ratio 2:1 is the octave; the ratio 3:2 is the fifth; 4:3 is the fourth, etc. Because the octave is very important in acoustical work, it is well to consider the mathematics of the octave. As the ratio of 2:1 is defined as the octave, its mathematical expression is:

$$\frac{f_2}{f_1} = 2^n, \tag{1.2}$$

where f_2 is the frequency of the upper edge of the octave interval, f_1 is the frequency of the lower edge of the octave interval and n is the number of octaves. Harmonics and octaves are compared in figure 1.7. Another fundamental concept is the spectrum that tells how the energy of the signal is distributed in frequency and, at the same time, gives the harmonics composition of the signal. For an ideal sine wave, all the energy is concentrated at one frequency. The triangular wave, instead, has both odd and even components and if you know the amplitude and phases of each of these, the original triangular wave shape can be synthesized by combining them [1]. A comparable analysis reveals the spectrum of the square wave shown in figure 1.8. It has harmonics of far greater amplitude than the triangular wave with a distinct tendency toward more prominent odd than even harmonics. A glance at the spectra of sine, triangular, and square waves reveals energy concentrated at harmonic frequencies, but nothing between. The fourth example in figure 1.8 is a random noise which, from a mathematical point of view, is a non-deterministic signal. This spectrum tells us that the energy of the

[1]Indeed the function we displayed in fig. 1.8, from a mathematical point of view is not only a triangular wave but a multiplication of a triangular wave by a theta function. As is well known clipping a function means, in the frequency domain, the introduction of an infinite series of harmonics. In our case if the triangular function is spread in the negative part of the t-axis, according to an even parity, we can have odd harmonics disappeared. Otherwise, in the odd case, disappear the even harmonics.

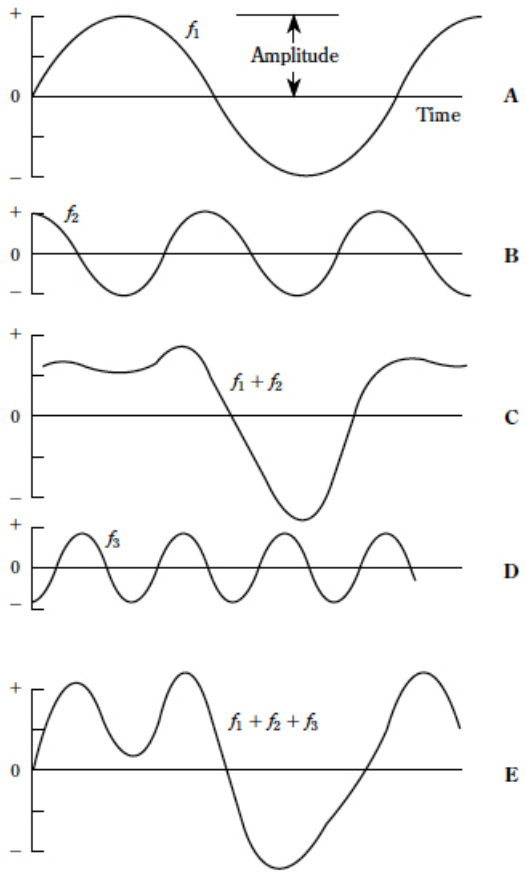

Figure 1.6: A study of the combination of sine waves that are not in phase. (A) The fundamental of frequency f_1. (B) The second harmonic f_2 with twice the frequency and half the amplitude of f_1 advanced 90 degrees with respect to f_1. (C) The combination of f_1 and f_2 obtained by adding ordinates point by point. (D) The third harmonic f_3 with phase 90 degrees behind f_1, and with half the amplitude of f_1. (E) The sum of f_1, f_2, and f_3. Compare this waveshape with that of figure 1.5 (E). The difference in waveshapes is due entirely to the shifting of the phase of the harmonics with respect to the fundamental.

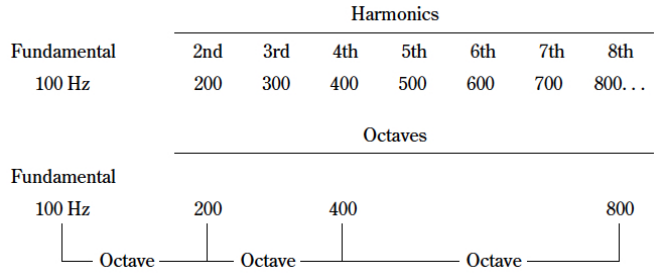

Figure 1.7: Comparison of harmonics and octaves. Harmonics are linearly related; octaves are logarithmically related.

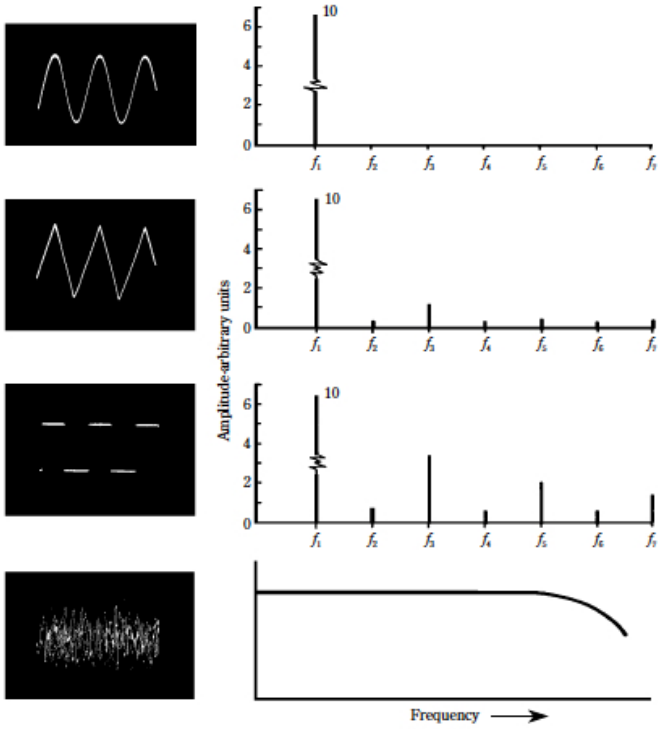

Figure 1.8: The spectral energy of a pure sinusoid is contained entirely at a single frequency. The triangular and square waves each have a prominent fundamental and numerous harmonics at integral multiples of the fundamental frequency. Random noise (white noise) has energy distributed uniformly throughout the spectrum up to some point at which energy begins to fall off due to generator limitations. Random noise may be considered a mixture of sine waves with continuously shifting frequencies, amplitudes, and phases.

random-noise signal is equally distributed throughout the spectrum until the drooping at high frequencies indicates that the upper frequency limit of the random noise generator has been reached.

1.2 Sound levels and the decibel

The decibel unit is commonly used in sound managing, because make easy to handle the extremely wide range of sensitivity in human hearing. A level in decibels is a convenient way of handling the wide range of sound pressures to which the ear is sensitive without use a long strings of zeros.
A power level of a power W_1 can be expressed in terms of a reference power W_0 through the Fechner-Weber's law:

$$L = \log_{10} \frac{W_1}{W_0} \text{bels}. \tag{1.3}$$

Because the decibel, from its very name, is $\frac{1}{10}$ bel (from Alexander Graham Bell), the level in decibels of a power ratio becomes:

$$L = 10 \log_{10} \frac{W_1}{W_0} \text{ decibels}. \tag{1.4}$$

Equation 1.4 applies equally to acoustic power, electric power, or any other kind of power. A question often arises when levels other than power need to be expressed in decibels. For example, acoustic intensity is acoustic power per unit area in a specified direction, hence equation 1.4 is appropriate. Acoustic power is proportional to the square of the acoustic pressure, p, hence the power level is:

$$L_P = 10 \log_{10} \frac{p_1^2}{p_0^2} = 20 \log_{10} \frac{p_1}{p_0} \text{ decibels}. \tag{1.5}$$

Because sound pressure is usually the most accessible parameter to measure in acoustics, equation 1.5 is more often encountered.
Thus sound-level meter is used to read a certain sound-pressure level (SPL). If the corresponding sound pressure is expressed in normal pressure units, a great range of very large and very small numbers results. Ratios are more closely related to human senses than linear numbers, and the level decibels approach compresses the large and small ratios into a more convenient and

comprehensible range. Some standard reference sound pressure for p_0 is needed. Several such reference pressures have been used over the years, but for sound in air the standard reference pressure is $20\mu Pa$ (micropascal), corresponding to the threshold of human hearing.
Clearly knowing the SPL level in decibel at each time the sound pressure can be obtained from equation 1.5 by:

$$\left(\frac{p}{p_0}\right)^2 = 10^{\frac{L_P}{10}}. \tag{1.6}$$

Table 1.9 lists sound pressure and sound-pressure levels of some common sounds. In the sound-pressure column, it is a long stretch from 100,000 Pa (100 kPa), which is atmospheric pressure to 0.00002 Pa (20 μPa), but this range is reduced to quite a convenient form in the level column. The same information is present in graphical form in figure 1.10 Often, two levels have

Sound Source	Sound pressure (Pa)	Sound level* (decibels, A-weighted)
Saturn rocket	100,000. (one atmosphere)	194
Ram jet	2,000.	160
Propeller aircraft	200.	140
Threshold of pain		135
Riveter	20.	120
Heavy truck	2.	100
Noisy office, Heavy traffic	0.2	80
Conversational speech	0.02	60
Private office		50
Quiet residence	0.0002	40
Recording studio		30
Leaves rustling	0.0002	20
Hearing threshold, good ears at frequency of maximum sensitivity		10
Hearing threshold, excellent ears at frequency maximum response	0.00002	0

* Reference pressure (take your pick, these are identical):
20 micropascal (μPa)
0.00002 pascal
2×10^{-5} newton/meter^2
0.0002 dyne/cm^2 or microbar

Figure 1.9: Some common sound-pressure levels and sound pressures.

to be summarised to one. For incoherent signal this can be done by the

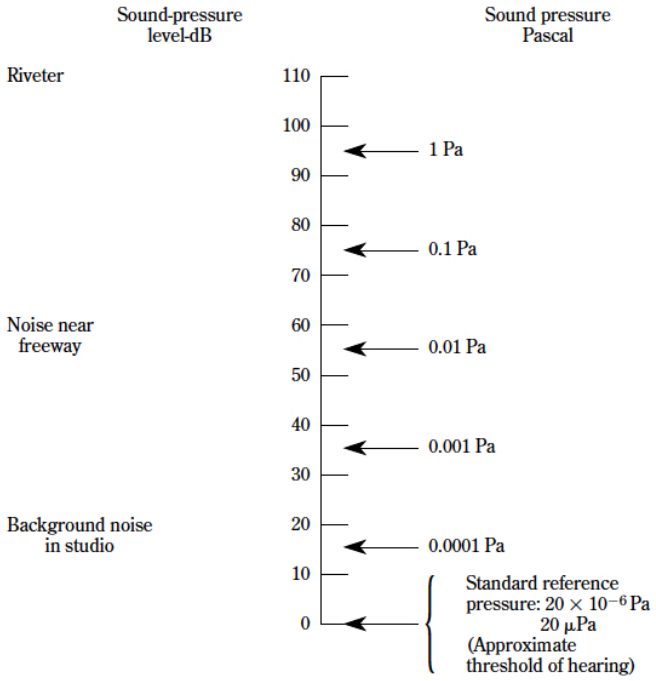

Figure 1.10: An appreciation of the relative magnitude of a sound pressure of 1 Pascal can be gained by comparison to known sounds. The standard reference pressure for sound in air is 20 microPascal, which corresponds closely to the minimum audible pressure.

following expression:

$$L_{Tot} = 10 \log_{10} \sum_{i=1}^{N} \frac{p_i^2}{p_0^2} = 10 \log_{10} \sum_{i=1}^{N} 10^{\frac{L_i}{10}}. \tag{1.7}$$

Equation 1.7 is called law of level summation. It states that the levels are in fact not summed, but the individual levels must be transformed to sound pressure values, before they are added together to yield the total level.
Until now we consider only sound sources with a sound level constant in time. If level is not constant in time, to obtain a mean information about the phenomenon, one consider the equivalent continuous sound pressure level L_{eq} defined as

$$L_{eq} = 10 \log_{10} \left(\frac{1}{T} \int_0^T \frac{p^2(t)}{p_0^2} dt \right), \tag{1.8}$$

that represents a sort of mean on period T (see figure 1.11). In similar way the Single Event Level is defined shrinking all the sound energy in $T = 1s$

$$SEL = 10 \log_{10} \left(\int_0^T \frac{p^2(t)}{p_0^2} dt \right) = L_{eq} + 10 \log_{10} T. \tag{1.9}$$

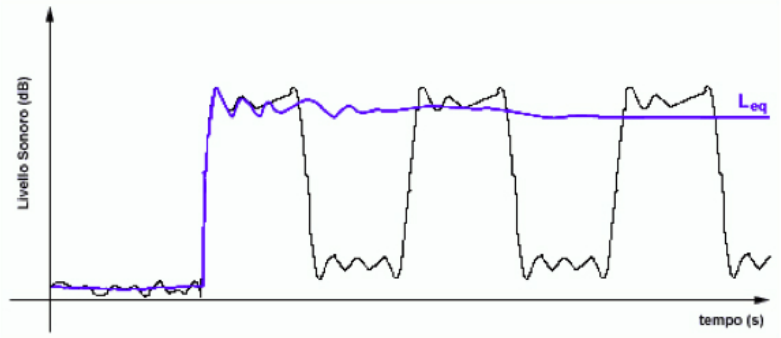

Figure 1.11: Equivalent continuous sound pressure level (blue line) of a time-dependent signal (black line).

1.3 The ear and the perception of sound

As already said, understanding how humans hear is a complex subject involving the fields of physiology, psychology and acoustics. In this section we

will focus on the acoustics of hearing. We will attempt to understand how the human ear serves as an astounding transducer, converting sound energy to mechanical energy to a nerve impulse which is transmitted to the brain. The ear's ability to do this allows us to perceive the pitch of sounds by detection of the wave's frequencies, the loudness of sound by detection of the wave's amplitude and the timbre of the sound by the detection of the various frequencies which make up a complex sound wave.

The ear consists of three basic parts: the outer ear, the middle ear, and the inner ear. Each part of the ear serves a specific purpose in the task of detecting and interpreting sound. The outer ear serves to collect and channel sound to the middle ear. The middle ear serves to transform the energy of a sound wave into the internal vibrations of the bone structure of the middle ear and ultimately transform these vibrations into a compressional wave in the inner ear. The inner ear serves to transform the energy of a compressional wave within the inner ear fluid into nerve impulses which can be transmitted to the brain. The three parts of the ear are shown in figure 1.12.

The outer ear consists of an ear flap and an approximately 2-cm long ear canal. The ear flap provides protection for the middle ear in order to prevent damage to the eardrum. The outer ear also channels sound waves which reach the ear through the ear canal to the eardrum of the middle ear. Because of the length of the ear canal, it is capable of amplifying sounds with frequencies of approximately 3000 Hz. As sound travels through the outer ear, the sound is still in the form of a pressure wave, with an alternating pattern of high and low pressure regions. It is not until the sound reaches the eardrum at the interface of the outer and the middle ear that the energy of the mechanical wave becomes converted into vibrations of the inner bone structure of the ear.

The middle ear is an air-filled cavity which consists of an eardrum and three tiny, interconnected bones - the hammer, anvil, and stirrup. The eardrum is a very durable and tightly stretched membrane which vibrates as the incoming pressure waves reach it. As shown below, a compression forces the eardrum inward and a rarefaction forces the eardrum outward, thus vibrating the eardrum at the same frequency of the sound wave.

Being connected to the hammer, the movements of the eardrum will set the hammer, anvil, and stirrup into motion at the same frequency of the sound wave. The stirrup is connected to the inner ear; and thus the vibrations of the stirrup are transmitted to the fluid of the inner ear and create a compression wave within the fluid. The three tiny bones of the middle ear act

as levers to amplify the vibrations of the sound wave. Due to a mechanical advantage, the displacements of the stirrup are greater than that of the hammer. Furthermore, since the pressure wave striking the large area of the eardrum is concentrated into the smaller area of the stirrup, the force of the vibrating stirrup is nearly 15 times larger than that of the eardrum. This feature enhances our ability of hear the faintest of sounds. The middle ear is an air-filled cavity which is connected by the Eustachian tube to the mouth. This connection allows for the equalization of pressure within the air-filled cavities of the ear. When this tube becomes clogged during a cold, the ear cavity is unable to equalize its pressure; this will often lead to earaches and other pains.
The inner ear consists of a cochlea, the semicircular canals, and the auditory nerve. The cochlea and the semicircular canals are filled with a water-like fluid. The fluid and nerve cells of the semicircular canals provide no roll in the task of hearing; they merely serve as accelerometers for detecting accelerated movements and assisting in the task of maintaining balance. The cochlea is a snail-shaped organ which would stretch to approximately 3 cm. In addition to being filled with fluid, the inner surface of the cochlea is lined with over 20000 hair-like nerve cells which perform one of the most critical roles in our ability to hear. These nerve cells have a differ in length by minuscule amounts; they also have different degrees of resiliency to the fluid which passes over them. As a compressional wave moves from the interface between the hammer of the middle ear and the oval window of the inner ear through the cochlea, the small hair-like nerve cells will be set in motion. Each hair cell has a natural sensitivity to a particular frequency of vibration. When the frequency of the compressional wave matches the natural frequency of the nerve cell, that nerve cell will resonate with a larger amplitude of vibration. This increased vibrational amplitude induces the cell to release an electrical impulse which passes along the auditory nerve towards the brain. In a process which is not clearly understood, the brain is capable of interpreting the qualities of the sound upon reception of these electric nerve impulses.

1.4 Hearing levels and A-weighting

Results of acoustic measurements are also often specifed using another single value called the A-weighted sound pressure level. Some basic principles of the frequency dependence of the sensitivity of human hearing are now explained,

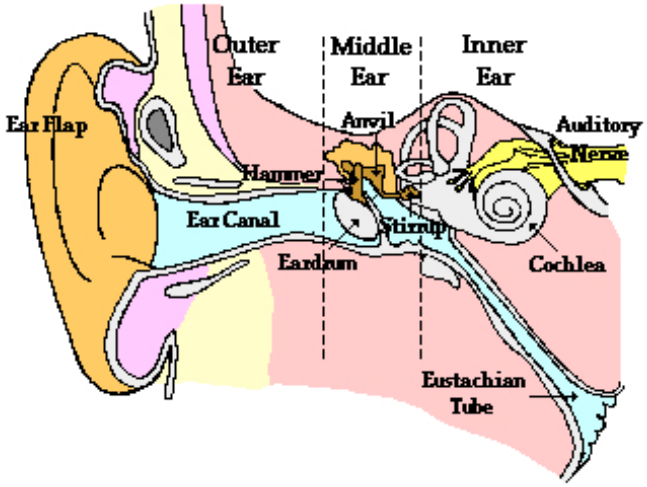

Figure 1.12: The four principal parts of the human ear: the ear flap, the Ear canal, the middle ear, and the inner ear.

as the measurement procedure for the A-weighted level is roughly based on this.
The sensitivity of the human ear is strongly dependent on the tonal pitch. The frequency dependence is depicted in 1.13. The

figure is based on the findings from audiometric testing. The curves of perceived equal loudness (which have the unit "phon") are drawn in a sound pressure level versus frequency plot. One can imagine the development of these curves as follows: a test subject compares a 1 kHz tone of a certain level to a second tone of another frequency and has to adjust the level of the second tone in such a way that it is perceived with equal loudness. The curve of one hearing level is obtained by varying the frequency of the second tone and is simply defined by the level of the 1 kHz tone. The array of curves obtained by varying the level of the 1 kHz tone is called hearing levels. It reveals, for example, that a 50 Hz tone with an actual sound pressure level of 80 dB is perceived with the same loudness as a 1 kHz tone with 60 dB. The ear is more sensitive in the middle frequency range than at very high or very low frequencies.
The relationship between the objective quantity sound pressure or sound pressure level, respectively, and the subjective quantity loudness is in fact quite complicated, as can be seen in the hearing levels shown in figure 1.13.

The frequency dependence of the human ear's sensitivity, for example, is also level dependent. The curves with a higher level are significantly flatter than the curves with smaller levels. The subjective perception "loudness" is not only depending on frequency, but also on the bandwidth of the sound incident. The development of measurement equipment accounting for all properties of the human ear could only be realized with a very large effort. A frequency-weighted sound pressure level is used both nationally and internationally, which accounts for the basic aspects of the human ear's sensitivity and can be realized with reasonable effort. This so-called "A-weighted sound pressure level" includes contributions of the whole audible frequency range. In practical applications the dBA-value is measured using the A-fillter. The frequency response function of the A-fllter is drawn in figure 1.14. The lower frequencies and the very high frequencies are evaluated compared to the middle frequency range when determining the dBA-value. As a matter of fact, the A-weighted level can also be determined from measured third-octave band levels. The levels given in figure 1.14 are added to the third-octave band levels and the total sound pressure level, now A-weighted, is calculated according to the law of level summation. The A-weighting function is standardized in EN 60651.

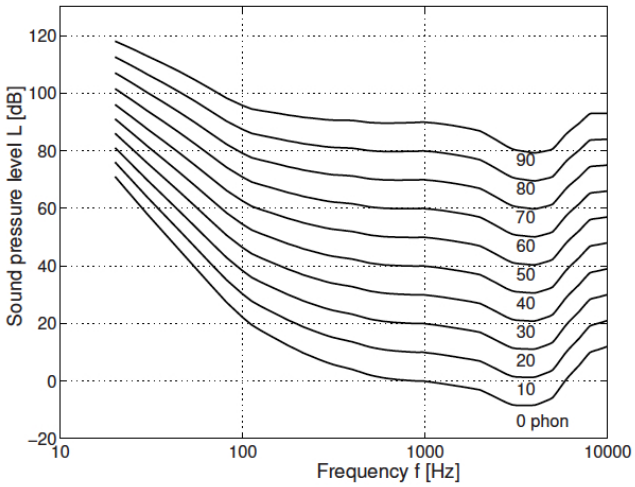

Figure 1.13: Hearing levels.

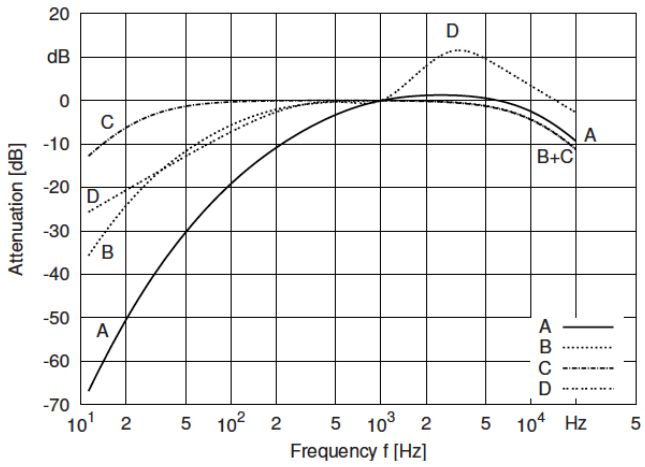

Figure 1.14: Frequency response functions of A, B, C and D weighting filters.

1.5 Propagation and radiation of sound

As we know from experience sound sources have a directivity. The sound level perceived by the observer is not dependent on the distance from the source alone. If the source is rotated, the level changes with angle. When estimating the radiation of sound sources, where the details of their directivity are unknown, one has to assume that their sound field is omnidirectional (which might actually not be the case). Thus, we begins with a discussion of omnidirectional sound radiation in free field where secondary influences such as weather conditions are neglected.

1.5.1 Sound radiation of point sources

The intensity I of sound decreases as the distance r to the source is increased. In free space, far from the influence of surrounding objects, sound from a point source is propagated uniformly in all directions. The intensity of sound decreases as shown in figure 1.15. The same sound power flows out through A1, A2, A3, and A4, but the areas increase as the square of the radius, r. This means that the sound power per unit area (intensity) decreases as the square of the radius. Doubling the distance reduces the intensity to one-fourth the initial value, tripling the distance yields $\frac{1}{9}$, and increasing the distance four times yields $\frac{1}{16}$ of the initial intensity. The inverse square law states that

the intensity of sound in a free field is inversely proportional to the square of the distance from the source. Thus the acoustic power W penetrating an arbitrary surface which surrounds the source must be identical for every surface (assuming that propagation losses can be neglected for distances not too far from the source). So we get for the acoustic power:

$$W = \frac{p^2}{\rho c} 4\pi r^2, \tag{1.10}$$

where ρ is the density of medium and c the speed of sound. Being the density $I = \frac{p^2}{\rho c}$ we get the following expression similar to the Coulomb law for electromagnetism:

$$I = \frac{W}{4\pi r^2}. \tag{1.11}$$

If the logarithm to the base 10 is taken for both sides we get the propagation law for the point source:

$$L_P = L_W - 20 \log_{10} r - 11, \tag{1.12}$$

where L_P represents the sound pressure level at distance r. Based on the distance law 1.12, the level falls off at 6 dB per doubling of distance. If the noise source is located on a totally reflecting surface (like the ground), the power flows through a hemisphere only. In this case, instead of 1.12 we obtain:

$$L_P = L_W - 20 \log_{10} r - 8, \tag{1.13}$$

In general one can assume a directivity factor Q that is 1 for "isotropic emission", 2 for "hemisphere source", etc. Thus the intensity read $I = \frac{QW}{4\pi r^2}$ and equation 1.12 become

$$L_P = L_W - 20 \log_{10} r - 11 + 10 \log_{10} Q, \tag{1.14}$$

1.5.2 Sound radiation of line sources

Sometimes in practice, extended noise sources occur, which may consist of multiple, omnidirectional radiating (and incoherent) point sources. The

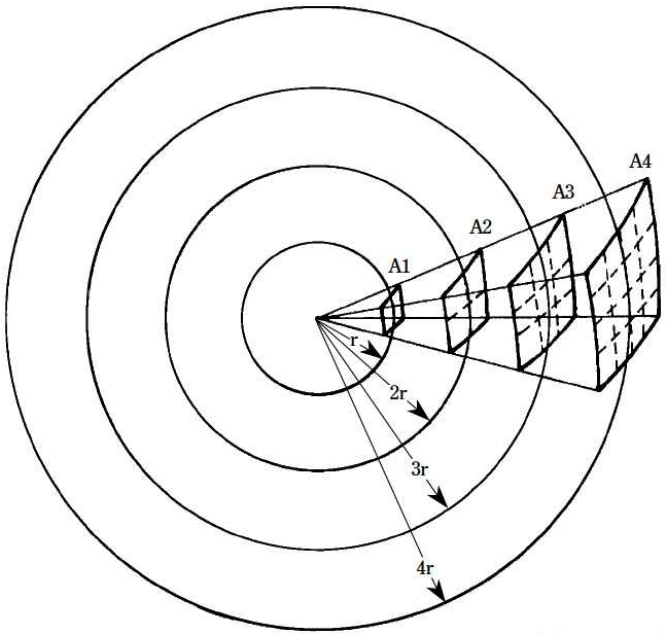

Figure 1.15: In the solid angle shown, the same sound energy is distributed over spherical surfaces of increasing area as r is increased. The intensity of the sound is inversely proportional to the square of the distance from the point source.

power in this case is calculated using a cylindrical surface (see figure 1.16 and with l being the length of the line source. Thus we obtain:

$$W = \frac{p^2}{\rho c} 2\pi r l, \tag{1.15}$$

resulting in a level of

$$L_P = L_W - 10 \log_{10} r - 10 \log_{10} l - 8, \tag{1.16}$$

or, if the source is again located on a reflecting surface

$$L_P = L_W - 10 \log_{10} r - 10 \log_{10} l - 5, \tag{1.17}$$

Here, the sound pressure level only decreases at 3 dB per doubling of distance. Consequently, very long sources are still audible at large distances.
In close vicinity to a source of finite length, the source characteristics resemble that of a long line source, whereas at larger distances, the individual sources shrink to a point. The transition between line and point source behavior occurs at a critical distance of $r_{cr} = l/2$, as can be seen by setting 1.10 and 1.15 to be equal to one another. At distances $r < r_{cr}$, the source behaves like a line source with the level decreasing by 3 dB per doubling of distance; at distances $r > r_{cr}$, it acts like a point source with the level decreasing by 6 dB per doubling of distance.

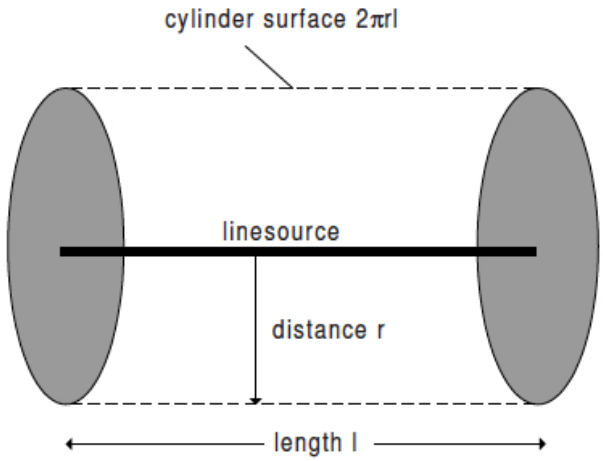

Figure 1.16: Cylindrical surface around an omnidirectional line source used for determining radiated sound power.

Chapter 2

Models of Road Traffic Noise

The development of models to predict traffic noise started more than 50 years ago and, the results have often been very accurate. Usually these kind of models are developed taking into account mainly traffic flow, both of light and heavy vehicles, features of the road surface, distance between carriage and receivers. Moreover, since several models have been developed all around the world, the peculiarities of different countries, in terms of roads, kind of vehicles and weather features have to be taken into account.
The aim of using a Traffic Noise Model (TNM) is twofold: on one side it can be used in the designing of new road infrastructures in order to evaluate the acoustical impact and to avoid post-construction mitigation actions that often present a greater cost; on the other side it can be used on an existing road network, so that the measurement campaign can be minimized and can be used just for the tuning of the model.
Many countries decided to regulate the use of these models, establishing which one can be adopted in a traffic noise simulation. In this chapter we present a quantitative review of the most used models, exploiting the main features and peculiarities of each of them. In particular we present the TNMs usually employed in Europe and U.S.A., following their historical evolution starting from a general and elementary concept of noise prediction to a more detailed formula which may include many corrective terms. In the next chapter we present our new proposal for traffic noise prediction.

2.1 Early models

First attempts of making a traffic noise prediction can be collocated into 1950/1960 decades; they mainly evaluate the percentile L_{50}, defined as the sound level exceeded by the signal in 50% of the measurement period. These models refer principally to a fluid continuous flux, considering a common constant velocity with no distinction between vehicle typologies. One of the first models, developed in 1952, is the one reported in Handbook of Acoustic Noise Control [6]. This model states that the 50 percentile of traffic noise for speed of 55-75 Km/h (35-45 mph) and distances greater than 20 feet (about 6 meters) is given by:

$$L_{50} = 68 + 8.5 \log_{10} Q - 20 \log_{10} d, \tag{2.1}$$

where Q is traffic volume in vehicles per hour and d is the distance from observation point to center of the traffic lane, in feet; no specification is included about vehicles and roads type. In the following years, Nickson et al. [7, 8] presented a new model in which a new parameter is included to relate the model with the experimental data. They proposed:

$$L_{50} = C + 10 \log_{10} \frac{Q}{d}, \tag{2.2}$$

where C is a constant value that can be evaluated making an analysis of experimental data and L_{50} is the sound level in dBA. Later, Johnson et al. [9] presented a new TNM taking also into account the mean speed of vehicles in mph, v. They proposed for L_{50} the following expression:

$$L_{50} = 3.5 + 10 \log_{10} \left(\frac{Q v^3}{d} \right). \tag{2.3}$$

This model presents a good agreement with the experimental data for a percentage of heavy vehicles from 0% to 40%. It also include some corrective factor for ground attenuation and gradient. Some years later, Galloway et. al. [10] improved this model taking into a account the percentage of heavy vehicles P. Their expression for the L_{50} level in dBA was:

$$L_{50} = 20 + 10 \log_{10} \left(\frac{Q v^2}{d} \right) + 0.4P. \tag{2.4}$$

The models developed in the next years introduced the equivalent level L_{eq} as sound level indicator. One of the most used is the Burgess Model [11]

applied for the first time in Sydney in Australia. Using the same notation of the previous expression, the sound level is given by:

$$L_{eq} = 55.5 + 10.2 \log_{10} Q + 0.3P - 19.3 \log_{10} d. \tag{2.5}$$

Another most used calculation formula is called "Griffiths and Langdon Method" [12]. In particular they propose the evaluation of equivalent level starting from the percentile level as follow:

$$L_{eq} = L_{50} + 0.018(L_{10} - L_{90})^2, \tag{2.6}$$

where the statistical percentile indicator have the expression:

$$L_{10} = 61.0 + 8.4 \log_{10} Q + 0.15P - 11.5 \log_{10} d, \tag{2.7}$$
$$L_{50} = 44.8 + 10.8 \log_{10} Q + 0.12P - 9.6 \log_{10} d, \tag{2.8}$$
$$L_{90} = 39.1 + 10.5 \log_{10} Q + 0.06P - 9.3 \log_{10} d, \tag{2.9}$$

where Q, P and d have the same meaning of previous formula. Several years later Fagotti et al. [13] improved the previous models introducing the motorcycles and buses flux, Q_M and Q_{BUS}. The formula they propose is the following:

$$L_{eq} = 10 \log_{10}(Q_L + Q_M + 8Q_P + 8.8Q_{Bus}) + 33.5- \tag{2.10}$$

Another model was formulated by the French "Centre Scientifique et Technique du Batiment" (C.S.T.B.) [14], which proposed a predictive formula of equivalent emission level, based on the average acoustic level (L_{50}) with the following expression:

$$L_{eq} = 0.65L_{50} + 28.8. \tag{2.11}$$

The value of L_{50} is calculated taking into account only the equivalent vehicular flows (Q_{eq}), and is given by:

$$L_{50} = 11.9 \log_{10} Q + 31.4, \tag{2.12}$$

for urban road and highway with vehicular flows lower than 1000 vehicles/hour and

$$L_{50} = 15.5 \log_{10} Q - 10 \log_{10} L + 36, \tag{2.13}$$

for urban road with elevated buildings near the carriageway edge, with L the width (in meters) of the road near the measurement point.

2.2 England standard: CoRTN procedure

The CoRTN procedure (Calculation of Road Traffic Noise) has been developed by the Transport and Road Research Laboratory and the Department of Transport of the United Kingdom in the 1975 [15] and has been modified in the 1988 [16]. It estimates the basic noise level L_{10} both on 1h and 18h reference time. This level is obtained at a reference distance of 10 m from the nearest carriageway edge of an highway. The parameters involved in this model are: traffic flow and composition, mean speed, gradient of the road and type of road surface. The basic hypothesis of the model are a moderate wind velocity and a dried road surface.
The CoRTN procedure is divided in five steps:

- Divide the road scheme into one or more segments, such that the variation of noise level within the segment is less than 2 dBA;
- Calculate the basic noise level 10 meters away from the nearside carriageway edge for each segment. It depends on the velocity, traffic flow and composition. The traffic is considered as a linear source positioned at 0.5 m from the road surface and at 3.5 m from the carriage edge;
- Evaluate the noise level, for each segment, taking into account the attenuation due to the distance and screening of the source line;
- Adjust the noise level taking into account:
  a) reflection due to buildings and facades on the other side of the road and reflective screen behind the reflection point.
  b) Size of source segment (view angle);
- Join the contributions from all segments to give the predicted noise level at the reception point for the whole road scheme.

Operatively the basic hourly noise level is predicted at a distance of 10 meters from the nearest carriageway, according to the following equation:

$$L_{10}(1h) = 42.2 + 10 \log_{10} q, \tag{2.14}$$

and the basic noise level in terms of total 18-hour flow is:

$$L_{10}(18h) = 29.1 + 10 \log_{10} Q, \tag{2.15}$$

where q and Q are the hourly traffic flow (vehicles/hour) and 18-hour flow (vehicles/hour), respectively. Here it is assumed that the basic velocity is v = 75 km/h, the percentage of heavy vehicles is P = 0 and road's gradient is G = 0%. It is also assumed that the source line is 3.5 m from the edge of the road for carriageways separated by less than 5.0 meters. Subsequently the level will be correct to take into account mean traffic speed, percentage of heavy vehicles and gradient contribute. In particular the corrections for heavy vehicles and speed are determined using the following expression:

$$\Delta_{pV} = 33 \log_{10}\left(v + 40 + \frac{500}{v}\right) + 10 \log_{10}\left(1 + \frac{5P}{v}\right) - 68.8, \tag{2.16}$$

where the mean speed v depends on road type and is reported in [16] for various roads. The percentage of heavy vehicles is then given by:

$$P = \frac{100f}{q} = \frac{100F}{Q}, \tag{2.17}$$

where f and F are respectively the hourly and 18-hour flows of heavy vehicles. The value of v to be used in equation 2.2 depends on the road gradient. In particular, for roads with gradient, traffic speed in the previous relation will be reduced by the value Δ_V which is predicted from:

$$\Delta_V = \left[0.73 + \left(2.3 - \frac{1.15p}{100}\right)\frac{p}{100}\right] G, \tag{2.18}$$

where G is the gradient expressed as a percentage. Once the traffic speed is known also the sound level is adjust for the extra noise from traffic on a gradients with the correction $\Delta_G = 0.3G$.
The noise depends also upon the road surface. In fact for roads which are impervious and where the traffic speed used in expression 2.2) is $V > 75Km/h$ a correction to the basic noise level is applied as:

- $\Delta_{TD} = 10 \log_{10}(90TD + 30) - 20$ for concrete surfaces;
- $\Delta_{TD} = 10 \log_{10}(20TD + 60) - 20$ for bituminous surfaces;

where TD is the texture depth. If instead $v < 75km/h$ the correction are:

- $\Delta_{TD} = -1$for impervious bituminous road surfaces;
- $\Delta_{TD} = -3.5$ for pervious road surfaces.

The model also consider the correction for receiver points located at distances $d < 4.0$ m from the edge of the nearest carriageway, which is:

$$\Delta_d = -10 \log_{10} \frac{d'}{13.5}, \tag{2.19}$$

where d' is the shortest distance between the effective source and receiver. The last correction is the one associated with the propagation obstacles, such as the nature of the ground surface between the edge of carriageway and the receiver point (for example grass land, cultivated fields, etc.) or the presence of buildings, walls, barriers, etc..

2.3 German standard: RLS90 model

In the Guideline for Noise Protection on Streets [17], the RLS90 (Richtlinien fur den Larmschutz an Straben) traffic noise model has been defined as an improvement of oldest standard RLS81 [18]. RLS90 is an effective calculation model, able to determine the noise rating level of road traffic and, at current day, is the most relevant calculation method used in Germany. The model requires an input of data regarding the average hourly traffic flow, separated into motorcycles, heavy and light vehicles, the average speed for each group, the dimension, geometry and type of the road and of any natural and artificial obstacles.
This model takes also into account the main features which influence the propagation of noise, such as obstacles, vegetation, air absorption, reflections and diffraction. In particular it makes possible to verify the noise reduction produced by barriers and takes into account also the reflections produced by the opposite screens. In addiction this is one of the few models present in literature that is able to evaluate the sound emission of a parking lot.
The starting point of the calculation is an average level $L_{m,E}$ measurable at a distance of 25 m from the centre of the road lane. This $L^{25}_{m,E}$ is a function of the amount of vehicles per hour Q and of the percentage of heavy trucks P (weight > 2.8 tons), under idealized conditions (i.e. a speed of 100 km/h, a road gradient below 5% and a special road surface). Analytically $L^{25}_{m,E}$ is given by

$$L^{25}_{m,E} = 37.3 + 10 \log_{10} \left[Q(1 + 0.082P) \right]. \tag{2.20}$$

The next step is to quantify the various deviations from these idealized conditions by means of corrections for the "real speed", the actual road gradient or

the actual surface, etc. In particular these correction depends upon whether day (6:00-22:00 h) or night (22:00-6:00 h) is considered. So for each lane the mean level in dBA Lm is calculated as

$$L_m = L^{25}_{m,E} + R_{SL} + R_{RS} + R_{RF} + R_E + R_{DA} + R_{GA} + R_{TB}, \tag{2.21}$$

where

- R_{SL} is a correction for the speed limit;
- R_{RS} is a correction for road surfaces. It's given in a table and depends upon kind of surface and vehicle speed. It ranges from 0 to 6 dB. In particular:
  $R_{RS} = 0.6|G| - 3$ for $|G| > 5\%$
  $R_{RS} = 0$ for —G— <= 5%;
- R_{RF} is a correction for rises and falls along the streets;
- R_E is a correction for the absorption characteristics of building surfaces;
- R_{DA} is a attenuation's coefficient that takes into account the distance from receiver and the air absorption;
- R_{GA} is a attenuation's coefficient due to ground and atmospheric conditions;
- R_{TB} is a attenuation's coefficient due to topography and buildings dimensions.

In particular the R_{SL} is given by the formula:

$$R_{SL} = L_{Pkw} - 37.3 + 10\log_{10}\left(\frac{100 + (10^{0.1D} - 1)P}{100 + 8.23P}\right), \tag{2.22}$$

with

$$L_{Pkw} = 27.7 + 10\log_{10}\left[1 + (0.02v_{Pkw})^3\right]; \tag{2.23}$$

$$L_{Lkw} = 23.1 + 12.5\log_{10}(v_{Pkw}); \tag{2.24}$$

$$D = L_{Lkw} - L_{pkw}; \tag{2.25}$$

where v_{Pkw} is the speed limit in the range of 30 to 130 km/h for light vehicles and v_{Lkw} is the speed limit in the range of 30 to 80 km/h for heavy vehicles. Evaluating the $L_{m,E}^{25}$ for each lane as described, we can obtain:

$$L_m = 10 \log_{10} \left[10^{0.1 L_{m,n}} + 10^{0.1 L_{m,f}} \right], \tag{2.26}$$

where n represent the nearer and f the further lane respectively. Finally the sound pressure level for the street is given by:

$$L_r = L_m + K, \tag{2.27}$$

K is the additional term for the increased effect of traffic light controlled intersections and other intersections.

2.4 Italian C.N.R. model

Nowadays the Italian legislation does not suggest any TNM of reference, but the most used by technician is the one developed by the Italian "Consiglio Nazionale delle Ricerche" (CNR) [19] and than improved by Cocchi et al. [20]. This model represents a modification of the German standard RLS 90, adapted to the Italian framework; a relation between the traffic parameters and the mean sound energy level is supposed and the traffic flow is modeled as a linear source placed in the center of the road. So the equivalent sound level in dBA is given by

$$L_{Aeq} = \alpha + 10 \log_{10}(Q_L + \beta Q_P) - 10 \log_{10} \left(\frac{d}{d_0} \right) + \Delta L_V + \Delta L_F + \Delta L_B + \Delta L_S + \Delta L_G + \Delta L_{VB}, \tag{2.28}$$

where Q_L and Q_P are the traffic flow in one hour, related to light and heavy vehicles respectively, d0 is a reference distance of 25 meter and d the distance between the lane center and observation point on the road's edge. Then:

- ΔL_V is the correction due to mean flux velocity defined in table 2.1;
- ΔL_F and ΔL_B are the correction for the presence of reflective facade near the observation point (+2.5 dBA) or in opposite direction (+1.5 dBA) respectively;
- ΔL_S is the correction for the road's pavement defined in the table 2.2;

- Δ_G is the correction for a road's gradient greater than 5% . The correction value is +0.6 dBA for each % gradient over 5%;

- Δ_{VB} is a coefficient that takes into account the presence of traffic lights (+1.0 dBA) or slow traffic (-1.5 dBA).

Whilst all the cited parameters have a general validity, independent by countries (because related just to physical or urban parameters), the α and β parameters are influenced by characteristics of countries roads and vehicles. In particular α is related to noise emission from the single vehicles and β is the weighting factor that takes into account the greater emission of heavy vehicles (for Italian roads $\alpha = 35.1$ and $\beta = 6$ are experimentally founded).

Table 2.1: Correction for flux mean speed

Mean speed (Km/h)	ΔL_V (dBA)
30-50	+0
60	+1
70	+2
80	+3
100	+4

Table 2.2: Correction for road's pavement

Road's pavement	ΔL_S (dBA)
Smooth Asphalt	-0.5
Rough Asphalt 0	0
Cement	+1.5
Rough pavement	+4

2.5 French model: NMPB - Routes 96

The European directive 2002/49/CE for what concern the traffic noise prevision model suggest to use the official interim French standard model "Nouvelle Methode de Prevision de Bruit" or simply NMPB-Routes-96 [21]. This method has been developed by different French Institutes of Ministere de

l'Equipement (CSTB, SETRA, LCPC, LRPC) and represents an improvement of an oldest one defined in the "Guide de Bruit" of 1980 [22] that takes into account the meteorological conditions and the long distance ($d > 250$m) prevision, as suggested in the ISO 9613. Nowadays it represents one of the most used TNM, being also integrated in some commercial software such as CadnaA by 01dB. In the 2000, under request of SETRA, a revision of NMPB-Routes-96 started, bringing to the NMPBRoutes- 2008.
The method is based on the concept of propagation path. Several paths between a source and a receiver can exist, depending on topography and obstacles and, at each of them, a long term sound level $L_{Ai,LT}$ may be associated. Despite of previous models, NMPB takes into account the standard meteorological conditions, as suggested by the ISO 9613, to adjust the prevision on long-period. They are classified in two types: meteorological conditions "favorable to the propagation" (as defined in ISO 9613) and "homogeneous acoustical conditions" (corresponding to the conditions used in the oldest French model). So, the long-period prediction level for each path $L_{Ai,LT}$ is evaluated adding the terms corresponding to this two conditions:

$$L_{Ai,LT} = 10\log_{10}\left(p_i 10^{0.1L_{Ai,F}} + (1-p_i)10^{0.1L_{Ai,H}}\right), \tag{2.29}$$

where $L_{Ai,F}$ and $L_{Ai,H}$ are the global levels evaluated respectively for favorable and homogeneous conditions and p_i represent the probability of occurrence of favorable conditions. These levels are calculated for each octave band and for each path from the source, according to the following formulas:

$$L_{Ai,F} = L_{A,w} - A_{div} - A_{atm} - A_{bnd} - A_{grd,F} - A_{diff,F}, \tag{2.30}$$

$$L_{Ai,H} = L_{A,W} - A_{div} - A_{atm} - A_{bnd} - A_{grd,H} - A_{diff,H} \tag{2.31}$$

For each path the algorithm computes three different attenuations: the geometrical spreading A_{div} and the atmospheric absorption A_{atm}, that are the same in both formulas, and the boundary attenuations A_{bnd}, which depends on the propagation conditions and are determined by ground effect (A_{grd}) and diffraction (A_{diff}). The sound power level, $L_{A,w}$, is evaluated considering the hourly flux Q, reported in [23], and directly obtaining the equivalent hourly level in dB(A), E, associated to a single light or heavy vehicle. By this procedure the pointlike source acoustical power representing the road is given by:

$$L_{Awi} = [(E_L + 10\log_{10} Q_L) + (E_P + 10\log_{10} Q_P)] + 20 + 10\log_{10} I_i + R(j), \tag{2.32}$$

where E_L and E_P are the emission levels obtained from [23] for light and heavy vehicle, I_i the length in meter of considered road and $R(j)$ is the value of normalized noise spectra from CEN 1793-3(1995) that take into account the frequency behavior of propagation. The predictions of NMPB-Routes-96 have been validated on a great number of experimental campaign with various topography and meteorological conditions, founding a very good agreement with the noise data but generally an overestimate level is found in downward propagation conditions. That's why SETRA required the revision of the model. The NMPBRoutes-2008 presents a better estimation of noise level in downward condition, takes into account reflections on embankments, is able to evaluate the correction due to diffraction by low barriers and has implemented other minor corrections.

2.6 Other models

In this section we give a list of other important traffic noise models with the relative references.

- **The FHWA Traffic Noise Prediction Model** [24] was developed for the United States of America Department of Transportation Federal Highway administration by Barry and Reagan, although they used some material from previous National Cooperative Highway Research Program (NCHRP) [25] reports. The prediction model was published as Report No. FHWA-RD-77-108 [26], which included a programmable calculator program. This program was further developed, separately, under the title STAMINA, in several successive versions.

- Modele de Calcul de Bruit du Traffic Routier Pour Ordinateur: Manuel d'utilisation du logiciel **StL-86** Version1.0 [27] is published by the Swiss Federal Office for Environmental Protection. It is consonant with Modele de Bruit du Traffic Routier dans les Zones Habitees [28], prepared by Balzari and Schudel, engineers and town planners, and Grolimund and Petermann, and also published by the Swiss Federal Office for Environmental Protection.

- In 1975, the Acoustical Society of Japan published the **ASJ Method** of predicting a pseudo-L_{50} resulting from free-flowing road traffic. It was reported by Koyasu [29], and up-dated by Takagi et al. [30], and

Yamamoto et al. [31]. The up-date contains a direct method of calculating L_{eq}, and deriving the pseudo-L_{50} from the result.

Chapter 3

A Stochastic Model for Traffic Noise Prediction

Many models able to predict noise emitted by different infrastructures, such as industrial areas, railways, airport, etc., have been developed (see for example [32, 33, 34, 35, 36]). In particular, in the last fifty years, the interest has been focused on noise coming from vehicular traffic. In literature, in fact, one can find many models (see chapter 2) aimed at this goal and it has been shown that some of them can be suitably adopted in most practical applications. For example a good traffic noise model (TNM) can be helpful in the stage of road project or to get an idea of acoustical impact generated by a new built infrastructure and, in addition, to avoid post-construction mitigation actions. One of the most significant advantages of a predictive traffic noise model concerns the possibility of collecting information about the road emission with little efforts in terms of time and costs.

Many countries have established a technical guideline to regulate the development of these mathematical models, with the aim of reducing the prediction error related to the different evaluations. Looking to Italy, it is the D.P.C.M. 01.03.1991 [5] which regulates noise pollution matters, giving the main acoustics elements definitions such as maximum limit of noise exposure in inner and external environment, acoustic zoning criteria, etc. Then the Framework Law n. 447/1995 has defined a general policy on the noise pollution that has been implemented in different decrees and regulations. Among these, one of the most interesting is the D.M.A. 16.03.1998 Noise pollution detection and measurement method (*Tecniche di rilevamento e di misurazione dell'inquinamento acustico*) which deals with the vehicular and railway noise

detection procedure. Moreover the D.Lgs 194/2005 (Ò*Attuazione della direttiva 2002/49/CE relativa alla determinazione e alla gestione del rumore ambientale*Ó) establishes the method to set the acoustic indicator for the different kind of noise sources such as vehicular traffic.

Together with the requirement of a satisfactory prediction of the equivalent and the statistical noise levels, it is required that the TNMs are simple enough in order to be user friendly for people managing with urban planning. In addition any TNM must be fully compatible with the International Standard ISO-9613 that deals with the sound propagation in open environment. This standard considers the influence of various environmental parameters (such as obstacles, geometric divergence, meteorological conditions, ground and air absorption etc.) on the sound propagation. Creating a simple, accurate and (first of all) general TNM is a very stimulant challenge because one should take into account a great number of variables: driving skills, total load, vehicle type and conditions, tire calibrations, exhaust system type and conditions, mechanical stress of the vehicle, meteorological conditions, road characteristics and configurations, etc. Furthermore, the traffic conditions, and the roads and vehicles features, differ from country to country and this makes difficult to develop a traffic noise model that can be used, with the same degree of accuracy everywhere. According to the above variables, differences will be experienced on the measured noise emission levels for different samples, even if the traffic flow and composition remain the same. Therefore, any mathematical model will be an approximated estimation since there are many random factors involved in the analysis.

Actually one can distinguish two main types of traffic noise model: predictive models with geometric approach and predictive models with statistical approach. The first ones, more sophisticated, usually adopt the ray tracing approach that consists in the trajectory and impact calculations of ray arriving to the observation point [37]. It requires as input the 3-dimensional cartography of analyzed site, buildings and air absorption data with respect to frequency, the source power and the hourly and daily traffic flow. Obtaining all these data for the site under analysis is in many cases, very difficult, so many authors produce simplified calculation methods using a statistical approach. The general expression of the equivalent level calculated according to a statistical traffic noise model is:

$$L_{eq} = A \log Q \left[1 + \frac{P}{100}(n-1)\right] + b \log(d) + C, \tag{3.1}$$

where Q is the total traffic charge (vehicle/hour), P the percentage of heavy vehicles (generally weight greater than 3.5 tons), d the distance between the lane centre and the receiver. The traffic flow parameter (Q and P) must be known in order to evaluate the noise emission from existing road or have to be inferred for a designing road. Moreover, since a heavy vehicle generally generates a greater noise than a light one, a factor n, called acoustical equivalent coefficient of heavy vehicles, can be considered. This coefficient is defined as the number of light vehicle that generate the same acoustic energy of an heavy one. Usually, an equivalent traffic flow, Q_{eq}, is introduced as follows:

$$Q_{eq} = Q \left[1 + \frac{P}{100}(n-1)\right]. \tag{3.2}$$

More recent models, starting from a more precise classification into several categories (adding also a motorcycle flow, say M), improve the accuracy of predictions. The A, b and C coefficients may be derived, for a fixed investigated area, by linear regression methods on many L_{eq} data measured at different traffic flows (Q, P) and distances (d). The acoustical equivalent, n, can be estimated both by regression method both by single vehicle emission measurements.
The general formula 3.1 can be easily adjusted by means of particular corrective addends, related to average velocity, kind of road (height gradient, asphalt, etc.), weather and traffic conditions, barriers and buildings existence etc.
The idea which led to the development of a new traffic noise model, move from the quite evident limits of the previous cited models. The majority of statistical models, such as the ones derived from formula (3.1), are in fact strongly dependent on the experimental data used for the regression. Therefore those particular parameters are influenced by the given kind of vehicles and the specific typology of flow occurred during the data taking, losing the correct generality. This feature is quite evident if one plots the equivalent noise level obtained according to different TNMs versus vehicles flow (Figure

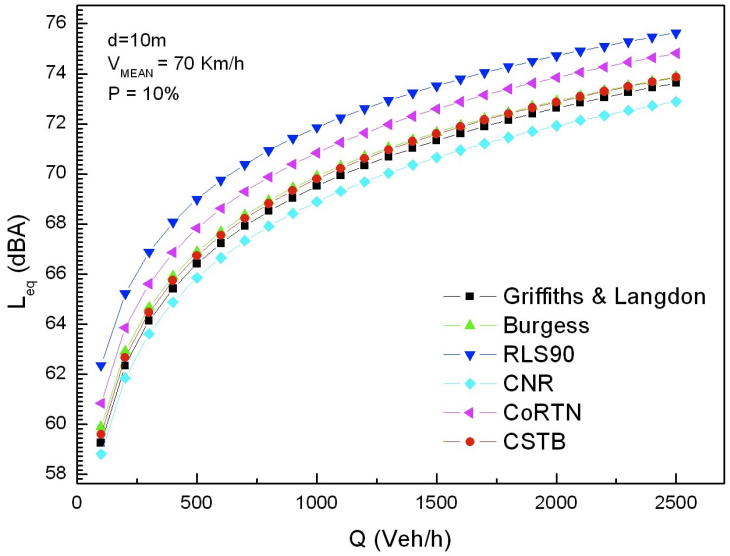

Figure 3.1: Comparison between L_{eq} prediction of different TNMs [11, 12, 14, 19, 17, 15, 16] in a standard situation with mixed flow composition (P = 10 %) at the distance d = 10 m and mean speed 70 Km/h.

3.1). From this graph one can easily notice that the spread of the different models results is quite large (about 4 dBA). This can be explained by the differences between data on which the evaluation of the models parameters has been made. A so evident dependance gives strong motivations to the development of a model which do not involve parameters that must be experimentally evaluated.
Moreover the TNMs assume a flat speed distribution and an unique emission value for all the vehicles in a chosen category, while, as will be shown in section 3 and 4, this two features strongly influence the amount of energy collected by the receiver and so the equivalent acoustical level. So, even if they are suitable for many prediction tasks, because their results are fully compatible with some common practical requests, a more efficient and realistic model must be designed for modeling not ordinary situations, and this is the main aim of this work.

3.1 Single vehicle noise emission

Knowledge of a single vehicle noise emission can be the first important step for a mathematical approach to the traffic noise prediction. Noise coming from a vehicle is originated from different sources since the vehicle is a complex system, in which many contributions are present (engine, transmission system, tyre rolling, aerodynamic, exhaust system, etc.). Thus the correct way to obtain the overall vehicle power level is to perform an energy sum $\oplus$ of these levels expressed in dB:

$$L_W = L_{Engine} \oplus L_{Rolling} \oplus L_{Exhaust} \oplus ... \tag{3.3}$$

Each of these contributions is preponderant in some particular conditions. For example, engine noise is preponderant at low velocity and high rpm, while for a vehicle running at constant speed, the engine load noise is negligible. In addition, in [38], Lelong et al. show that the effect of small accelerations on noise emitted by vehicle is negligible in comparison to the noise levels measured when the same vehicle is running at constant speed. Thus, in the simplest picture, is reasonable to assume that the two main noise sources of a vehicle running at constant speed are the mechanically originated noise (engine, exhaust system) and the rolling one (tyre-road contact noise). Such an assumption brings to the following assumption for the energy budget

$$L_W = L_{Engine}(s, gear) \oplus L_{Rolling}(v), \tag{3.4}$$

where s is the engine speed (rpm) which is related to the vehicle velocity v by the relation $s_i(v) = \frac{1000\, v}{\tau_i}$, with τ_i the transmission ratio when the gear i is engaged. The technical data sheets provided by the cars manufacturers give the value of τ_i for each gear i. An accurate study of difference between L_{Engine} and $L_{Rolling}$ can be found in [39] while the power source as a function of vehicle speed $L_W(v)$ is reported in figure 3.2 for different driving condition. In particular for a light vehicle we perform a fit of the experimental data to get an analytical expression of $L_W(v)$. Considering two velocity regimes: cruising/decelerating and accelerating. In the first case we find

$$L_W(v) = \begin{cases} \alpha + \beta \log v & \text{for } v > 11.5 Km/h\,, \\ 82 & \text{for } v < 11.5 Km/h\,, \end{cases} \tag{3.5}$$

with $\alpha = 53.6 \pm 0.3$ dBA and $\beta = 26.8 \pm 0.2$ dBA. In accelerating state, differently, the sound level rises suddenly from zero to a constant value

of $90.5dBA$ until $v \approx 25Km/h$, where it switches to the curve of cruising/decelerating state. Actually, while for light vehicles the noise emission for cruising, decelerating and accelerating state follows approximately the same curve, for heavy vehicles we found three different curves. All these curves show a common behavior, switching from a constant value at low speed to an approximately linear growth at high v. Also in this case the fit of data has been performed and fit errors are bounded between 0.3% and 0.8%.

$$L_W^{cru}(v) = \begin{cases} 100.6 + 0.089\, v & \text{for } v > 21Km/h\,, \\ 102.5 & \text{for } v < 21Km/h\,, \end{cases} \tag{3.6}$$

$$L_W^{acc}(v) = \begin{cases} 103.0 + 0.069\, v & \text{for } v > 20.5Km/h\,, \\ 104.5 & \text{for } v < 20.5Km/h\,, \end{cases} \tag{3.7}$$

$$L_W^{dec}(v) = \begin{cases} 91 + 0.20\, v & \text{for } v > 18Km/h\,, \\ 94.5 & \text{for } v < 18Km/h\,, \end{cases} \tag{3.8}$$

After the power source characterization we must consider the noise propagation to the receiver. Depending on the geometry of the problem, the source can be considered pointlike or linear, with a consequent difference in the sound level propagation. In particular, a common assumption is to consider the traffic flow as a linear source, while a single vehicle could be approached in a pointlike source approximation. In order to perform an accurate noise prediction, the noise emission of a single transit has been measured for each of the three relevant vehicles categories: light, heavy and motorcycles. The data have been taken in the same condition for the three vehicles and preventing the contamination of the pass-by vehicle noise from other vehicles and external sources, with a first class noise meter as required by the current international directive CEI 29-1 and by the art. 2 of Italian D.L. 16/03/1998. The obtained data have been fitted with the well know pointlike source formula

$$L_I(t) = L_W - 20 \log r(t) - 11, \tag{3.9}$$

where, according to the geometry shown in figure 3.3 we have:

$$r(t) = \sqrt{d^2 + \left(\frac{S}{2} - v\, t\right)^2}, \tag{3.10}$$

for a vehicle running at constant speed, and

$$r(t) = \sqrt{d^2 + \left(\frac{S}{2} - \frac{1}{2}at^2 - v_0\, t\right)^2}, \tag{3.11}$$

for a vehicle with constant acceleration a and initial speed v_0, with S the road length. In particular the power source level L_W has been obtained from the peak level (i.e. the level in front of the receiver) measured at the distance $d = 15$ m. Despite of a good agreement around the peak, the simulated curve deviate from experimental data in the region far from the receiver. A better agreement is found when the vectorial nature of the acoustical sound field is taken into account. The receiver, in fact, is able to detect mostly the component of the field orthogonal to the running path, because of its acceptance radius. Thus, if we make the projection of the sound level on the receiver direction, we find:

$$L_I(t)_\perp = 10 \log(\frac{I}{I_0} \cos\theta), \tag{3.12}$$

where $\theta(t)$ is the angle between the receiver direction and the propagation radius (see fig. 3.3). In particular being $\cos\theta = \frac{d}{r}$ we obtain a modified expression of eq. 3.9 that reads:

$$L_I(t) = L_W - 30\, \log r(t) + 10\, \log d - 11. \tag{3.13}$$

According to this formula, the simulated emission curves are generated and then compared with the experimental data, as shown in figure 3.4,3.5 and 3.6. Once the sound level is obtained we can evaluate the Single Event Level (in the following SEL) for each vehicle by the following well known expression

$$SEL = 10 \log \frac{1}{t_0} \int_{t_1}^{t_2} \tilde{p}^2\, dt = 10 \log \frac{1}{t_0} \int_{t_1}^{t_2} 10^{\frac{L_I(t)}{10}}\, dt, \tag{3.14}$$

with $t_0 = 1s$ and $\tilde{p}^2 = \frac{p^2}{p_0^2}$. For our aims the integration time has been chosen ($t_1 = -10$ s, $t_2 = +10$s), since the most of significant area under curve $10^{0.1\, L_I(t)}$ is comprised in the region around the peak. Let us remark that the SEL level, in particular, is a measure of the acoustical energy emitted by the source and, as we will see in the next section, can be put into a correspondence with the equivalent continuous sound pressure level.

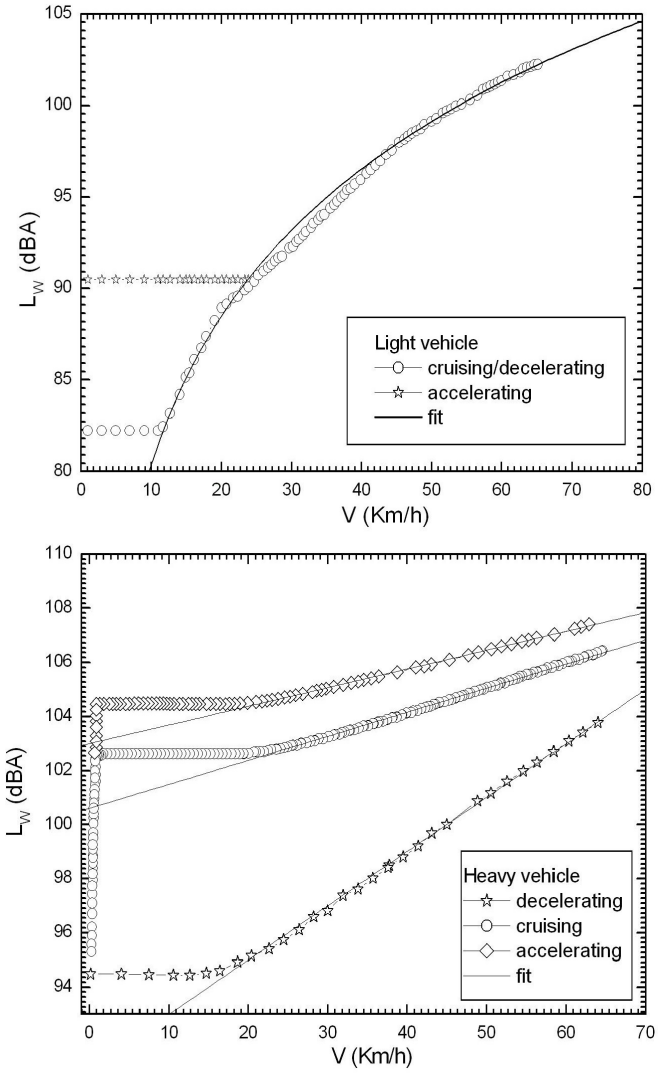

Figure 3.2: Speed dependence of light(upper) and heavy(lower) vehicle for different velocity and driving state [40]. The straight line represent the fit of experimental data (see text).

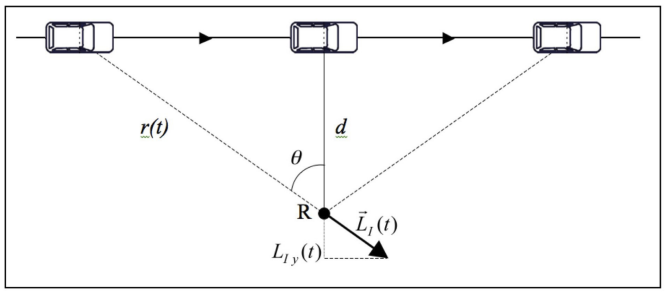

Figure 3.3: Geometry for noise calculation.

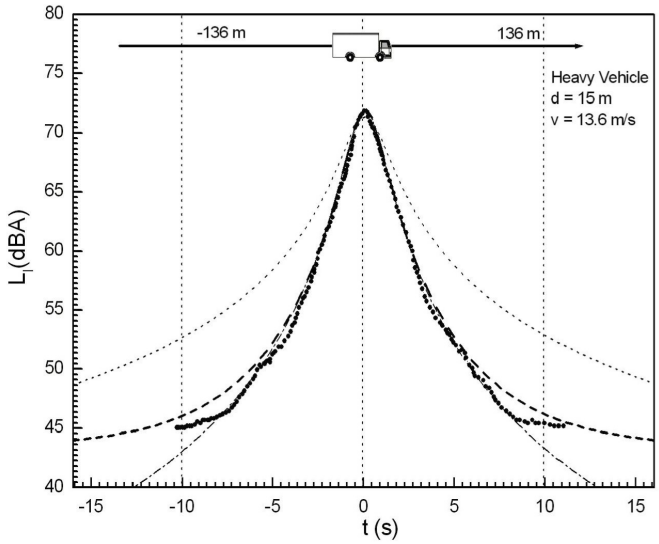

Figure 3.4: Noise emission of single transits of a light vehicle running at v=15.3 m/s at a vertical distance $d = 15m$ from the receiver. The arrow indicated the vehicles direction. The dotted curve is the simulation with eq. 3.9. The dot-dashed one is the projected level (eq. 3.13, while the dashed curve is given by the dot-dashed one plus a constant background noise level.

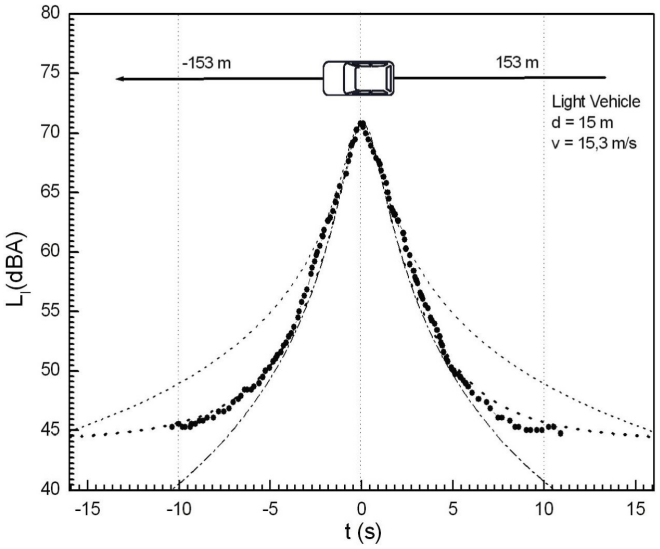

Figure 3.5: Noise emission of single transits of a heavy vehicle running at v=13.6 m/s at a vertical distance $d = 15m$ from the receiver. The arrow indicated the vehicles direction. The dotted curve is the simulation with eq. 3.9. The dot-dashed one is the projected level (eq. 3.13, while the dashed curve is given by the dot-dashed one plus a constant background noise level.

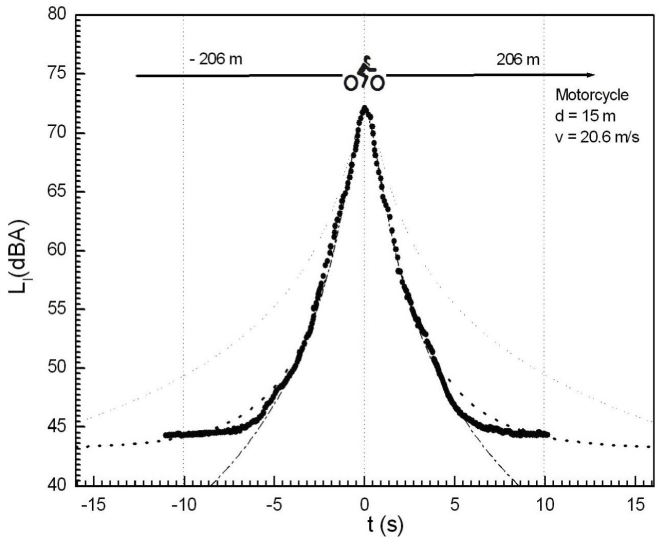

Figure 3.6: Noise emission of single transits of a motorcycle running at v=20.6 m/s at a vertical distance $d = 15m$ from the receiver. The arrow indicated the vehicles direction. The dotted curve is the simulation with eq. 3.9. The dot-dashed one is the projected level (eq. 3.13, while the dashed curve is given by the dot-dashed one plus a constant background noise level.

In the last part of this section we want to also recall an equivalent formulation of single vehicle sources one can found in the literature. In particular we refer toImagine/Harmonoise project developed by the European Community [50]. The goal of the Imagine project is to define a method to generate noise maps that contains the noise levels of road and rail traffic, aircraft and industrial noise, to identify problem areas and to evaluate noise action plans. For road noise, these noise levels are calculated using a vehicle noise source model represented by two pointlike sources. In particular, for the given reference condition, the sound power L_W of a vehicle from each of the main vehicle categories is a sum of rolling noise and propulsion noise. The sound level of the rolling noise L_{WR} is calculated by

$$L_{WR} = a_R(f) + b_R(f) \log\left(\frac{v}{v_{ref}}\right); \tag{3.15}$$

where v is the vehicle driving speed, $v_{ref} = 70$ Km/h is the reference speed and the coefficients a_R and b_R are given for each 1/3-octave band frequency f from 25 to 10000 Hz. The values for heavy vehicles can be found by adding $10\log(n_A/2)$ with n_A number of axes of the vehicle. The rolling noise is assumed to be distributed over two point sources, where 80% of the sound power is radiated by a point source at 0,01 m above the road surface and the remaining 20% is radiated by a second point source which is assumed to be located at 0,3 m height for light vehicles, and at 0,75 m for heavy one (see figure 3.7). For propulsion noise, the sound power level L_{WP} is given by

$$L_{WP} = a_P(f) + b_P(f) \log\left(\frac{v - v_{ref}}{v_{ref}}\right); \tag{3.16}$$

where the coefficients a_P and b_P are also given per 1/3-octave frequency band. For propulsion noise, 20% of the sound power is appointed to a point source at 0,01 m height, and 80% is appointed to the second noise source at 0,3 m or 0,75 m for light and heavy vehicles, respectively.

3.2 Flow type and speed distribution

Before starting the description of the proposed model, in this paragraph some general considerations about traffic flow and velocity distribution are given. Flow type is a parameter, complementary to speed, which includes acceleration, deceleration, engine load, and pulsed or continuous traffic motion. This

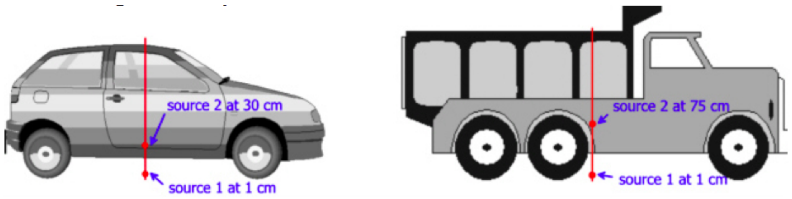

Figure 3.7: Drawing of noise sources position in Imagine/Harmonoise project.

is described by means of categories that are still approximated, but probably sufficient to predict noise levels.

Fluid continuous flow: This is a flow where vehicles move with a nearly constant velocity on the road section of interest. It is "fluid" in the sense that the flow is stable both in space and in time for periods of at least ten minutes. Variations during the day may be observed but without abrupt or rhythmic variations. Furthermore, it is neither accelerated nor decelerated but of steady velocity. This flow type corresponds to the traffic of a motorway link or an interurban road, on an urban expressway (outside rush hours), and on major roads in an urban environment, without traffic lights.

Pulsed continuous flow: A pulsed flow has a significant portion of vehicles in a transitory state (i.e. either accelerating or decelerating). It is stable neither in time (i.e. there exist abrupt variations of flow during small time periods) nor in space (i.e. at any given moment in time, irregular concentrations of vehicles exist on the road section of interest). However, it is possible to define an average overall velocity for a pulsed continuous flow of vehicles, which is stable and repetitive for a sufficiently long period of time. This flow type corresponds to that found on city-centre roads, on major roads close to saturation, on dispatching or connecting roads with numerous crossings, in car parks, at pedestrian crossings and at junctions to housings.

Pulsed accelerated flow: This is a pulsed flow with a great portion of all vehicles in accelerating state, which means that the notion of speed has a meaning only in discrete and local points as it is not stable during displacement. This is typically the case of traffic either on an expressways after a crossing, or at a motorway slip road, at a tollbooth, etc.

Pulsed decelerated flow: This is the opposite of the previous one, in which a significant portion of vehicles is decelerating. It is generally found on the approach of major urban crossings, on motorway or expressway exits or on the approach to a tollbooth, etc.

Speed of vehicles is the second fundamental parameter that must be considered modeling the traffic noise. Vehicles with different speeds, in fact, send to the receiver a different amount of acoustical energy, that can be directly related to the SEL value, so the equivalent level at the receiver strongly depends on the speed distribution associated to the road. The development of mathematical tools focused on the modeling of the speed distribution in a traffic flow is widely reported in the scientific literature [41, 42, 43, 44]. Many papers, in fact, consider this problem since vehicles speed distribution is an important input parameter also in other issues, such as kinematical traffic simulation model, road design, speed limit evaluation, air pollution prediction, etc.. In this section, we focus on the different probability distributions that can be chosen for vehicles speed, depending on the traffic flow conditions, postponing the integration with a dynamical traffic model to next chapters. Thus, the chosen distributions are implemented in a computing framework in order to randomly generate speeds to be used for the evaluation of the SEL of each vehicle transiting. In this way, the stochastic core of the traffic phenomena is implemented and reproduced in a new traffic noise model. Moreover the comparison between different distributions could be performed, related to the effective noise experienced in different traffic flow conditions.
The study of the speed distribution on a given road can be approached by means of frequency distribution or cumulative frequency distribution curves. When probability density is plotted, it may exhibit one or more modes, as, for example, shown in figure 3.8. These speed distributions are called unimodal or multimodal speed distributions, respectively. The nature of the speed distribution curve is described by various parameters signifying the central tendency, the spread, the skewness, the peakedness, and the uniformity. These parameters provide statistical properties of the speed distribution curve. However, some of them are purely arbitrary.
In general, with almost homogeneous traffic conditions, the speed of vehicles on a straight road follow a normal distribution [45, 46, 47, 48] as

$$P_G(v;x,t) = \frac{1}{\sqrt{2\pi\Theta(x,t)}} \exp\left(\frac{(v-V(x,t))^2}{2\Theta(x,t)}\right), \tag{3.17}$$

where $V(x,t) = \langle v \rangle$ denotes the average velocity and $\Theta(x,t) = \langle (v - V(x,t))^2 \rangle$

represents the velocity variance. This assumption is supported by many experimental works, that give also an estimation of the standard deviation of the distribution. In particular the mean value and the variance of velocity distribution, for a certain kind of road, will be clearly determined by the traffic conditions. In particular for the fluid continuous flow, vehicles are neither accelerated or decelerated but move with an almost steady velocity, so one can expect a small value of variance. For pulsed continuous flow, instead, one can expect a greater value of variance. At this stage, according to many data present in the scientific literature [51, 52, 53, 54, 55], one can assume that the standard deviation generally ranges from 1.4 m/s (5 Km/h) and 5.6 m/s (20 Km/h).
If the traffic conditions are not homogeneous, the normal distribution is not well suitable anymore. Haight and Mosher [52], for example, considered that the time speeds could be well represented by either a gamma or a log-normal distribution.
The conditions to turn to a different speed distribution is quite often realized in non-highway or urban roads, where, in general, the traffic stream is much more complicated, mainly because of the different composition. In fact, in such a road, one can find both fast vehicles (cars, motorbikes, light trucks, etc.) and slow ones (bicycles, animal drawn vehicles, heavy trucks, light scooters, buses, etc.). This large spread of typology, together with other parameters such as the presence of traffic lights and the road surface conditions, leads to a significant deviation of the speed distribution curve from the generally accepted single modal normal distribution. A better approximation in a mixed traffic condition could be a bimodal or a multimodal distribution, as referred in [44]. In this paper Dey et al., introduce the spread ratio (SR), defined as the ratio of the difference between percentile levels $SR = \frac{V_{85}-V_{50}}{V_{50}-V_{15}}$. This parameter is able to estimate the modality of speed distribution and results to be strongly correlated with the shape of the cumulative speed distribution curve. Starting from a fit of experimental data taken in India, the authors affirm that speed data follow the unimodal curve only when the spread ratio is in the range of 0.69-1.35.
In this paper the authors take into account the role of different speed distributions in the evaluation of the equivalent continuous sound pressure level. Since the best approximation for homogeneous conditions is a normal distribution, one can think to simulate a more general situation by means of a bimodal distribution obtained by the overlap of two different gaussian distributions, for example one related to heavy vehicles and the other related to

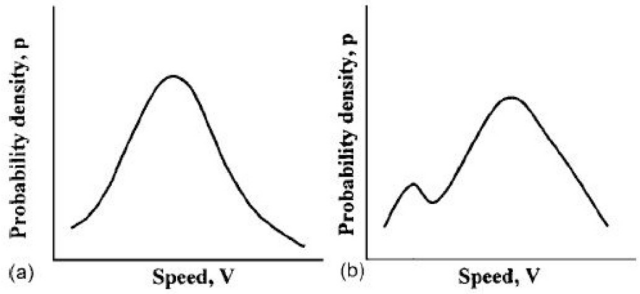

Figure 3.8: Probability density curves: a) unimodal distribution; b) bimodal distribution

light vehicles, generally faster than the heavy ones. A practical example is reported in figure 3.9, where the results of random speed generation for 3000 light vehicles and 600 heavy vehicles is shown. In particular, the two set of speeds are generated according to two gaussian distributions with mean respectively of 80 Km/h and 50 Km/h and $\sigma = 10$ Km/h. In the graph are also shown, as a guide to the eye, the gaussian behavior of the two starting distribution (dotted and dashed line) and the overall distribution (solid line). The bimodality is also evident looking at the cumulative distribution in the insert that, as referred in [44], shows two different slopes in a double log scale.

3.3 Model presentation

The idea which led to the development of a new traffic noise model move from the attempt to overcome some limits of the previous cited models. As widely discussed, the most relevant simplifications of the current models are mainly two: the use of an average speed and the unique emission value for all the vehicles in a chosen category. Concerning the first topic, we already largely explained that the speed distribution cannot be considered flat and that the assumption of an average speed is really restricting. This issue is very important because, as shown in section 4, the vehicle emission is strictly bounded to its speed. Regarding the second point, one had to consider that all the vehicles belonging to the same category (light vehicles, heavy vehicles, motorcycles) do not emit the same amount of acoustical energy/noise, also if

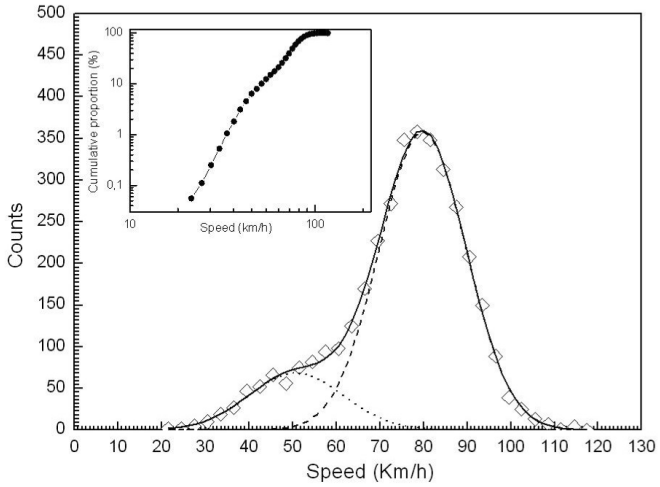

Figure 3.9: Bimodal speed distribution obtained from the random generation of speed of 3000 light vehicles and 600 heavy vehicles. The two set of speeds are generated according to two Gaussian distribution with mean respectively of 80 Km/h and 50 Km/h and $\sigma = 10$ Km/h. In the insert is also shown the overall cumulative distribution function in double log scale.

running at the same speed. Moreover many parameters should be taken into account, such as mechanical conditions of the vehicle, driver skills, power and capacity of the vehicle, fuel type, etc, which can heavily influence the emission of noise in term of peak level and frequency spectrum. Thus, random terms must be introduced to keep into account the intrinsic stochastic nature of the traffic composition. All of these considerations, together with the idea of developing a model more adherent to the reality, brought us to the development of GERIAN2009 model that stays for: Gaussian Equivalent Road Impact Acoustical Noise.

3.3.1 General consideration

The flow chart relative to GERIAN2009 is reported in Figure 3.10. The model starts taking four different type of data as input. First of all the traffic data are considered by means of hourly traffic flow of light, heavy and motorcycles, mean speed and flow type. Then geometrical parameters, such as the receiver distance and height, road data such pavement, dimensions, number of lane and slope, are considered. Finally the statistical data related

to the power source emission for any vehicle's category are collected. After the data input, following the flow chart in fig. 3.10, one arrives to the central core of our model. The principal and new ingredient of such a method is given, in fact, by its random intrinsic kernel. The traffic process, which is intrinsically stochastic, is therefore modeled by a random approach, in order to obtain a result more adherent to reality. For each vehicle, in fact, a random velocity is generated according to a Gaussian distribution (see before). The mean value and the variance of velocity distribution for a certain kind of road is clearly determined by the traffic conditions. In particular, for the fluid continuous flow, vehicles are neither accelerated or decelerated but move with a steady speed, so we expect a small value of variance. For pulsed continuous flow, instead, we expect a greater value of variance. Either in fluid continuous flow or pulsed accelerated one, suitable values for the variance can be easily obtained through a preliminary study of all the parameters that can influence the spread of the velocity distribution. In the same way for pulsed accelerated and decelerated flow, one can assume a random initial velocity v_0 according to a Gaussian distribution and use a mean acceleration (deceleration) value a estimated for each the particular road section. Looking at the scientific literature [51, 52, 53, 54, 55], we found that the standard deviation is generally bounded between 2,8 m/s (10 Km/h) for a fluid continuous flow and 5.6 m/s (20 Km/h) for a pulsed continuous one.
The power source for each vehicle is then evaluated starting from its speed by the means of expressions (3.5) for light vehicles and (3.6),(3.7),(3.8) for heavy truck and motorcycle. In particular we choose to use cruising curve for fluid continuos and pulsed continuos flow, and the accelerated (decelerated) $L_W(v)$ for pulsed accelerated (decelerated) flow. In addition, to take into account the presence of stochastic parameters such as driving conditions and skills, vehicles mechanics and maintenance, different vehicle model etc., we correct the previous expressions with a stochastic additive term. This is obtained choosing a gaussian correction with mean zero and unitary variance. The Gaussian hypothesis is supported by the analysis of a set of experimental data [57] (merged with the data coming from many vehicles datasheets) which show the distribution of noise emission at $d = 7.5$ m for many commercial vehicle of different companies. As it can be seen from data reported in figure 3.11, noise levels distribution ranges from 66 dBA to 74 dBA, with a mean value of 70 dBA and a standard deviation of 1 dBA and follows a gaussian like shape. This methodology considers the intrinsic stochastic feature of the traffic phenomenon, and it allows us to take into account the

different energy emission of vehicles also inside the same category such as those due to older vehicles which are in worst conditions of maintenance, to low skill in driving (high rpm engine regime), horn sounds, etc..

3.3.2 L_{eq} calculation

The next step of our scheme, as suggested by the flow chart of figure 3.10, is to evaluate a physical observable in order to implement our approach in the framework of a measurable acoustical quantity. Thus, let us evaluate the noise propagation from each vehicles to the receiver, i.e. $L_I(t)$ signal. In order to obtain such a quantity, a geometrical approach is adopted by means of expression (3.13) as described in the previous section. Once the sound pressure level is obtained, the SEL can be evaluated for each vehicle according to expression (3.14), with an additive term L_R due to the background noise (see figure 3.4,3.5,3.6 in section 4). Starting from the SEL level of each vehicle, the hourly equivalent continuous sound pressure level L_{eq} can be easily obtained. In particular the equivalent noise level is defined by

$$L_{eq} = 10 \log \frac{1}{\Delta t} \int_{t_1}^{t_2} \tilde{p}^2 \, dt, \tag{3.18}$$

with $\Delta t = t_2 - t_1$. Considering $k = L, H, M$ for light, heavy and motorcycle respectively, we can write

$$10 \log \int_{t_1}^{t_2} \sum_k \left(\sum_{j=1}^{N_k} \tilde{p}^2 \right) dt = 10 \log \sum_k \sum_{j=1}^{N_k} \int_{t_1}^{t_2} \tilde{p}^2 \, dt = 10 \log \sum_k \sum_{j=1}^{N_k} 10^{\frac{SEL_j}{10}} \tag{3.19}$$

where N_k in the number of vehicles belonging to the k-esim category. Multiplying and dividing for Δt, one can relate L_{eq} to SELs:

$$\begin{aligned} L_{eq} = 10 \log \frac{1}{\Delta t} + 10 \log (& \sum_{i=1}^{N_L} 10^{0.1 SEL_i^{light}} + \\ & + \sum_{i=1}^{N_H} 10^{0.1 SEL_i^{heavy}} + \sum_{i=1}^{N_M} 10^{0.1 SEL_i^{mcycle}}), \end{aligned}$$

where N_L,N_H and N_M are the number of light, heavy and motorcycle vehicles respectively and $\Delta t = 1h = 3600$. This procedure has been described for a single-lane road. For a multi-lane configuration one must apply the same

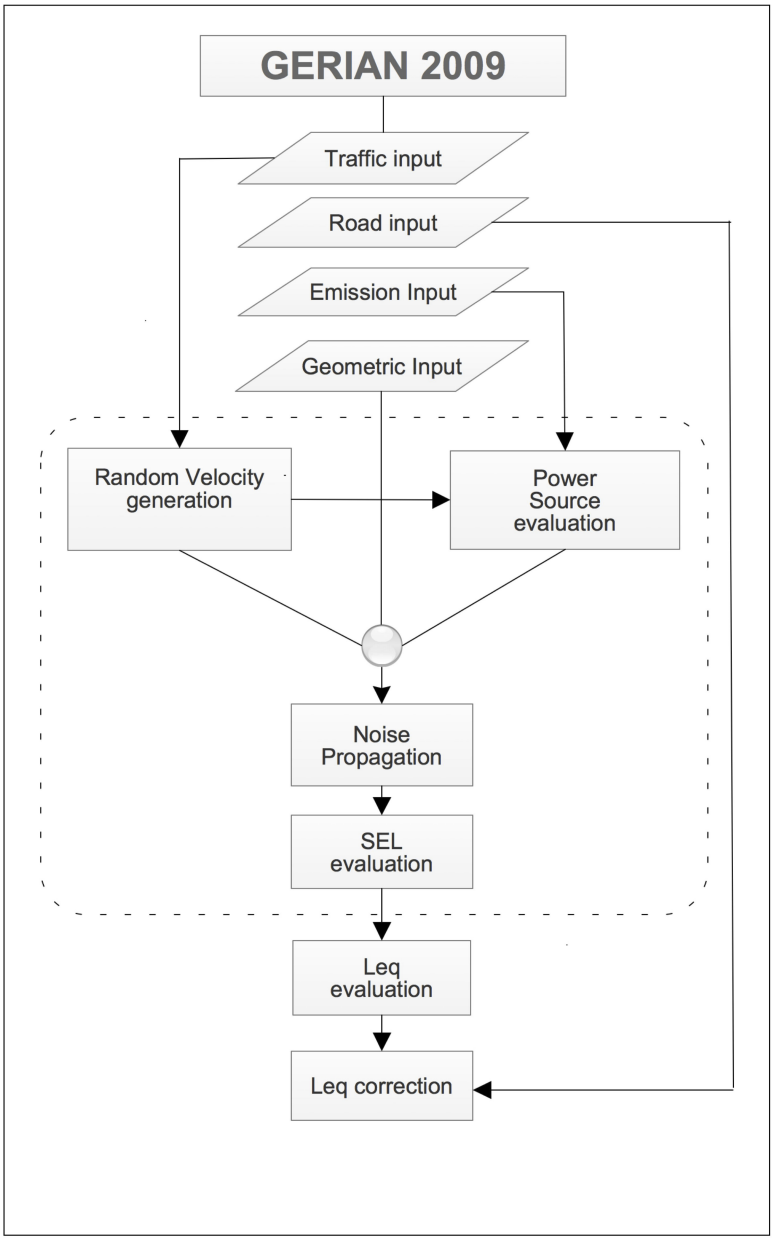

Figure 3.10: Flow chart for Gerian2009. The dashed line denote a loop on each vehicle for the three category.

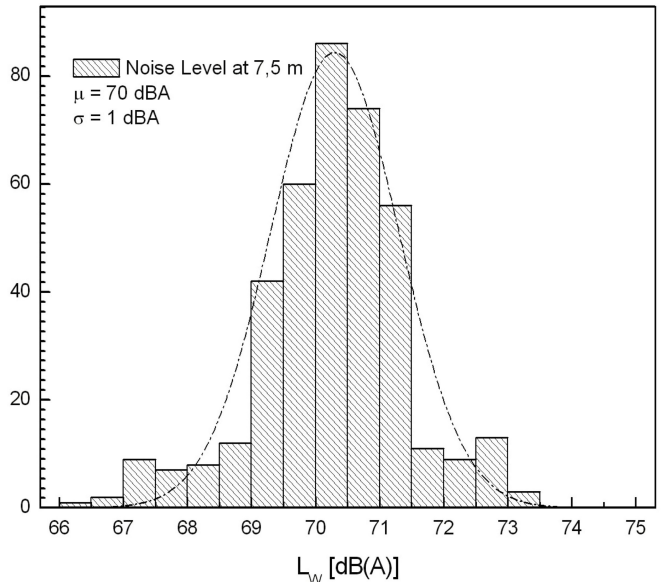

Figure 3.11: Noise level distribution at 7,5 m for 398 light vehicles of 33 different company with different engine capacity and fuel type. The dashed line is just a guide to the eye to put in evidence the gaussian-like behavior. Similar graph are obtained for heavy vehicles and motorcycles.

procedure for each of n-esim lane (both forward and backward direction) getting to N equivalent level L_{eq_n}. The equivalent continuous sound pressure level is then calculated by the energetic-sum over n-index.

3.3.3 Noise level correction

The last step of our procedure concerns the correction of noise level by means of different terms compatible with the international ISO-9613.
The first term we analyze is the correction due to the road's surface. Above a certain speed the overall noise emitted by a vehicle is dominated by the noise produced at the road-tyre contact points tha typically depends on road surface. The road surface corrections used in the model here are compatible with EN ISO 11819-1 [56] (see table 1). In particular we can distingue:

- *Porous Surface*: is a surface with a void volume of at least 20% . The surface has to be less than 5 years old. The age restriction accounts for the tendency of porous surfaces to become less absorptive over time as the voids fill up. If special maintenance is applied, the age restriction may be lifted.

- *Smooth asphalt (concrete or mastic)*: is the reference road surface defined in EN ISO 11819-1. It is a dense, smooth-textured, either concrete or stone-mastic asphalt surface, with a maximum chipping size of 11 - 16 mm.

- *Cement Concrete and corrugated asphalt*: includes both the cement concrete and coarse texture asphalt.

- *Smooth texture paving stones*: paving stones with a distance smaller than 5 mm between the blocks.

- *Rough texture paving stones*: paving stones with a distance greater than or equal to 5 mm between the blocks.

A second correction we introduce is due to the road's gradient greater than 5%. In particular the correction ΔL_{slope} is +0.6 dBA for each % gradient over 5%.
The last correction we consider is due to the presence of wind. In particular the corrective value ΔL_{wind} depends on wind velocity U_w and by the angle θ between wind direction and source-receiver distance as

Road surface	Correction
Porous $\bar{v} = 0 - 60$ Km/h	-1 dBA
Porous $\bar{v} = 61 - 80$ Km/h	-2 dBA
Porous $\bar{v} = 81 - 130$ Km/h	-3 dBA
Smooth asphalt	0 dBA
Cement Concrete	+ 2 dBA
Smooth texture	+ 3 dBA
Rough texture	+ 6 dBA

Table 3.1: Noise level correction $\Delta L_{surface}$ for different road pavement.

$$\Delta L_{wind} = -0.88 \log_{10}\left(\frac{d}{15}\right) U_w \cos\theta. \tag{3.20}$$

For the intrinsic structure of the methods, other additive correction factor (such that for air absorption, traffic light, etc.) can be easily implemented following the ISO-9613 suggestions.

3.4 Main results

In this section, we briefly report the main results obtained implementing the procedure introduced above in the framework of Wolfram Mathematica^{TM}. The first remarkable result is shown in Figure 3.12, where the L_{eq} vs Q simulated by GERIAN is plotted, for different V_{mean} and $\sigma = 10$ Km/h. As we can note the logarithmic behavior, forced by all the previous cited statistical TNMs, is obtained without any preliminary assumption. Thus the macro behavior is induced by a microscopical approach, i.e. the single vehicle emission and random velocity approach. In some sense, this result gives a further validation to the statistical models, since it ensures that the logarithmical dependance of the equivalent level from the vehicles flow, that the TNMs introduce by hand, is well suited. Moreover the simulation gives another remarkable result, that is the dependance of the equivalent noise level from the mean velocity of traffic flow shown in Figure 3.13. As it was foreseen, the equivalent level grows with the velocity, and the slope is almost linear. This result can be compared with the additive correction implemented in some models, such as the italian CNR [19], and obtained with a strong experimental effort. This correction is in quite perfect agreement with our

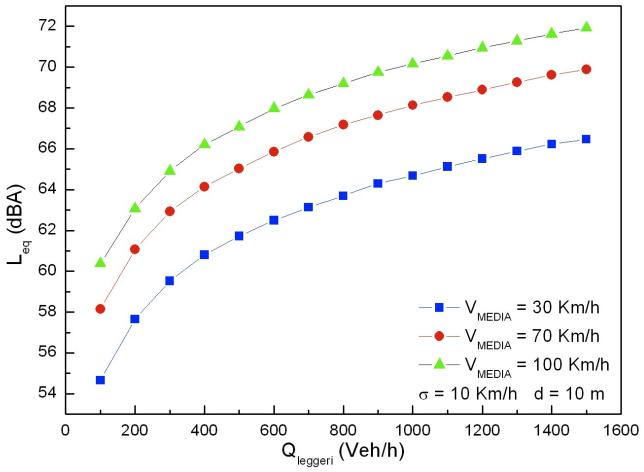

Figure 3.12: Equivalent noise level L_{eq} versus traffic flow Q, for different values of flow mean velocity V_{mean} and fixed standard deviation σ.

results, since it assumes a reference speed between 30 and 50 km/h and, for example, it adds 3 dB if the velocity is 80 Km/h, which is very similar with the results shown inFigure 3.13.

3.5 Comparison with experimental data

In order to validate the model, an experimental session has been performed and the resulting set of data has been compared with the correspondent values simulated with GERIAN. The data have been taken on an extraurban road in fluid continuos flow condition, with a first class noise meter, as required by the current international directive CEI 29-1 and by the art. 2 of Italian D.L. 16/03/1998. The mean speed of about 60 Km/h has been measured with a stopwatch and markers. A further comparison has been performed with other experimental data taken from literature referring to different peculiar mixed traffic situations, so that an unbiased test can be done. In particular, data from [58] refer to an urban highway while [59] and [60] refers to a low speed urban road. In Figure 3.15 the simulated equivalent levels are plotted versus the measured ones. The solid line is the bisector and the dashed lines correspond to $\pm$ 2 dBA levels. The level of accordance can be easily estimated looking at the distribution of absolute difference between

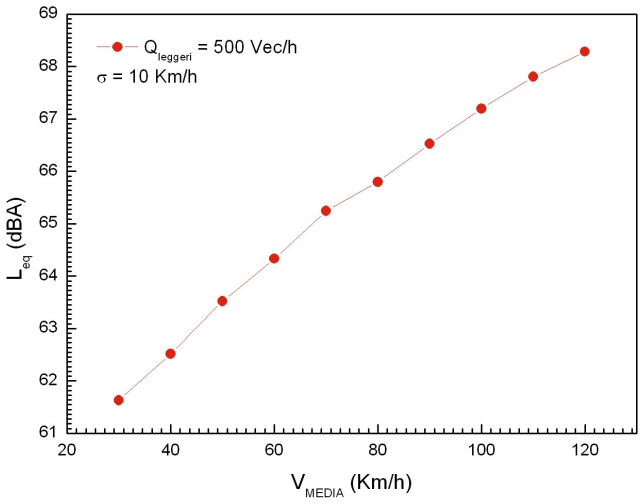

Figure 3.13: Equivalent noise level L_{eq} versus flow mean velocity V_{mean}, with fixed values of traffic volume Q and standard deviation σ.

simulated and measured data. A statistical analysis shows, in fact, a mean value of about 1 dBA, with a standard deviation of 0.66 dBA; in addition the 75-th percentile level is founded to be 1.5 dBA so the majority of data are strictly bounded within a $\pm$ 1.5 dBA interval around the axes bisector. As a further proof of the correct working of our model, we performed the fit of the experimental data with formula 3.1 to evaluate the parameters (A, b, C), comparing the result of this procedure with GERIAN curve for a standard mixed traffic situation with $P = 10\%$. As we can note from figure 3.14 there is a quite perfect agreement between results from the two models, even though in our approach no experimental measurements were needed, with a consequent strong gain in simpleness and time of prediction.

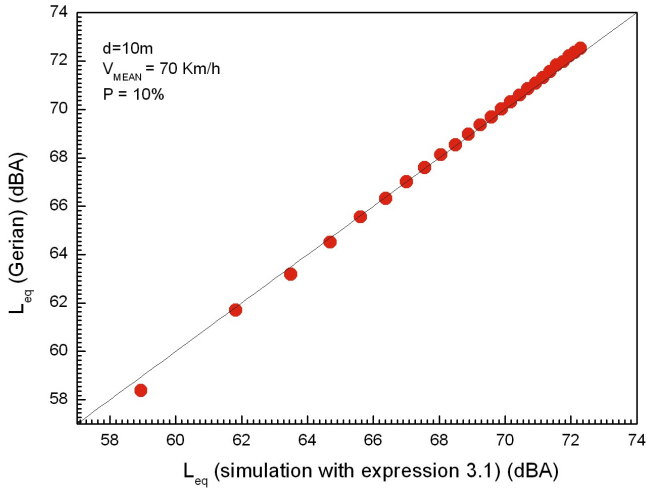

Figure 3.14: Comparison between results of formula 3.1 and GERIAN2009 for a standard mixed traffic situation with $P = 10\%$.

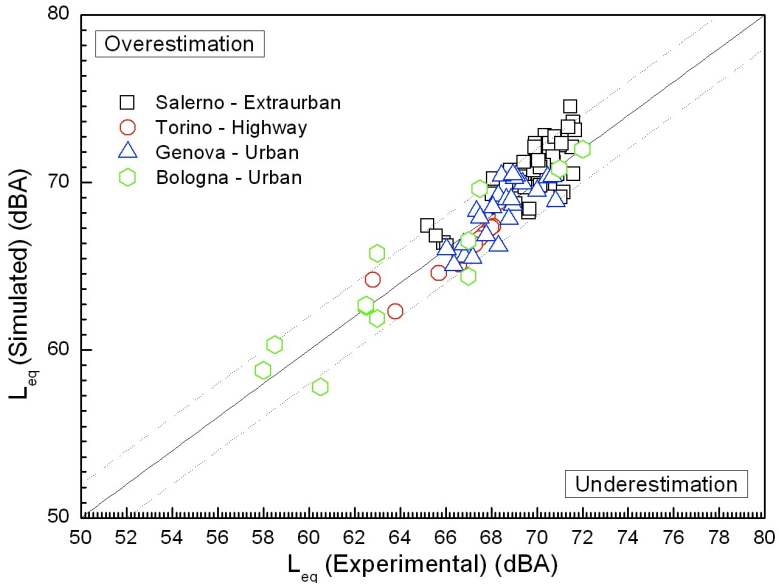

Figure 3.15: Simulated equivalent noise level L_{eq}^{SIM} versus experimental equivalent noise level L_{eq}^{EXP} for different set of data. The solid line is the axes bisector and the dashed lines correspond to $\pm$ 2 dBA levels. Literature data have been taken from [58, 59, 60].

Chapter 4

The Physics of Road Traffic and Transportation

4.1 A brief history of traffic flow theory

Historically, traffic physics got its roots as a rather practical discipline, entailing most of the time a common sense of its practitioners to solve particular traffic problems. However, all this changed at the dawn of the 1950s, when the scientific field began to mature, attracting scholar from all sorts of trades. Most notably, John Glen Wardrop instigated the evolving discipline now known as traffic flow theory, by describing traffic flows using mathematical and statistical ideas [61].

Two examples of the progress during this decade, include the fluid-dynamic model of Michael James Lighthill, Gerald Beresford Whitham, and Paul Richards (or the *LWR model* for short) for describing traffic flows [62, 63], and the car-following experiments and theories of the group of people working at General Motors' research laboratory [64, 65, 66, 67].

In spite of the intense booming during the 1950s and 1960s, all progress seemingly came to sudden stop, as there were almost no significant results for the next two decades.

At the beginning of the 1990s, researchers found a revived interest in the field of traffic flow modelling. On the one hand, researchers' interests got kindled again by the appealing simplicity of the LWR model, whereas on the other hand one of the main boosts came from the world of statistical physics. In this latter framework, physicists tried to model many particle

systems using simple and elegant behavioural rules. As an example, the now famous particle hopping (cellular automata) model of Kai Nagel and Michael Schreckenberg [68] still forms a widely-cited basis for current research papers on the subject and will be explained in the next chapter. In parallel, with this kind of modelling approach, many of the old "beliefs" (e.g., the fluid-dynamic approach to traffic flow modelling) started to get questioned. As a consequence, a wide number of models quickly found its way to the transportation community, whereby most of these models didn't give a thought as to whether or not their associated phenomena corresponded to real-life traffic observations.
Nowadays, the research and application of traffic flow theory and intelligent transportation systems continues. The scientific field has been largely diversified, encompassing a broad range of aspects related to sociology, psychology, environment, economy, etc.

4.2 Microscopic traffic flow characteristics

Road traffic flows are composed of drivers associated with individual vehicles, each of them having their own characteristics. These characteristics are called *microscopic* when a traffic flow is considered as being composed of such a stream of vehicles. If instead we now zoom out to a more aggregate level (traffic streams are regarded e.g., as a fluid) we refer to a *macroscopic* model. In this dissertation we mainly focus on microscopic models that, in our opnion, are more suitable for noise prediction.
The dynamical aspects of these traffic flows (i. e. microscopic) are formed by the underlying interactions between the drivers of the vehicles. This is largely determined by the behaviour of each driver, as well as the physical characteristics of the vehicles.
Because the process of participating in a traffic flow is heavily based on the behavioural aspects associated with human drivers, it would seem important to include these human factors into the modelling equations. However, this leads to a severe increase in complexity, which is not always a desired artifact.
Considering individual vehicles, we can say that each vehicle i in a lane of a traffic stream has the following informational variables:

- a *length*, denoted by l_i,

- a *longitudinal position*, denoted by x_i,
- a *speed*, denoted by $v_i = \dfrac{dx_i}{dt}$,
- and an *acceleration*, denoted by $a_i = \frac{d^2x_i}{dt^2}$

Note that the position x_i of a vehicle is typically taken to be the position of its rear bumper. In this first approach, a vehicle's other spatial characteristics (i.e., its width, height, and lane number) are neglected. In spite of our narrow focus on the vehicle itself, the above list of variables is also complemented with a driver's *reaction time*, denoted by τ_i.
Referring to 4.1, we can consider two consecutive vehicles in the same lane in a traffic stream: a follower i and its leader $i+1$. From the figure 4.1, it can be seen that vehicle i has a certain *space headway* h_{s_i} to its predecessor (it is expressed in metres), composed of the distance (called the *space gap*) g_{s_i} to this leader and its own *length* l_i:

$$h_{s_i} = g_{s_i} + l_i. \tag{4.1}$$

By taking the rear bumper as a vehicle's position, the space headway $h_{s_i} = x_{i+1} - x_i$. The space gap is thus measured from a vehicle's front bumper to its leader's rear bumper.
Analogously to equation 4.1, each vehicle also has a *time headway* h_{t_i} (expressed in seconds), consisting of a *time gap* g_{t_i} and an *occupancy time* ρ_i:

$$h_{t_i} = g_{t_i} + \rho_i. \tag{4.2}$$

Both space and time headways can be visualised in a *time-space diagram*, such as the one in 4.2. Here, we have shown the two vehicles i and $i+1$ as they are driving. Their positions x_i and x_{i+1} can be plotted with respect to time, tracing out two *vehicle trajectories*. As the time direction is horizontal and the space direction is vertical, the vehicles' respective speeds can be derived by taking the tangents of the trajectories (for simplicity, we have assumed that both vehicles travel at the same constant speed, resulting in parallel linear trajectories). Accelerating vehicles have steep inclining trajectories, whereas those of stopped vehicles are horizontal.

When the vehicle's speed is constant, the time gap is the amount of time necessary to reach the current position of the leader when travelling at the current speed (i.e., it is the elapsed time an observer at a fixed location would

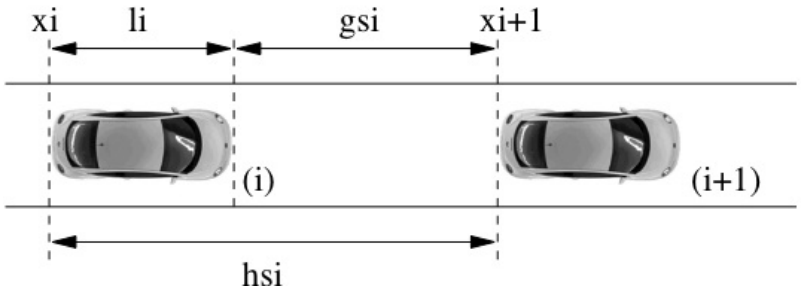

Figure 4.1: Two consecutive vehicles (a follower i at position x_i and a leader $i+1$ at position x_{i+1}) in the same lane in a traffic stream. The follower has a certain space headway h_{s_i} to its leader, equal to the sum of the vehicle's space gap g_{s_i} and its length l_i.

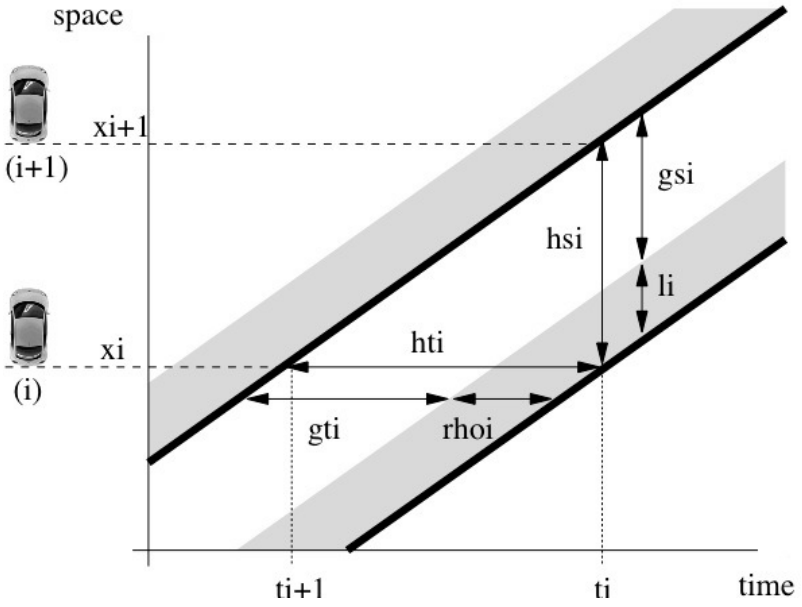

Figure 4.2: A time-space diagram showing two vehicle trajectories i and $i+1$, as well as the space and time headway h_{s_i} and h_{t_i} of vehicle i. Both headways are composed of the space gap g_{s_i} and the vehicle length l_i, and the time gap g_{t_i} and the occupancy time ρ_i, respectively. The time headway can be seen as the difference in time instants between the passing of both vehicles, respectively at t_{i+1} and t_i.

measure between the passing of two consecutive vehicles). Similarly, the occupancy time can be interpreted as the time needed to traverse a distance equal to the vehicle's own length at the current speed, i.e., $\rho_i = l_i/v_i$; this corresponds to the time the vehicle needs to pass the observer's location. Both equations 4.1 and 4.2 are furthermore linked to the vehicle's speed v_i as:

$$\frac{h_{s_i}}{h_{t_i}} = \frac{g_{s_i}}{g_{t_i}} = \frac{l_i}{\rho_i} = v_i. \tag{4.3}$$

As the above definitions deal with what is called single-lane traffic, we can easily extend them to multi-lane traffic. In this case, four extra space gaps related to the vehicles in the neighbouring lanes should be introduced. This topic will be discussed in detail in the following chapter.

4.3 Fundamental Diagrams of traffic flow

Considering a stream of traffic flow, we can distinguish different types of operational characteristics, called regimes or phases, each of them characterised by a certain set of unique properties. In the following sections, we discuss the regimes known as free-flow traffic, capacity- flow traffic, congested, stop-and-go, and jammed traffic. Our discussion of these regimes is based on the commonly adopted way of looking at traffic flows. We conclude the section with a discussion on the correlations between traffic flow characteristics expressed by the fundamental diagrams of traffic flow (TFDs).

4.3.1 Free-flow traffic

Under light traffic conditions, vehicles are able to freely travel at their desired speed. As they are largely unimpeded by other vehicles, drivers strive to attain their own comfortable travelling speed. Crearly drivers have to take into account the maximum allowed speed (denoted by v_{max}), as well as road, engine, and other vehicle characteristics. The free-flow speed (by some called the nominal speed) is the mean speed of all vehicles and is denoted $\overline{v}_{ff}$. Free-flow traffic occurs exclusively at low densities, implying large average space headways. As a result, small local disturbances in the temporal and spatial patterns of the traffic stream have no significant effects, hence traffic flow is stable in the free-flow regime.

4.3.2 Capacity-flow traffic

When the traffic density increases, vehicles are driving closer to each other. Considering the number of vehicles that pass a certain location alongside the road, an observer will notice an increase in the flow. At a certain moment, the flow will reach a maximum value (which is determined by the mean speed of the traffic stream and the current density). This maximum flow is called the capacity flow, denoted by q_c, q_{cap}, or even q_{max}. The average time headway is minimal at capacity-flow traffic, indicating the local formation of tightly packed clusters of vehicles, which are moving at a certain capacity-flow speed v_c or v_{cap}) which is normally a bit lower than the free-flow speed. Note that some of these fast platoons are very unstable when they are composed of tailgating vehicles: whenever in such a string a vehicle slows down a little, it can have a cascading effect, leading to exaggerate braking of following vehicles. Hence, these latter manoeuvres can destroy the local state of capacity-flow, and can in the worst case lead to multiple rear-end collisions. At this point, traffic becomes unstable.

4.3.3 Congested, stop-and-go, and jammed traffic

Considering the regime of capacity-flow traffic, it is reasonable to assume that drivers are more mentally aware and alert in this regime, as they have to adapt their driving style to the smaller space and time headways under high speeds. However, when more vehicles are present, the density is increased even further, allowing a sufficiently large disturbance to take place. For example, a driver with too small space and time headways, will have to brake in order to avoid a collision with the leader directly in front; this can lead to a local chain of reactions that disrupts the traffic stream and triggers a breakdown of the flow. The resulting state of saturated traffic conditions, is called congested traffic. The moderately high density at which this breakdown occurs, is called the critical density, and is denoted by k_c or k_{crit} (for a typical motorway, its value lies around 25 vehicles per kilometre per lane [69]). From this knowledge, we can derive the optimal driving speed for single-lane traffic flows as $v_s = \frac{q_{cap}}{k_{crit}}$.
Higher values for the density indicate almost always a worsening of the traffic conditions; congested traffic can result in stop-and-go traffic, whereby vehicles encounter so called stop-and-go waves. These waves require them to slow down severely, or even stop completely. When traffic becomes motionless, the

space headway reaches a minimum as all vehicles are standing bumper-to-bumper; this extreme state is called jammed traffic. Clearly, there exists a maximum density at which the traffic seems to turn into a "parking lot", called the jam density and it is denoted by k_j, k_{jam}, or k_{max}. For a typical motorway, its value lies around 140 vehicles per kilometre per lane [69] (Note that the jam density is typically expressed in vehicles per kilometre and ignores the effects of traffic composition and vehicle lengths).

4.3.4 Transitions between different regimes

Streams of traffic flows can be regarded as many-particle systems (e.g., gasses, magnetic spin systems etc.); as they have a large number of degrees of freedom, it is often intractable when it comes to solving them exactly. However, from a physical point of view, these systems can be described in the framework of statistical physics, whereby the collective behaviour of their constituents is approximately treated using statistical techniques. Within this context, the changeover from one traffic regime to another, can be looked upon as a phase transition. Within thermodynamics and statistical physics, an order parameter is often used to describe the phase transition: when the system shifts from one phase to another the order parameter expresses a different behaviour. There exists a difference in which a phase transition can express itself. This difference is designated by the order of the transition; generally speaking, the two most common phase transitions are first-order and second-order transitions. According to Ehrenfest's classification, first-order transitions have an abrupt, discontinuous change in the order parameter that characterizes the transition. In contrast to this, the changeover to the new phase occurs smoothly for second-order transitions [70]. With respect to the description of regimes in traffic flows, it is commonly agreed that there exists a first-order phase transition when going from the capacity-flow to the congested regime. The point at which this transition occurs, is the critical density. For an accourate study about these question we refer the reader to the work of Tampeére, where an excellent overview is given, detailing the different traffic flow regimes, their transitions, and mechanisms with respect to jamming behaviour [71].

4.3.5 Correlations between traffic flow characteristics: Fundamental Diagrams

The first idea to investigate the correlation between traffic flow characteristics is due to Greenshields that in 1935 provide the basis for the empirical fundamental diagrams. In particular in his seminal paper, he sketched a linear relation between the density and the mean speed, based on empirically obtained data [72]:

$$\overline{v} = \overline{v}_{ff}\left(1 - \frac{k}{k_j}\right). \tag{4.4}$$

As can be seen from Greenshields's relation, when increasing the density from zero to the jam density k_j, the mean speed will monotonically decrease from the free-flow speed v_{ff} to zero. Although Greenshields's derivation of the linear relation between density and space mean speed appears elegant and simple, it is deeply incorrect. The fact of the matter is that his hypothesis is based on only seven measurement points and six of these observations were obtained for free-flow conditions, whereas the one single point that indicates congested conditions, was obtained at an entirely different road, on a different day [73].
Some twenty years later, Lighthill and Whitham developed a theory that describes the traffic flows on long crowded roads using a first-order fluid-dynamic model [74]. The term fundamental diagram itself, is historically based on Lighthill and Whitham's fundamental hypothesis of the existence of such a flow-concentration curve.
TFDs consist of mainly 2 different graphs: flow-density and speed-density; all the graphs are two dimensional and the variables are related each other by the traffic fundamental relation

$$q = \overline{v}(k)k \tag{4.5}$$

were q (in veh/h) is the traffic flow, k the vehicles density (in veh/Km) and $v(\lambda)$ in the vehicles mean speed (in Km/h).
We now give an overview of some of the qualitative features of the different possible fundamental diagrams.
Space-mean speed versus density:
Noteworthy features of this type of fundamental diagram are:

- the density is restricted between 0 and the jam density k_j;

- the space-mean speed is restricted between 0 and the free-flow speed $\overline{v}_{ff}$;
- as density increases, the space-mean speed monotonically decreases;
- there exists a small range of low densities, in which the space-mean speed remains unaffected and corresponds more or less to the free-flow speed.

Flow versus density:
Probably the most encountered form of a fundamental diagram, is that of flow versus density. An example of this fundamental diagram is depicted in figure 4.3. Noteworthy features of this type of fundamental diagram are:

- for moderately low densities (i.e., below the critical density k_c), the flow increases more or less linearly (this is called the free-flow branch of the fundamental diagram);
- near the critical density k_c, the fundamental diagram can bend slightly, due to faster vehicles being obstructed by slower vehicles, thereby lowering the free-flow speed;
- at the critical density k_c, the flow reaches a maximum, called the capacity flow q_{cap};
- in the congested regime (i.e., for densities higher than the critical density), the flow starts to decrease with increasing density, until the jam density k_j is reached and traffic comes to a stand still, resulting in a zero flow (this is called the congested branch of the fundamental diagram);
- the space-mean speed $\bar{v}_s$ for any point on the $q(k)$ fundamental diagram, can be found as the slope of the line through that point and the origin;
- when taking the slope of the tangent in any point of the diagram, we obtain what is called the kinematic wave speed. These speeds w correspond to shock waves encountered in traffic flows (e.g., the stop-and-go waves). As can be seen from the figure, the shock waves travel forwards, i.e., downstream, in free-flow traffic ($w > 0$), but backwards, i.e., upstream, in congested traffic ($w < 0$).

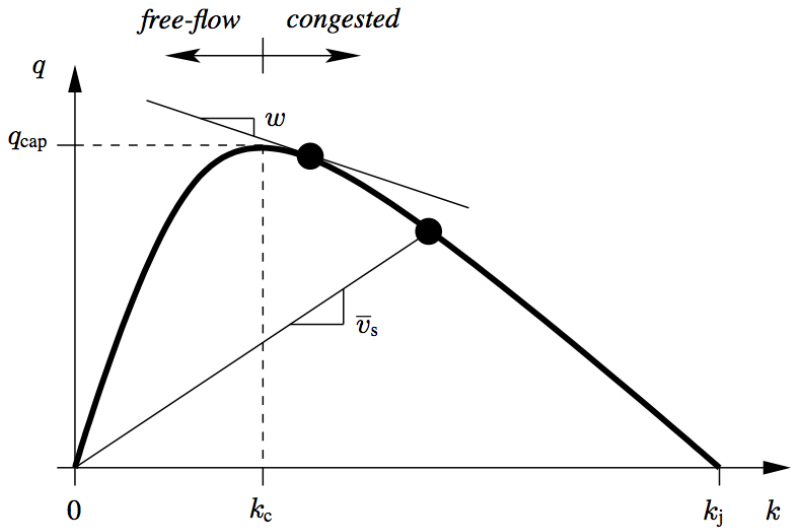

Figure 4.3: A fundamental diagram relating the density k to the flow q. The capacity flow q_{cap} is reached at the critical density k_c.

The shape of the $q(k)$ depicted in figure 4.3 fundamental diagram is just one possibility. There exist many different flavours, originally derived by traffic engineers seeking a better fit of these curves to empirical data (see for example [75, 76, 77] and figure 4.4). The most extreme argument with respect to the shape of the fundamental diagram, came from Kerner with his fundamental hypothesis of three-phase traffic flow theory [78].

4.4 Poisson Law and Road Traffic

If the passage of vehicles is a stationary phenomenon and the flow is often enough rarefied so that the vehicles do not influence each other, the probability $p(n,t)$ that in a fixed section of a road occurs the passage of n vehicles in a generic time t, is given by the Poisson law [79]:

$$p(n,t) = e^{-Qt}\frac{(Qt)^n}{n!}, \tag{4.6}$$

where Q is the mean value of vehicles passage in the unitary time. Thus, the probability that no vehicles passages are achieved in a certain time t is given

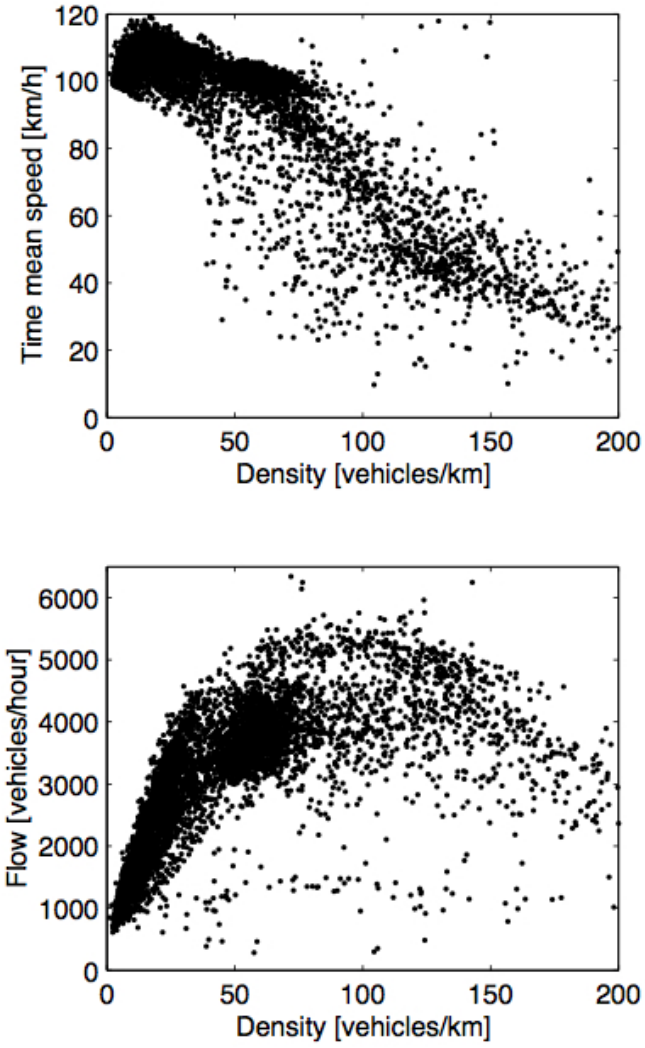

Figure 4.4: Illustrative scatter plots of the relations between traffic flow characteristics as measured by video camera CLO3 located at the E17 three-lane motorway near Linkeroever, Belgium.

by

$$p(0,t) = e^{-Qt}. \tag{4.7}$$

If we now denote τ the random variable representing the time distance between two subsequent vehicles passages, thus, from 4.7, we obtain that the probability that this time gap is greater then t is:

$$p(\tau >= t) = e^{-Qt}. \tag{4.8}$$

Denoting $f_\tau(\tau)$ and $F_\tau(t)$ respectively the probability density function and the cumulaltive function of the random variable τ, we obtain that $p(\tau >= t) = e^{-Qt} = 1 - F_\tau(t)$, so:

$$f_\tau(\tau) = F'_\tau(t) = Qe^{-Q\tau}, \tag{4.9}$$

that represents the probability density function of an exponential random variable. Thus, when the flow can be approximated to a poissonian current, the time-gap distance follows an exponential law. In particular, this happens when $Q < 400$ so that vehicles can be considered independent. For flux greater than $Q = 400$ vehicles cannot be assumed independent anymore, so time-gap follows an Erlang Distribution [79].

Chapter 5

Traffic Noise Prediction with Follow-the-leader models

Microscopic models are based on the explicit consideration of the interactions between individual vehicles within a traffic stream. These classes of models typically employ characteristics such as vehicle lengths, speeds, accelerations, and time and space headways, vehicle and engine capabilities as well as some rudimentary human characteristics that describe the driving behaviour.
The material in this chapter is organised as follows: we first introduce the classical car- following formulation, after which we focus our attention on the Optimal Velocity Model (OVM). In the second part of the chapter we present an integration between the OVM and noise prediction tools reported in chapter 3, accounting the traffic noise directly from the system dynamics in different traffic situation.

5.1 Car-following model: general formulation

Probably the most widely known class of microscopic traffic flow models is the so called family of car-following or follow-the-leader models. One of the oldest models in this case, is the one due to Reuschel [80], Pipes [81], and Forbes et al. [82]. The first mathematical car-following models that have been developed, were based on a description of the interaction between two neighbouring vehicles in a traffic stream, i.e., a follower and its leader.
The above mentioned model was originally formulated as the following ordi-

nary differential equation (ODE) for single-lane traffic:

$$\frac{dv_i(t)}{dt} = \frac{v_{i+1}(t) - v_i(t)}{T_r}, \tag{5.1}$$

with $v_i(t)$ and $v_{i+1}(t)$ the speeds of the following, respectively leading, vehicle at time t, and T_r a relaxation parameter. For the above case, the underlying assumption is that vehicle i (the follower) tries to achieve the speed $v_{i+1}(t)$ of vehicle $i+1$ (its leader), whilst taking a certain relaxation time T_r into account.

Chandler et al. were among the first to include in equation 5.1 an explicit reaction time τ into the model (typically, $\tau = 1.5$ s), leading to destabilization of vehicle platoons [83]. This reaction encompasses both a perception-reaction time (PRT), i.e., the driver sees an event occurring (for example the brake lights of the leading vehicle), as well as a movement time (MT), i.e., the driver needs to take action by applying pressure to the vehicle's brake pedal [73]. Introducing this behaviour resulted in what is called a stimulus-response model, whereby the right- hand side of equation 5.1 describes the stimulus and the left-hand side the response (the response is frequently identified as the acceleration, i.e., the action a driver takes by pushing the acceleration or brake pedal). The relaxation parameter is then reciprocally reformulated as the sensitivity to the stimulus, i.e., $\lambda = T_r^{-1}$, resulting in the following expression:

$$\text{response} = \text{sensitivity x stimulus} \tag{5.2}$$

$$\frac{dv_i(t+\tau)}{dt} = \lambda \left(v_{i+1}(t) - v_i(t)\right). \tag{5.3}$$

The latter equation is called a delayed differential equation (DDE), which, in this case, is known to behave in an unstable manner, even resulting in collisions under certain initial conditions. Gazis et al. remedied this situation by making the stimulus λ dependent on the distance, i.e., the space gap g_{s_i} between both vehicles [84]:

$$\frac{dv_i(t+\tau)}{dt} = \lambda \left(\frac{v_{i+1}(t) - v_i(t)}{x_{i+1}(t) - x_i(t)}\right). \tag{5.4}$$

Further advancements to this car-following model were made by Edie, who introduced the current speed of the following vehicle [85] such as:

$$\frac{dv_i(t+\tau)}{dt} = \lambda v_i^m(t) \frac{v_{i+1}(t) - v_i(t)}{\left(x_{i+1}(t) - x_i(t)\right)^l}, \tag{5.5}$$

with now λ, l, and m model parameters (in the early days, the model was also called the L-M model [86]). A recent extension to the classical car-following theory, is the work of Treiber and Helbing, who developed the intelligent driver model (IDM). Its governing equation is the following [87]:

$$\frac{dv_i}{dt} = a_{max}\left[1 - \left(\frac{v_i}{v_{des}}\right)^{\delta} - \left(\frac{g_s^*(v_i, \Delta v_i)}{g_{s_i}}\right)^2\right], \tag{5.6}$$

with a_{max} the maximum acceleration, v_{des} the vehicles's desired speed, and Δv_i the speed difference with the leading vehicle. The first terms within the brackets denote the tendency of a vehicle to accelerate on a free road, whereas the last term is used to allow braking in order to avoid a collision (the effective desired space gap $g_s^*(v_i, \Delta v_i)$ is based on the vehicle's speed, its relative speed with respect to its leader, a comfortable maximum deceleration, a desired time headway, and a jam space gap). The finest qualities of the IDM are that it elegantly generalises most existing car-following models and is quite capable of generating all known traffic regimes. For a complete review of microscopic model we refer to [88].

5.2 Car Following Deduction of Fundamental Diagram

In chapter 4 we summarized the main features of the Traffic Fundamental Diagram. Now we obtain the fundamental diagram in the framework of Car-following model for single lane traffic. Let the cars in a single lane be numbered consecutively beginning with the leading car, and let $x_n(t)$ denote the position of the n-th car at time t, $x_n'(t)$ its velocity, and $x_n''(t)$ its acceleration. Although a large number of differential difference relations have been proposed [88], we shall concentrate on three basic simple equations which can be plausibly deduced and which yield specific flow-concentration relationships. The first one starts by the consideration that, in general, authorities recommend a minimum spacing between consecutive cars which is proportional to the velocity of the following car. Taking into account a car length, so that the same coordinate point of each car is specified, the rule can be written

$$x_{n+1}' = C_1(x_n - x_{n+1}) + cost., \tag{5.7}$$

which it is convenient to represent in terms of acceleration as

$$x''_{n+1} = C_1(x'_n - x'_{n+1}). \tag{5.8}$$

Equation 5.8 does not involve the distance between cars, and a more sophisticated model can be obtained by regarding C as the sensitivity of response, which is supposed to be inversely proportional to spacing, giving

$$x''_{n+1} = C_2 \frac{x'_n - x'_{n+1}}{x_n - x_{n+1}}. \tag{5.9}$$

It can be argued still further that the sensitivity in equation 5.9 should be inversely proportional to headway, since the driver of the $(n+1)$ car will be more alert with smaller headway than with greater headway. The headway of the $(n+1)$ car is $\frac{x_n - x_{n+1}}{x'_{n+1}}$. Therefore, this new conjecture leads to the equation

$$x''_{n+1} = C_3 x'_{n+1} \frac{x'_n - x'_{n+1}}{(x_n - x_{n+1})^2}. \tag{5.10}$$

Since the fundamental relation which we are trying to obtain contains a velocity (or mean velocity), it is only necessary to integrate equations 5.8, 5.9 and 5.10 once. However, some very strong equilibrium assumptions are necessary, namely that each car finally assumes exactly the same speed and spacing as every other, so that individual values can safely be replaced by population means. Equations 5.8, 5.9 and 5.10 yield, respectively to:

$$x'_{n+1} = C_1(x_n - x_{n+1}) + cost., \tag{5.11}$$

$$x'_{n+1} = C_2 \log(x_n - x_{n+1}) + cost., \tag{5.12}$$

$$\log x'_{n+1} = -C_3(x_n - x_{n+1})^{-1} + cost., \tag{5.13}$$

or, in equilibrium,

$$\bar{v} = \frac{C_1}{k} + cost., \tag{5.14}$$

$$\bar{v} = C_2 \log \frac{1}{k} + cost., \tag{5.15}$$

$$\log \bar{v} = -C_3 k + cost. \tag{5.16}$$

Since there are two boundary conditions available, $\bar{v}(0) = \bar{v}_{ff}$ and $\bar{v}(k_j) = 0$, it should be possible to evaluate both C_i and the integration constant. However, an examination of 5.14, 5.15, 5.16 shows that the first two cannot

be valid near $k = 0$ and the third cannot be valid near $k = k_j$. Therefore, we restrict 5.14 and 5.15 to dense traffic and 5.16 to sparse traffic and evaluate the costant at the appropriate boundary. Multiplying the previous equations by k, we find for the three car following postulates, the following flow-concentration curves:

$$q = C_1(1 - \frac{k}{k_j}), \tag{5.17}$$

$$q = C_2 k \log \frac{k_j}{k}, \tag{5.18}$$

$$q = \bar{v}_{ff} \lambda e^{-C_3 k}. \tag{5.19}$$

5.3 Optimal velocity model

Closely related to the previously discussed classical car-following models, are the so-called optimal velocity models (OVM) of Newell and Bando et al. Whereas the previous car-following models mostly describe the behaviour of a vehicle that is following a leader, the OVMs modify the acceleration mechanism, such that a vehicle's desired speed is selected on the basis of its space headway, instead of only considering the speed of the leading vehicle [88]. Newell was the first to suggest such an approach, using an equilibrium relation for the desired speed as a function of its space headway [89].
Bando et al. later improved this model, resulting in the following equation that describes a vehicle's acceleration behaviour [90]:

$$\frac{dv_i(t)}{dt} = \alpha \left[V_{opt}(h_{s_i}(t)) - v_i(t) \right] \tag{5.20}$$

in which $V_{opt}(.)$ is called the Optimal Velocity Function (OVF) and $h_{s_i} = x_{i+1} - x_i$. The difference between this desired speed, associated with the driver's current space headway, and the vehicle's current speed, is corrected with an acceleration $\alpha V_{opt}()$, with now α a coefficient expressing the sensitivity of a driver. This sensitivity corresponds to the inverse of the relaxation time, which is the time needed to reach the speed dictated by the OVF. Specification of the optimal velocity function is done such that it is zero for $h_{s_i} \to 0$, and bounded to v_{max} for $h_{s_i} \to +\infty$; this latter condition means that the model is able to describe the acceleration of vehicles without the explicit need for a leader as in the previous car-following models.

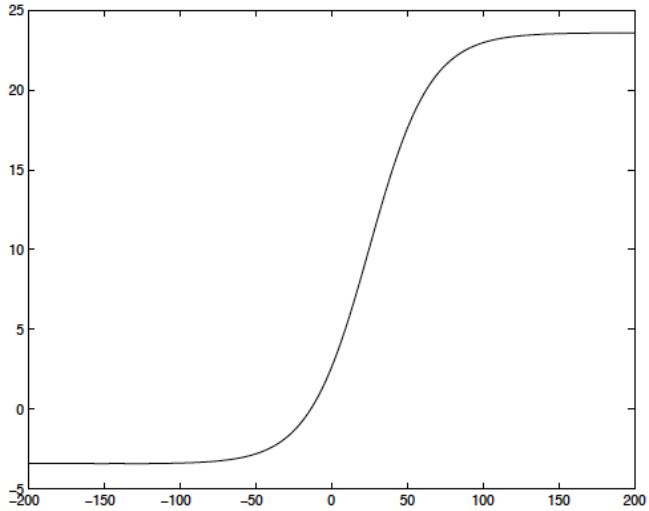

Figure 5.1: Optimal Velocity Function (ordinate) 5.21 as function of headway (abscissa) for $d = 25m$, $w = 40m$, $c = 0.7465$ and $v_{max} = 27m/s$.

In this dissertation we choose to use the OVF suggested by Bando et al. in [90] that reads:

$$V_{opt} = \frac{v_{max}}{2}\left[\tanh\left(\frac{h_{s_i} - d}{w}\right) + c\right], \tag{5.21}$$

where v_{max} is the maximum speed allowed and d, w and c are model parameters that must be tuned on experimental data. In figure 5.1 the behaviour of OVF 5.21 has been reported.

This model has been numerically implemented in the framework of Wolfram Mathematica ^{TM}, for a single and double lane road.

5.3.1 Single Lane Dynamics

In the framework of Wolfram Mathematica ^{TM} we numerically implement the dynamics of single lane road. In particular we implemented the car dynamics with open boundary conditions: at each time step with a given probability p a new car enters the system if its distance from the previous car (i.e. the one that entered before) is greater then a minimum distance Δx_{min}. Then, for each car, the speed at the next time step is evaluated according to the

OVF function 5.21 and expression 5.20 such as:

$$v_i(t+\Delta t) = v_i(t) + \alpha \left[V_{opt}(h_{s_i}(t)) - v_i(t)\right] \Delta t \quad \text{if} \quad h_{s_i} > \Delta x_{min} \tag{5.22}$$

$$v_i(t+\Delta t) = 0 \quad \text{if} \quad h_{s_i} < \Delta x_{min}. \tag{5.23}$$

Thus the positions are subsequently updated as $x_i(t+\Delta t) = x_i(t) + v_i(t)\Delta t$. To keep into account the random behaviour of driver, a stochastic noise term f is introduced as $v_i(t+\Delta t) = \left(v_i(t) + \alpha \left[V_{opt}(h_{s_i}(t)) - v_i(t)\right] \Delta t\right)(1+f\xi)$ where $\xi \in (-0.5, 0.5)$ is a random term.
In addition, to monitor the actual traffic situation, we introduce a "congestion" parameter η that is evaluated at each time step as $\eta(t) = \sum_i \frac{v_i}{v_{max}}$. Its value ranges from $\eta = 1$, that corresponds to free flow speed (i.e. all vehicles has $v_i = v_{max}$), to $\eta = 0$, that corresponds to a super traffic jam with all vehicle stopped (i.e. $v_i = 0$ for all vehicles). In figure 5.2 we report the behaviour of this parameter in two different traffic situations. In particular, in the up panel of figure 5.2 we can observe the behaviour of the congestion parameter in a nearly free flow situation, while in the down panel a more congested situation is represented.

5.3.2 Double Lane Dynamics

In the same way as done for single lane traffic we develop a numerical code for traffic dynamics on double lane road. In particular all the lanes point in the same direction so, respect to single lane traffic, we include the possibility that a vehicle overtakes its predecessor and then return to the previous lane. Thus we distinguish the two lanes in a slow lane (with maximum speed V_{max1} and a fast lane (with maximum speed V_{max2}. A vehicle can overtake another if some conditions are respected in order to avoid accidents. In particular it is necessary that:

- The space headway from its predecessor *on the fast* lane is greater than a minimum distance Δx_{front}.
- The space headway respect to the follower *on the fast* lane is greater than a minimum distance Δx_{back}
- The driver has the intention to overtake its predecessor. In particular this is modeled assigning a global overtaking probability $p_{overtaking}$

In similar way a vehicle goes back to the slow lane if:

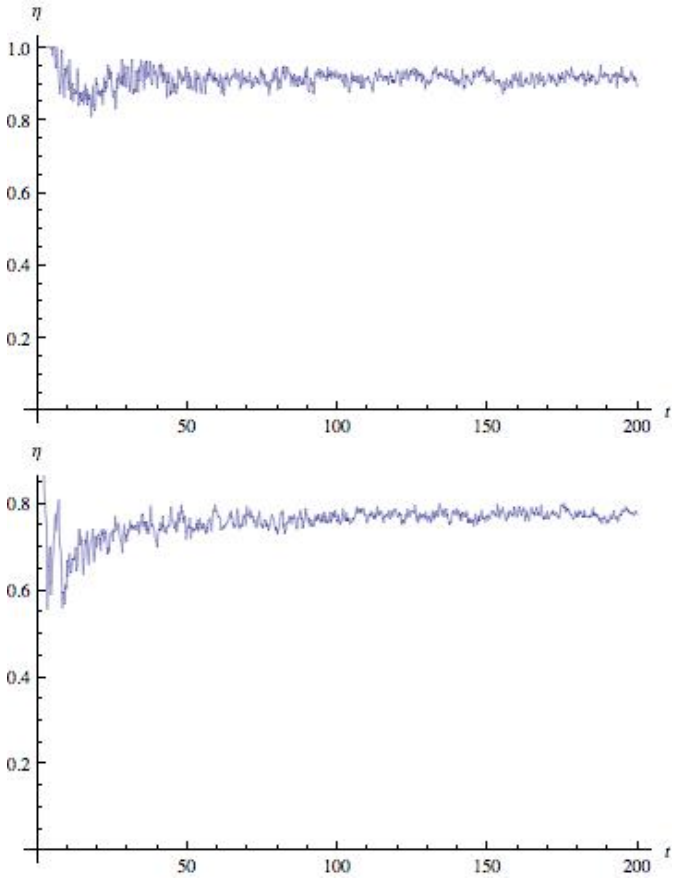

Figure 5.2: Congestion parameter as function of time for $w = 23.3$, $d = 25$, $\alpha = 2$, $c = 0.913$ and $f = 0.3$ over a period of T=200 time steps (each time step correspond to $\Delta t = 0.2$ s). *Up:* Simulation for $p = 0.05$ and $\Delta x_{min} = 30$m. *Down:* Simulation for $p = 0.5$ and $\Delta x_{min} = 10$m.

- The space headway from its predecessor *on the slow* lane is greater than a minimum distance Δx_{front}.
- The space headway respect to the follower *on the slow* lane is greater than a minimum distance Δx_{back}
- The driver has the intention to go back to slow lane. In particular this is modeled assigning a global probability p_{goback}

In figure 5.3 we report the behaviour of this congestion parameter for single lane (left) and double lane (right) traffic for the same traffic situations. Looking at the graphs can be noticed that in double lane traffic we achieve a less congested situation clearly because vehicles can improve their speed overtaking their predecessor.

5.3.3 Dynamics with a Forced Slowdown

In some cases external effects, such as for example the presence of obstacles or "men at work", can lead to a modification of maximum speed in a defined section of the road. This can lead to the formation of an external inducted local jam because the slowdown of leader is back-propagated to following cars, such asa kind of slowdown wave.
Also in this case we develop a numerical code for traffic dynamics from which we achieve the behaviour of congestion parameter η. As can be noticed by figure 5.4 the congestion parameter suddenly converge to a very low value revealing the presence of a traffic jam in proximity of the slowdown region where the maximum speed is set to V_{obs}. The system dynamics at different time is reported in figure 5.5.

5.3.4 Dynamics with Traffic Lights

Another interesting situation that can be investigated is the effect of traffic lights on system dynamics. In this case, vehicles can not move when the traffic light is red, and the stop of leader is back-propagated to followings cars such a kind of stopping wave.
Also in this case, we develop a numerical code for traffic dynamics from which we achieve the behaviour of congestion parameter η when a traffic light of duration ΔTL is present on the road. As can be noticed by figure 5.6, the congestion parameter is on the high value (corresponding to free flow) when

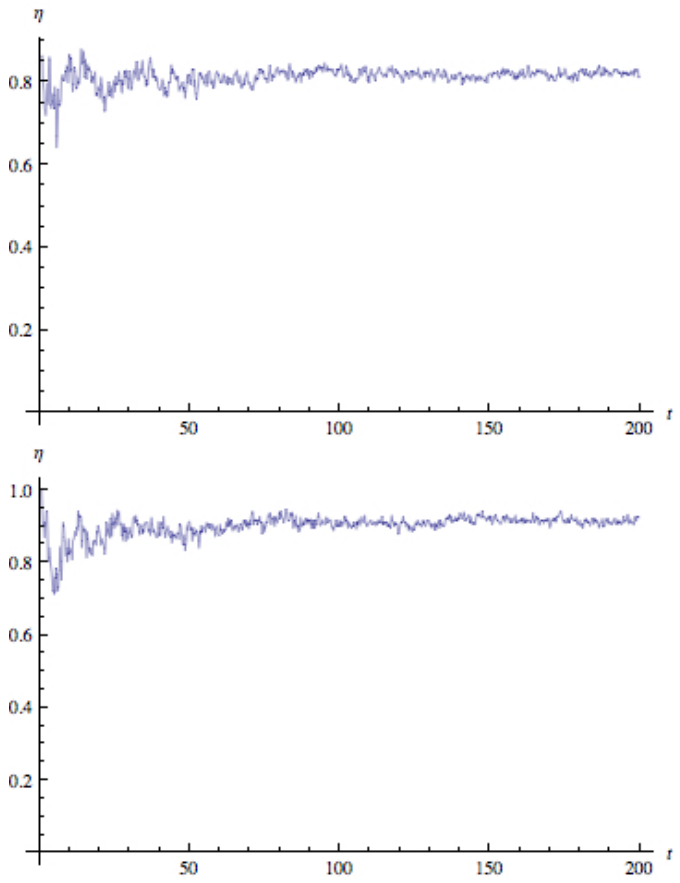

Figure 5.3: Congestion parameter as function of time for single lane (*up*) and double lane (*down*) traffic for the same traffic situations over a period of T=200 time steps (each time step correspond to $\Delta t = 0.2$ s). The model parameter are $w = 23.3$, $d = 25$, $\alpha = 2$, $c = 0.913$ and $f = 0.3$, $p = 0.3$, $\Delta x_{min} = 20$m, $\Delta x_{front} = 20$m, $\Delta x_{back} = 30$m, $V_{max} = 130$Km/h, $V_{max1} = 90$Km/h, $V_{max2} = 130$Km/h, $p_{overtaking} = 0.01$, $p_{goback} = 0.02$.

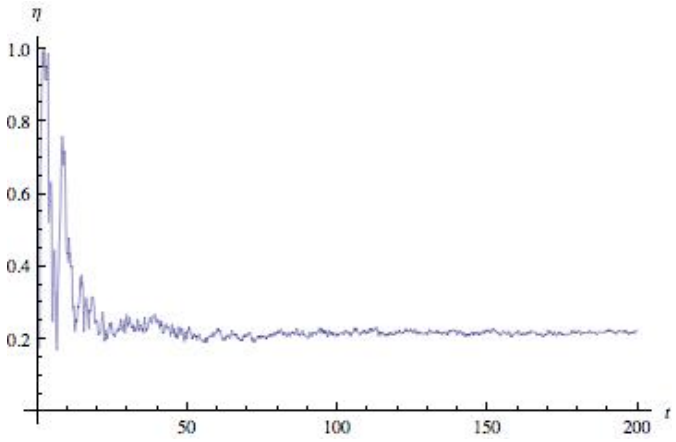

Figure 5.4: Congestion parameter as function of time for single lane traffic with a slowdown region with spatial extension of 50 m. Simulation runs over a period of $T = 200$ time steps (each time step correspond to $\Delta t = 0.2$ s). The model parameter are $w = 23.3$, $d = 25$, $\alpha = 2$, $c = 0.913$ and $f = 0.3$, $p = 0.3$, $\Delta x_{min} = 20$m, $V_{max} = 90$ Km/h, $V_{obs} = 50$ Km/h.

the traffic light is green and drop to zero when the traffic light is set red, because a huge congestion is present; after ΔTL time steps the traffic light become green and so the congestion parameter grows. To get another look at this effect we report the system dynamics at different time in figure 5.7. In the upper figure of 5.7 we have a snapshot of dynamics when the green light is on and the system is in an free flow situation; then in middle up figure we observe the situation when the light is red and vehicles are stopped. In the last two figures we report, instead, the dynamics when the green light is on and the vehicles slowly start to move until they reach a free flow situation.

5.4 Dynamical noise estimation in OVM model

The main purpose of this section is to introduce the noise estimation in the framework of OVM model. In order to evaluate the road noise emission, we have implemented a numerical algorithm in the framework of Wolfram Mathematica ^{TM}. In particular, the main idea is to evaluate the noise emission directly from the dynamics, recording for each vehicle the position $x_i(t)$ and the speed $v_i(t)$ at each time step. Thus, by the knowledge of the contextual vehicle speed $v_i(t)$, is possible to assign to each vehicle a noise source power

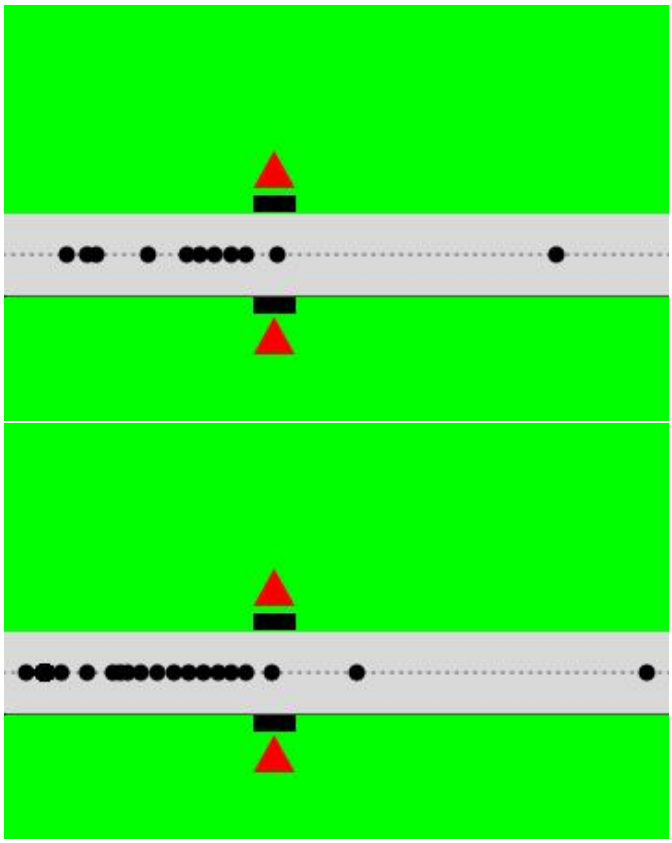

Figure 5.5: System dynamics at $t = 10$ (*up*) and $t = 60$ (*down*) for single lane traffic with a slowdown region with spatial extension of 50 m. Simulation runs over a period of $T = 200$ time steps (each time step correspond to $\Delta t = 0.2$ s). The model parameter are $w = 23.3$, $d = 25$, $\alpha = 2$, $c = 0.913$ and $f = 0.3$, $p = 0.3$, $\Delta x_{min} = 20$m, $V_{max} = 90$ Km/h, $V_{obs} = 50$ Km/h.

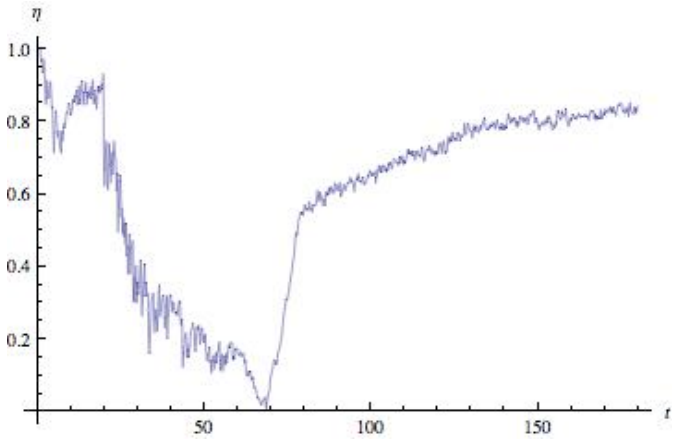

Figure 5.6: Congestion parameter as function of time for single lane traffic with traffic lights. Simulation runs over a period of $T = 180$ time steps (each time step correspond to $\Delta t = 0.2$ s). The model parameter are $w = 23.3$, $d = 25$, $\alpha = 2$, $c = 0.913$ and $f = 0.3$, $p = 0.1$, $\Delta x_{min} = 20$m, $V_{max} = 90$ Km/h, $\Delta TL = 30$ time steps.

level L_W^i at each time step, according to the experimental relations 3.5 already presented in section 3.1. In particular, for light vehicles, the expression reads:

$$L_W^i(v) = 53.6 + 23.8Log[v_i] \tag{5.24}$$

for $v > 11.5Km/h$ and $L_W^i(v) = 82$ for $v < 11.5Km/h$. In addition, to take into account the presence of stochastic parameters, such as driving conditions and skills, vehicles mechanics and maintenance, different vehicle model etc., we correct the previous expressions with a stochastic additive term. This is obtained choosing a gaussian correction with mean zero and unitary variance, as widely explained in section 3.3.1.. Thus, from the knowledge of geometrical and emission parameters, for each vehicle, at each time step t, the noise level can be propagated to the receiver, choosing an appropriate source model. Following a procedure similar to what described in paragraph 3.1 we use the point-like source propagation, described by the expression:

$$L_I^i(t) = L_W^i - 20Log[r_i(t)] - 11 \tag{5.25}$$

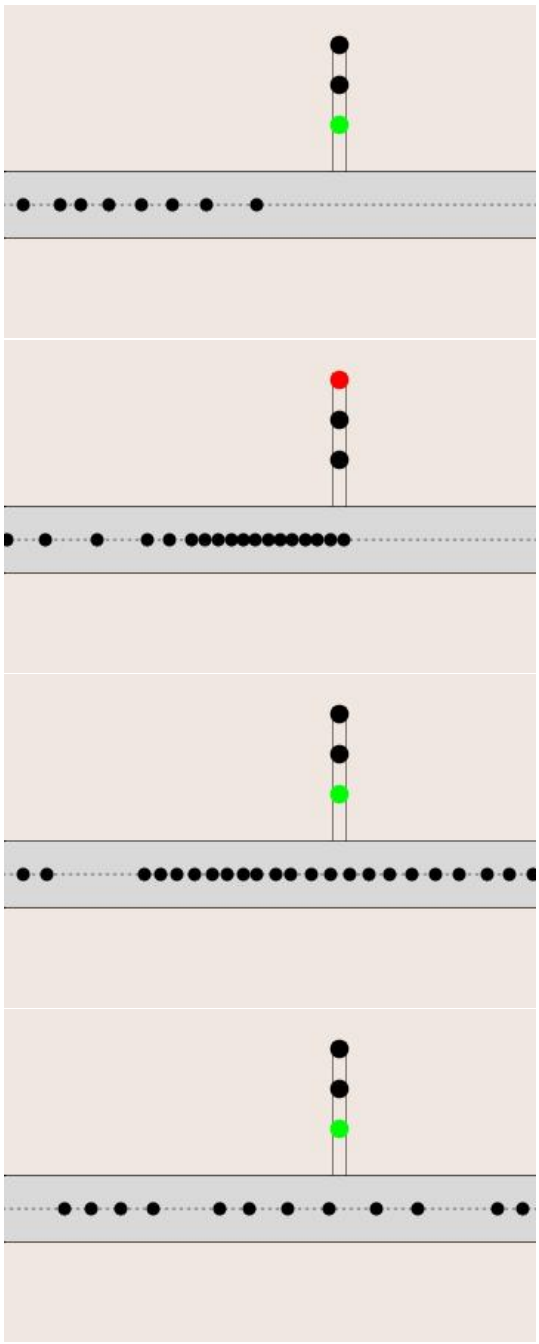

Figure 5.7: System dynamics at different time step (from up to down $t = 15$, $t = 50$, $t = 120$ and $t = 180$) for single lane traffic with traffic lights. Simulation runs over a period of $T = 180$ time steps (each time step correspond to $\Delta t = 0.2$ s). The model parameter are $w = 23.3$, $d = 25$, $\alpha = 2$, $c = 0.913$ and $f = 0.3$, $p = 0.1$, $\Delta x_{min} = 20$m, $V_{max} = 90$ Km/h, $\Delta TL = 30$ time steps.

where $r_i(t)$ is the distance between the i-th vehicle and the receiver, that, according to figure 5.8, is defined as:

$$r_i(t) = \sqrt{d^2 + \left(\frac{S}{2} - v_i(t)\right)^2} \tag{5.26}$$

where S is the road length and d is the vertical distance between road and receiver. In this way we are able to rebuild, for each vehicle, the sound

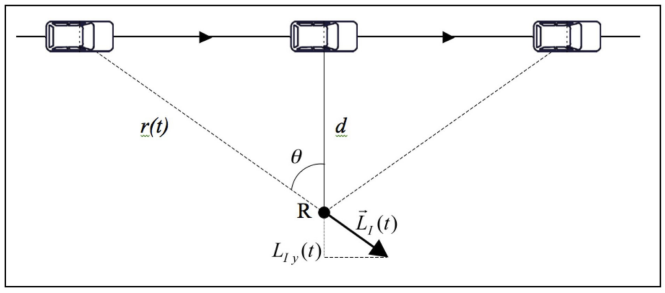

Figure 5.8: Geometry for noise calculation in OVM model.

intensity level $L_I(t)$ as function of time. Iterating this procedure for all transiting vehicles and performing the logarithmical sum, we are able to construct the global sound intensity level at the receiver as function time. Now, by the knowledge of the time-history of the entire signal it is possible to evaluate the equivalent continuous sound pressure level in the simulation period ΔT by the use of expression 3.18. In figure 5.9 we report the equivalent continuous sound pressure level as function of time for a single lane road, in two different traffic situations for a receiver at the perpendicular distance of 10 m from the road. In particular in the left panel of figure 5.2 we can see the noise level in a nearly free flow situation, while in the right panel a more congested situation is represented. These two situations correspond to those reported in figure 5.2. In the first case, we achieve an equivalent noise level $L_{eq} = 69.8$ dBA, while in the second case we achieve a greater value of $L_{eq} = 71.1$. In both figures some noise peaks are clearly evident, that roughly correspond to each vehicle passage in front of the receiver. Let's now see what happens for double lane road, where we let the vehicle overtaking each other. In this case we have two competiting effects that contribute to change the global noise level: on one hand not all vehicles are at the same distance from the receiver, while on the other the mean speed increases.

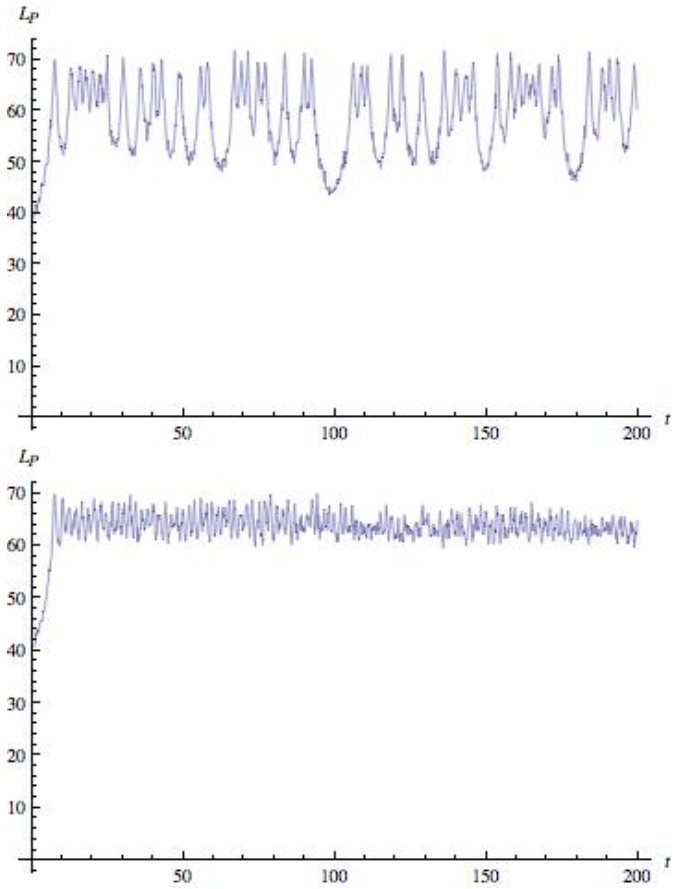

Figure 5.9: Equivalent continuous sound pressure level as function of time for $w = 23.3$, $d = 25$, $\alpha = 2$, $c = 0.913$ and $f = 0.3$ over a period of T=200 timesteps (each timestep correspond to $\Delta t = 0.2$ s). *Left:* Simulation for $p = 0.05$ and $\Delta x_{min} = 30$. *Right:* Simulation for $p = 0.5$ and $\Delta x_{min} = 10$. In both cases we assume the receiver at the perpendicular distance of 10 m from the road.

The competition between this two effects results in a small decreasing of global noise level respect to the single lane case, as can be evidenced from figure 5.10 where, for single lane traffic we find $L_{eq} = 75.0$ dBA while for double lane $L_{eq} = 73.3$ dBA. It could be also interesting to perform a traffic noise prediction in presence of an external induced slowdown region or with traffic lights. In the first case, recalling the system dynamics exposed in section 5.3.3, we can evaluate the equivalent continuous sound pressure level, when in a particular region of the road the maximum speed is set to a lower value respect to the maximum speed of entire road. In particular, the sound intensity level as function of time, is reported in figure 5.11. In the same way, recalling the dynamics exposed in section 5.3.4, we can evaluate the equivalent continuous sound pressure level, when traffic lights are present on the road. In particular, the sound intensity level as a function of time, is reported in figure 5.12.

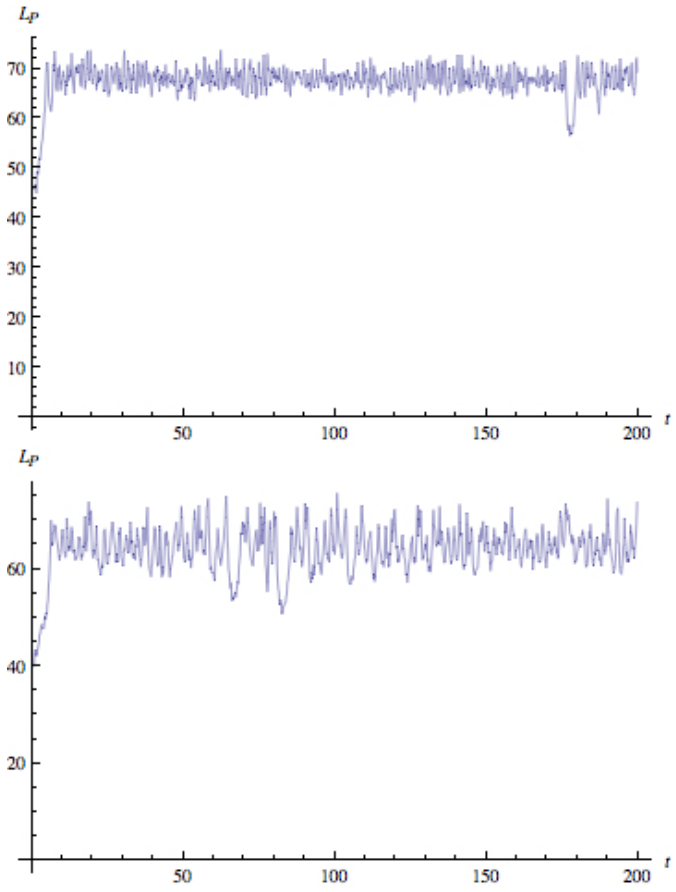

Figure 5.10: Equivalent continuous sound pressure level as function of time for single lane (up) and double lane (down) traffic for the same traffic situations over a period of T=200 time steps (each time step correspond to $\Delta t = 0.2$ s). The model parameter are $w = 23.3$, $d = 25$, $\alpha = 2$, $c = 0.913$ and $f = 0.3$, $p = 0.3$, $\Delta x_{min} = 20$, $\Delta x_{front} = 20$, $\Delta x_{back} = 30$, $V_{max} = 130$, $V_{max1} = 90$, $V_{max2} = 130$, $p_{overtaking} = 0.01$, $p_{goback} = 0.02$. In both cases we assume the receiver at the perpendicular distance of 10 m from the road.

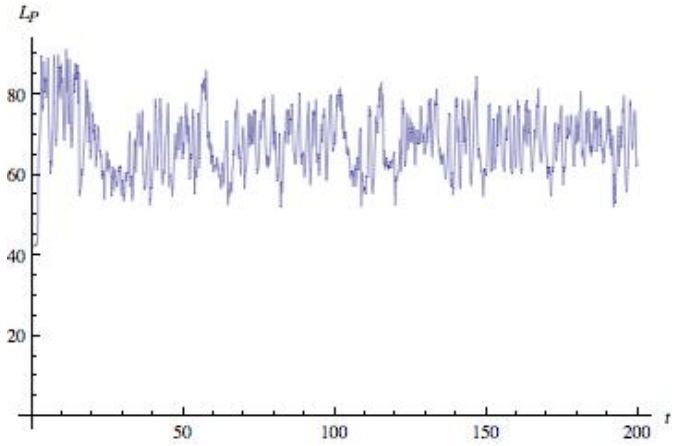

Figure 5.11: Equivalent continuous sound pressure level as function of time for single lane traffic with a slowdown region with spatial extension of 50 m. Simulation runs over a period of $T = 200$ time steps (each time step correspond to $\Delta t = 0.2$ s). The model parameter are $w = 23.3$, $d = 25$, $\alpha = 2$, $c = 0.913$ and $f = 0.3$, $p = 0.3$, $\Delta x_{min} = 20$m, $V_{max} = 90$ Km/h, $V_{obs} = 50$ Km/h. We assume the receiver at the perpendicular distance of 10 m from the road.

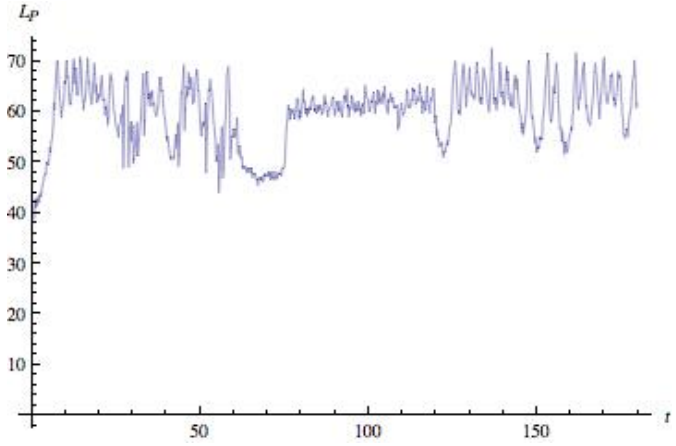

Figure 5.12: Equivalent continuous sound pressure level as function of time for single lane traffic with traffic lights. Simulation runs over a period of $T = 180$ time steps (each time step correspond to $\Delta t = 0.2$ s). The model parameter are $w = 23.3$, $d = 25$, $\alpha = 2$, $c = 0.913$ and $f = 0.3$, $p = 0.1$, $\Delta x_{min} = 20$m, $V_{max} = 90$ Km/h, $\Delta TL = 30$ time steps. We assume the receiver at the perpendicular distance of 10 m from the road.

Chapter 6

Traffic Noise Prediction with Cellular Automata models

In the field of traffic flow modeling, microscopic traffic simulation such that implemented in chapter 5, has always been regarded as a time consuming, complex process involving detailed models that describe the behaviour of individual vehicles. Approximately a decade ago, however, new microscopic models were being developed, based on the cellular automata programming paradigm from statistical physics. The main advantage was an efficient and fast performance when used in computer simulations, due to their rather low accuracy on a microscopic scale.
In this chapter, we exploit the suitability of different cellular automata (CA) models in the framework of traffic noise control. In particular, by the use of some traffic cellular automata (TCA), the traffic dynamics has been simulated in different situations and the related equivalent continuous sound pressure level has been evaluated. The final goal is to obtain a sort of fundamental diagram of traffic noise, relating the equivalent continuous sound pressure level to vehicles density on the road, so that different traffic conditions can be easily implemented and simulated in the noise control framework.

6.1 Mathematical Background on Cellular Automata

The simple structure of cellular automata has attracted researchers from various disciplines, from the first proposal given by Von Neumann and Ulam [91],

to the recent book of Wolfram "A New Kind of Science" [92]. During the last fifty years, they have been subjected to rigorous mathematical and physical analysis and their application has been proposed in different branches of science. The reason behind the popularity of cellular automata can be traced to their simplicity and to the enormous potential they hold in modeling complex systems. CA can be viewed as a simple model of a spatially extended decentralized system made up of a number of individual components (cells). The communication between constituent cells is limited to local interaction. Each individual cell is in a specific state which changes over time depending on the states of its local neighbors. The overall structure can be viewed as a parallel processing device. However, this simple structure, when iterated several times, produces complex patterns displaying the potential to simulate different sophisticated natural phenomena. Starting from the theoretical concept of universality, researchers have tried to develop simpler and more practical architectures of CA which can be used to model widely divergent application areas. In this respect, two notable developments can be credited to Wolfram and Conway.
In the beginning of the eighties, Stephen Wolfram studied much in detail a family of simple one-dimensional cellular automata rules (now famous as Wolfram rules [97]) and showed that even these simplest rules are capable of emulating complex behavior. In this book Wolfram related cellular automata to all disciplines of science (e.g., sociology, biology, physics, mathematics, engineering, urbanist etc) [98, 99, 100, 101].
In the 1970s, CA models found their way to one of the most popular applications called "simulation games", of which John Horton Conway's "Game of Life" [102, 103] is probably the most famous. The game found its wide spread fame due to Martin Gardner who, at that time, devoted to it a Scientific American column, called "Mathematical Games". Life, as it is called for short, is traditionally "played" on an infinitely large grid of cells. Each cell can be either "alive" or "dead". The game evolves by considering all surrounding neighbors of a cell, deciding whether or not the cell should live or die, leading to phenomenon called "birth", "survival", and "overcrowding" (or "loneliness"). In particular Game of Life follows the following evolution rules:

- A dead cell with exactly three live neighbors becomes a live cell (birth).
- A live cell with two or three live neighbors stays alive (survival).

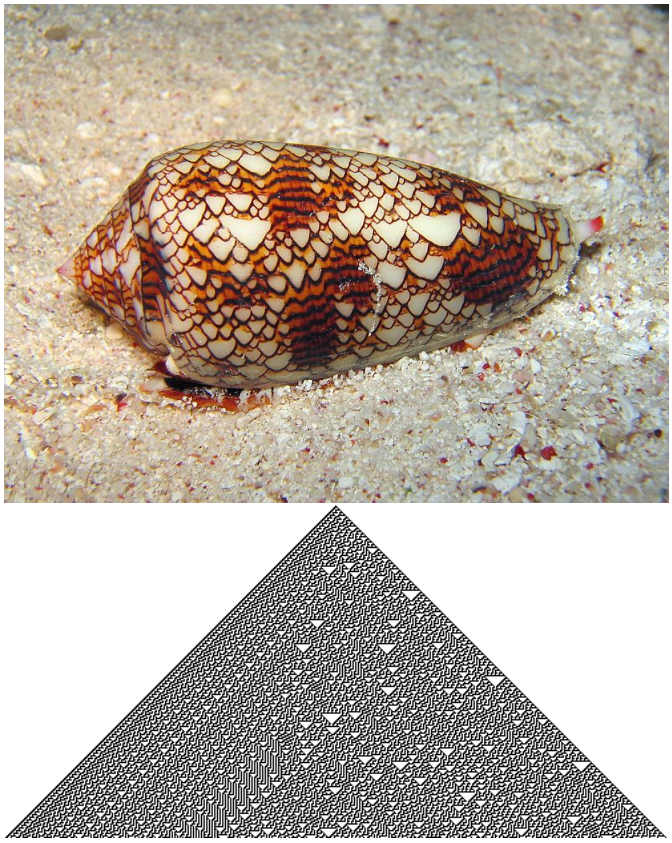

Figure 6.1: Simulation of Wolfram's Rule 30 and its similarity with natural pattern.

- In all other cases, a cell dies or remains dead (overcrowding or loneliness).

Let us see what happens to a variety of simple patterns. A single organism or any pair of counters, wherever placed, will obviously vanish on the first move. A beginning pattern of three counters also dies immediately unless at least one counter has two neighbors. The illustration in figure 6.2 shows the five triplets that do not fade on the first move. The first three (a, b, c) vanish on the second move. In connection with c it is worth noting that a single diagonal chain of counters, however long, loses its end counters on each move until the chain finally disappears. Pattern d becomes a stable "block" (two-by-two square) on the second move. Pattern e is the simplest of what are called "flip-flops" (oscillating figures of period 2). It alternates between horizontal and vertical rows of three. Conway calls it a "blinker". The illustration in figure 6.3 shows the life histories of the five tetrominoes (four rookwise-connected counters). The square a is, as we have seen, a still-life figure. Tetrominoes b and c reach a stable figure, called a "beehive," on the second move. Beehives are frequently produced patterns. Tetromino d becomes a beehive on the third move. Tetromino e is the most interesting of the lot. After nine moves it becomes four isolated blinkers, a flip-flop called "traffic lights." It too is a common configuration. The illustration 6.2 and 6.3 shows the 12 commonest forms of still life. Many other structure has been evidenced by many scholar in the last years showing the amazing nature of this system. The Conway Game of Life has been numerically implemented for a 30 x 30 grid starting from random initial condition. In figure 6.4 the global state of system is reported for different time step. As we can see, even if we start from random configuration, after a certain number of steps the system converge towards stable structure and oscillator.

In this chapter, we present an application of CA in the framework of environmental control. In particular TCA method has been used to evaluate traffic dynamics and the related global acoustical noise level. Before the presentation of the TCA we will use in this chapter, it can be useful to recall some basilar concept of CA models.
The basic ingredients of any cellular automata are essentially four: the physical environment, the cell's state and neighbourhoods and, finally, the evolution rules.
Concerning the physical environment, it represents the universe on which the CA is computed and consists of a discrete lattice of cells (typically equal in

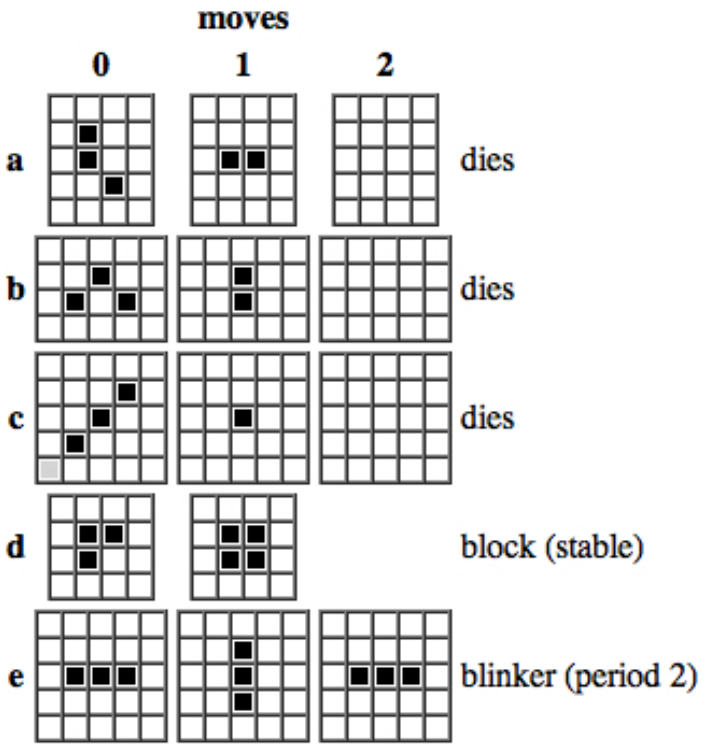

Figure 6.2: Pictures of cell's state evolution in Conway's Game of Life.

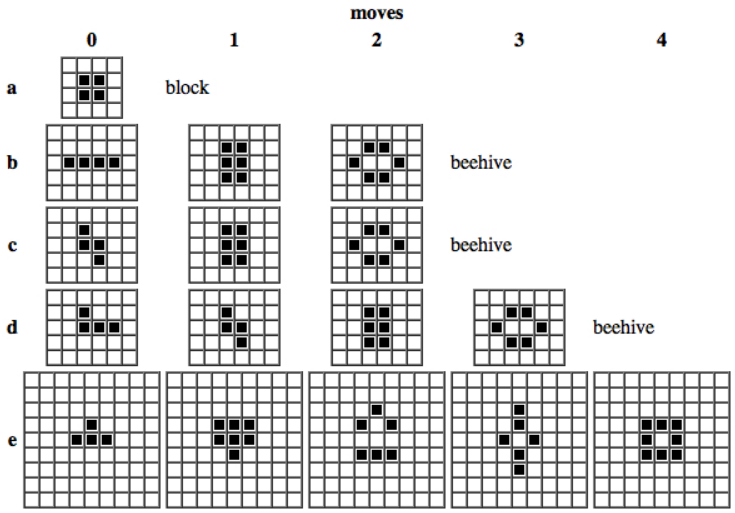

Figure 6.3: Pictures of cell's state evolution in Conway's Game of Life.

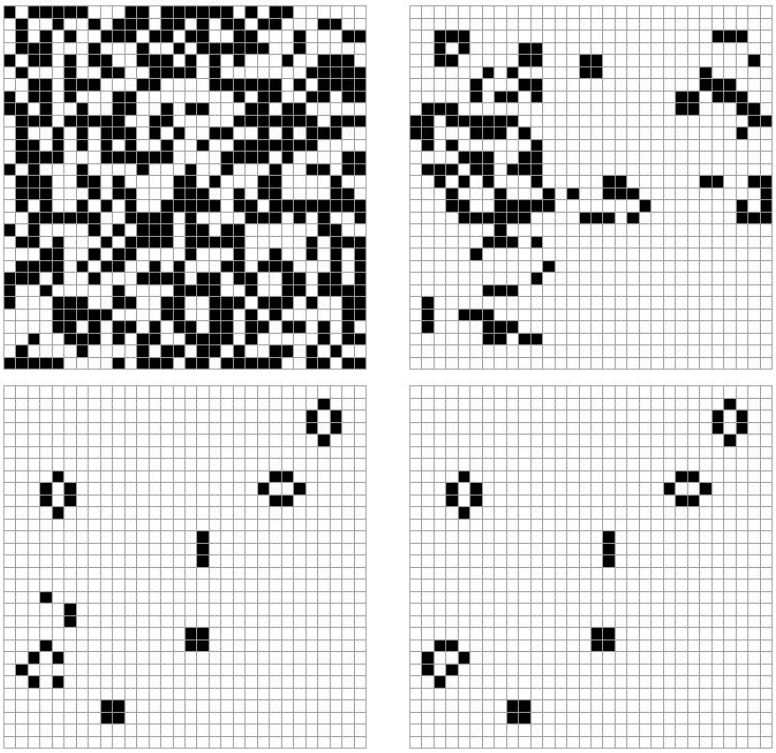

Figure 6.4: Pictures of cell's state evolution in Conway's Game of Life implemented for a 30 x 30 grid over 600 timestep starting from random initial condition for $t = 1, 25, 50, 100$.

size) with a rectangular, hexagonal, or other topology. The lattice can be finite or infinite in size, and its dimensionality can be 1 (a linear string of cells), 2 (a grid), or even higher dimensional. A common assumption is that the CAs lattice is embedded in a Euclidean space.
The second fundamental ingredient is the cell's state. Each cell of lattice, in fact, can be in a certain state, where typically an integer represents the number of distinct states a cell can be in, e.g. a binary state. Note that a cell's state is not restricted to such an integer domain and a continuous range of values is also possible, in which case we are dealing with coupled map lattices (CML). We call the states of all cells collectively a CA global configuration. This convention asserts that states are local and refer to cells, while a configuration is global and refers to the whole lattice.
For each cell, we define a neighbourhood, that has the same dimension for

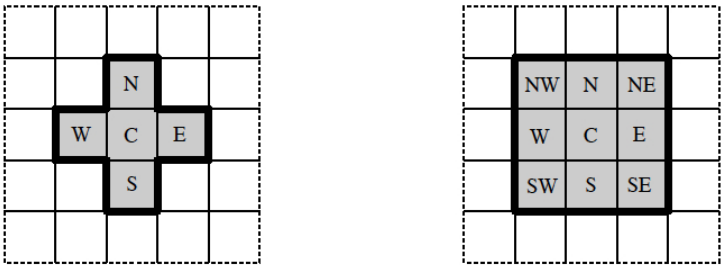

Figure 6.5: Two commonly used two-dimensional CA neighbourhoods with a radius of 1: the von Neumann neighbourhood (left) consisting of the central cell itself plus 4 adjacent cells, and the Moore neighbourhood (right) where there are 8 adjacent cells. Note that for one-dimensional CAs, both types of neighbourhoods are the same.

each cell in the lattice. In the one-dimensional lattice, for example, the neighbourhood consists of the cell itself plus its adjacent cells. In a two-dimensional rectangular lattice, there are several possibilities. For example, if one considers, besides the cell itself, the four north, east, south, and west adjacent cells is working with a von Neumann neighbourhood, while, accounting the previous five cells as well as the four north-east, south-east, south-west, and north-west diagonal cells one work with Moore neighbourhood (see figure 6.5). Of course as the dimensionality of the lattice increases, the number of direct neighbours of a cell increases exponentially.
After the definition of the cell's state and its neighbourhood we must define some transition rules that lead the cell's state change each timestep. The CA evolves in time and space as the rule is subsequently applied to all the cells in parallel. Typically, the same rule is used for all the cells (if the converse is true, then the term hybrid CA is used). When there are no stochastic components present in this rule, we call the model a deterministic CA, as opposed to a stochastic (also called probabilistic) CA. As the local transition rule is applied to all the cells in the CA's lattice, the global configuration of the CA changes.

6.2 Modeling the traffic dynamics with cellular automata

When applying the cellular automaton analogy to vehicular road traffic flows, the physical environment of the system is the road and lattice is composed by cells that can be empty or occupied by exactly one vehicle. In this section we focus on unidirectional, single-lane traffic so the layout consists of a one-dimensional lattice and the neighbourhood of a certain cell is represented by the previous and following cell. A typical discretization scheme assumes the time step $\Delta t = 1s$ based on a typical driver's reaction time [88] ,whereas the cell's dimension is chosen to be $\Delta x = 7.5m$, that corresponds to the average length that a conventional vehicle occupies in a closely jam packed configuration (focusing on single-lane traffic the vehicle's width has been neglected). This choice corresponds to a speed increments of $v = \frac{\Delta x}{\Delta t} = 27Km/h$.
Strongly important is also the question of boundary conditions that can be periodic (i.e a closed ring of cells) or open. In this section we always refer to periodic boundary conditions (PBC) while for noise mapping in section 6.5 we will use open boundary conditions.
The propagation of the individual vehicles in a traffic stream is described by means of a rule set that reflects the car-following behavior of a traffic cellular automaton evolving in time and space. The TCA's local transition rule actually comprises this set of rules that are consecutively applied to all vehicles in parallel. So, for each vehicle, the new speed is computed, after which its position is updated according to this speed. For single-lane traffic, we assume the the car-following behavior, so vehicles respond only to frontal stimuli from the direct frontal neighborhood of the cell to which the rules are applied. In addition to individual vehicles behavior, we can evaluate in the CA world the collective quantities according to the following formulas:

$$\lambda' = \frac{N}{L},$$
$$Q' = \frac{1}{TL}\sum_{t=1}^{T}\sum_{i=1}^{N} v_i(t),$$
$$\bar{v}' = \frac{Q'}{\lambda'},$$

where λ' is the vehicles density in veh/cells, Q' is the vehicular flow in veh/time step and $\bar{v}'$ is the average speed in cell/time step. The conversion from CA world to "Real world" is possible thanks to the following expressions that use the discretization parameters:

$$\lambda = \lambda' \cdot \frac{1000}{\Delta X},$$
$$Q = Q' \cdot \frac{3600}{\Delta T},$$
$$\bar{v} = \bar{v}' \cdot 3.6 \frac{\Delta X}{\Delta T}.$$

In the following subsections we introduce the evolution rules of some different TCA, whereas in the next section we discuss about how to evaluate the acoustical noise from traffic dynamics. All the described models has been implemented in a numerical algorithm in the framework of Wolfram Mathematica ^{TM}.

6.2.1 Wolfram's rule 184

The first deterministic model we consider, is a one-dimensional TCA model with binary states. It is often referred as Wolfram's rule 184. This name came from Wolfram classification of binary cellular automata upon 256 rules [92]. If we consider the states 1 as particles (that are vehicles), and the states 0 as holes, then rule 184 dictates that all particles move one cell to the right, on the condition that its right neighbor cell is empty. At the same time, all holes have the tendency to move to the left for each particle that moves to the right, a phenomenon which is called "'the particle hole symmetry"'. For a TCA model, we can rewrite the previous actions as the following two rules:

(R1) acceleration and braking:
$$v_i(t) = min\left[g_{s_i}(t-1)\,,\,1\right]$$

(R2) vehicle movement:
$$x_i(t) = x_i(t-1) + v_i(t)$$

where g_{s_i} is defined as the space gap (given in number of empty cell) between the i-th vehicle and the one that precedes.

Rule R1 sets the speed of the i-th vehicle, for the current updated configuration of the system; it states that a vehicle always strives to drive at a speed of 1 cell/time step, unless it's impeded by its direct leader, in which case $g_{s_i}(t-1) = 0$, and the vehicle consequently stops in order to avoid a collision.
The second rule R2 is not actually a 'real' rule; it just allows the vehicles to advance in the system.
In figure 6.6 we have applied these rules to a lattice consisting of 150 cells showing the evolution over a period of 300 time steps. The time and space axes are oriented from left to right, and from bottom to top, respectively. In the left part, we show a free-flow regime with a global density k = 0.2 vehicles/cell, in the right part we have a congested regime with k = 0.75 vehicles/cell. Each vehicle is represented as a single coloured dot; as time advances, vehicles move to the upper right corner, whereas congestion waves move to the lower right corner, i.e., backwards in space. From both parts of Fig. 6.6, we can see that the CA-184 TCA model constitutes a fully deterministic system that continuously repeats itself. A characteristic of the encountered congestion waves is that they have an eternal life time in the system. In fig. 6.7, the foundamental diagrams have been reported. In particular, in the upper graph we report the flux-density diagram that, in this case, has an isosceles triangular shape with a capacity $Q_{max} = 0.5$. As it can be seen from the bottom graph, instead, the mean speed $\bar{v}'$ remains constant at $v_{max} = 1$ until the density $\lambda \approx 0.5$ is reached, at which point it starts to diminish towards zero, where the critical density is reached.

6.2.2 Deterministic Fukui-Ishibashi model DFI

The Wolfram rule 184 was later generalized by Fukui and Ishibashi in [93]. This model has been developed both in a deterministic version and in a stochastic one. In this subsection, we will first discuss the deterministic version. The main idea of the model is the introduction of both a maximum speed v_{max} that is different from 1 cell/time step (as it is in rule 184) and an instantaneous acceleration to the highest speed allowed. These considerations lead to the reformulation of the Wolfram transition rule R1 as follow:

(R1) acceleration and braking:

$$v_i(t) = min\left[g_{s_i}(t-1)\,,\, v_{max}\right]$$

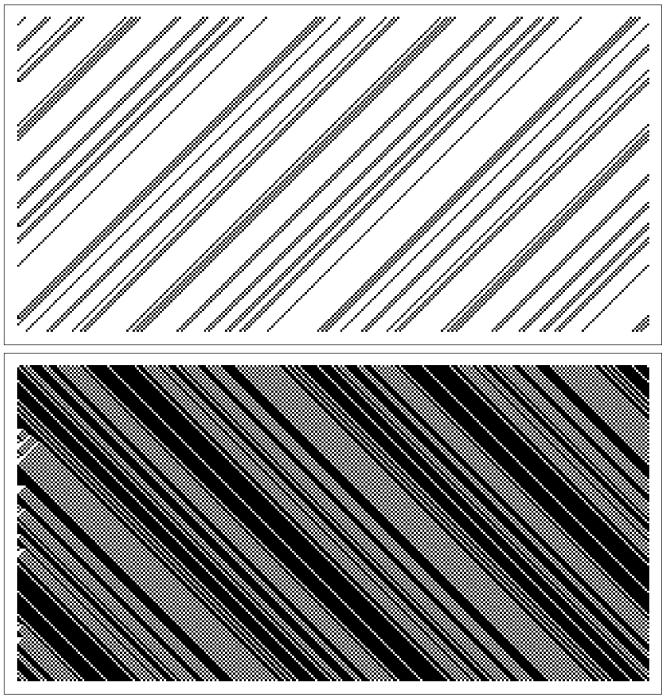

Figure 6.6: Typical time-space diagrams of the Wolfram's rule 184 on 150 cells lattices over a period of 300 time steps. Each vehicle is represented as a black square. Up: Traffic in a free-flow regime with a density $\lambda = 0.2$ vehicles/cell. Bottom: Traffic in a congested regime with a density $\lambda = 0.7$ vehicles/cell. The congestion waves can be seen as propagating in the opposite direction of traffic.

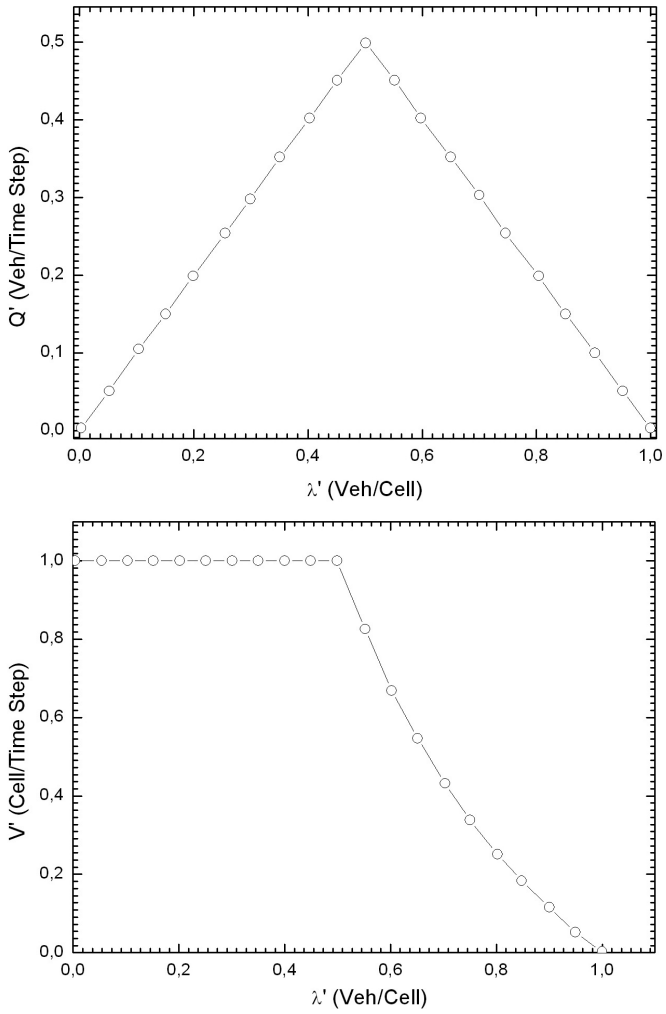

Figure 6.7: Up. Flux-density fundamental diagram for Wolfram's rule 184 with its typical triangular shape. Bottom: Speed-Density fundamental diagram for Wolfram's rule 184.

If eventually the vehicle cannot proceed in its time-space evolution, for instance because of a traffic jam, it will instantaneously stop, dropping its speed from v_{max} to 0 in one time step. This will avoid also the possibility of collisions. The rule R1 can also be modified to be more adherent to the reality, assuming a gradual acceleration of one cell per time step:

$$\text{(R1) acceleration and braking:}$$
$$v_i(t) = min\left[v_i(t-1) + 1\,,\, g_{s_i}(t-1)\,,\, v_{max}\right]$$

In fig. 6.8, the fundamental diagrams have been reported. In particular, in the upper graph we report the flux-density diagram for different V_{max}. In this case a triangular shape with a capacity $Q_{max} = \frac{V_{max}}{V_{max}+1}$ is observed. As it can be seen from the bottom graph, instead, the mean speed $\bar{v}'$ remains constant at V_{max} up to a well defined density and then it starts to diminish towards zero where the critical density is reached. In both type of diagram the curves are well separate and overlap themselves only at high density.

6.2.3 Nagel-Schreckenberg model STCA

The Nagel-Schreckenberg TCA is known as *NaSch TCA* or as *stochastic traffic cellular automaton* (STCA) and it is able to reproduce some real-life traffic phenomena, such as the spontaneous birth of traffic jams [94, 95]. This model includes a stochastic term in one of the transition rules, that can be resumed as follow:

$$\text{(R1) acceleration and braking:}$$
$$v_i(t) = min\left[v_i(t-1) + 1\,,\, g_{s_i}(t-1)\,,\, v_{max}\right]$$

$$\text{(R2) randomization:}$$
$$\xi(t) < p \Rightarrow v_i(t) = max\left[0, v_i(t) - 1\right]$$

$$\text{(R3) vehicle movement:}$$
$$x_i(t) = x_i(t-1) + v_i(t)$$

The rules are quite similar to previous models, except for the presence of a stochastic term. At each time step, a random number $\xi(t) \in [0, 1[$ is

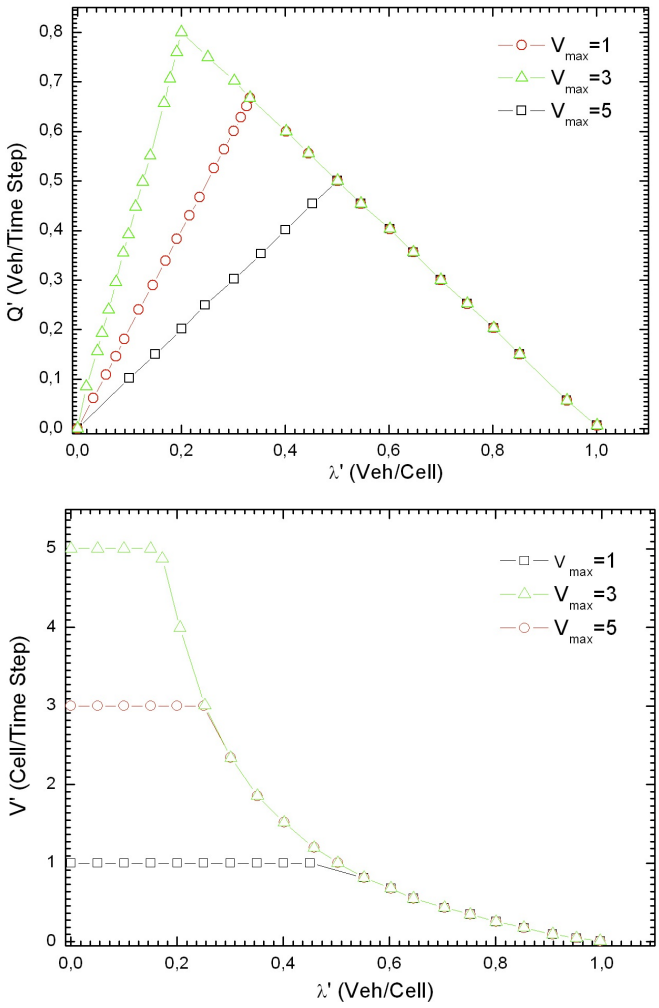

Figure 6.8: Up. Flux-density fundamental diagram for Fukui-Ishibashi model with differentV_{max}. Bottom: Speed-Density fundamental diagram for Fukui-Ishibashi model with different V_{max}.

generated according to an uniform distribution and it is compared with a stochastic parameter $p \in [0, 1]$, also called *slowdown probability*. This means that there is a probability p that a vehicle will slow down to $v_i(t)-1$ cells/time step.
The reason behead rule R2 is the attempt to capture natural speed fluctuations due to human behaviour, introducing overreactions of drivers when braking. This provides the key to the formation of spontaneously emerging jams, as can be seen in the space-time diagram in figure 6.9. In fig. 6.10, the fundamental diagrams have been reported. In particular, in the upper graphs we report the flux-density diagrams for different V_{max} and slow down probability. In this case, a more irregular shape is observed due to the presence of the stochastic term p. As it can be seen from the bottom graphs, instead, the mean speed $\bar{v}'$ vs density presents a behavior similar to Fukui-Ishibashi model, with speed which remains constant at low density (at value lower than v_{max} for the presence of slow down probability) and then it starts to diminish towards zero when the critical density is reached.

6.2.4 STCA with cruise control STCA-CC

A shortcoming of STCA model is that it can produce unstable artificial jams. The stochastic feature, in fact, can lead to local breakdown of traffic at any density and even in free-flow traffic regime. A way to overcome this artifact is to establish the free-flow branch of (λ, Q) diagram, by adding to STCA rules, an additional rule R0 that is in charge of turning off the randomisation for high-speed vehicles. This procedure has been proposed by Nagel and Paczuski in [96], and the new rule R0 can be written as follow:

$$\begin{aligned} &\text{(R0) determine stochastic noise:} \\ &v_i(t-1) = v_{max} \Rightarrow p'(t) = 0, \\ &v_i(t-1) < v_{max} \Rightarrow p'(t) = p. \end{aligned}$$

with p replaced by $p'(t)$ in STCA rule R2 This rule implies that only "jammed" vehicles will have stochastic behavior. This feature is called *cruise-control limit* (STCA-CC). In fig. 6.11, the fundamental diagrams of STCA-CC model have been reported for a lattice of 150 cells over a period of 300 timesteps. In particular, in the upper graphs we report the flux-density diagram for different V_{max} and slow down probability while, in the lower graphs,

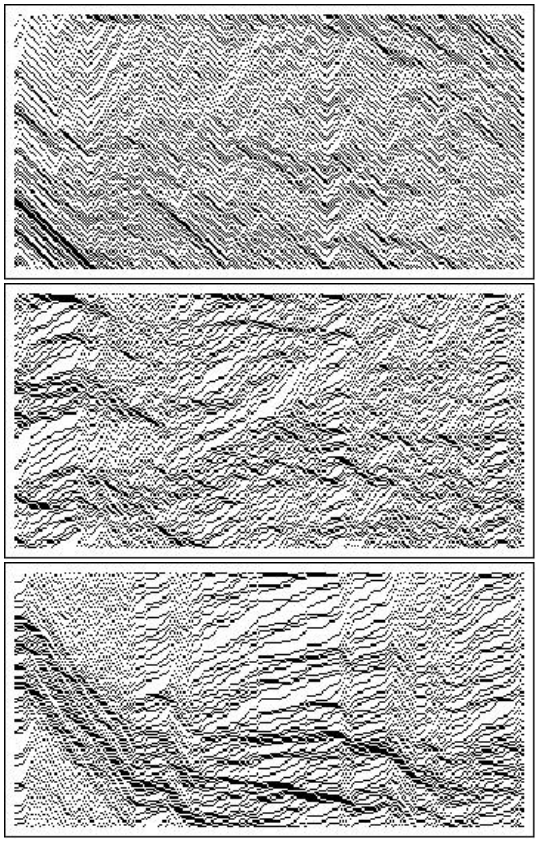

Figure 6.9: Typical time-space diagrams of the Nagel-Schreckenberg model on 150 cells lattices over a period of 300 time steps with different slow down probability. Up: Density $\lambda = 0.3$ vehicles/cell and $p = 0.1$. Middle: $\lambda = 0.3$ vehicles/cell and $p = 0.5$ Bottom: Density $\lambda = 0.3$ vehicles/cell and $p = 0.7$. The effects of the randomisation rule R2 are clearly visible as there occur artificial phantom mini-jams.

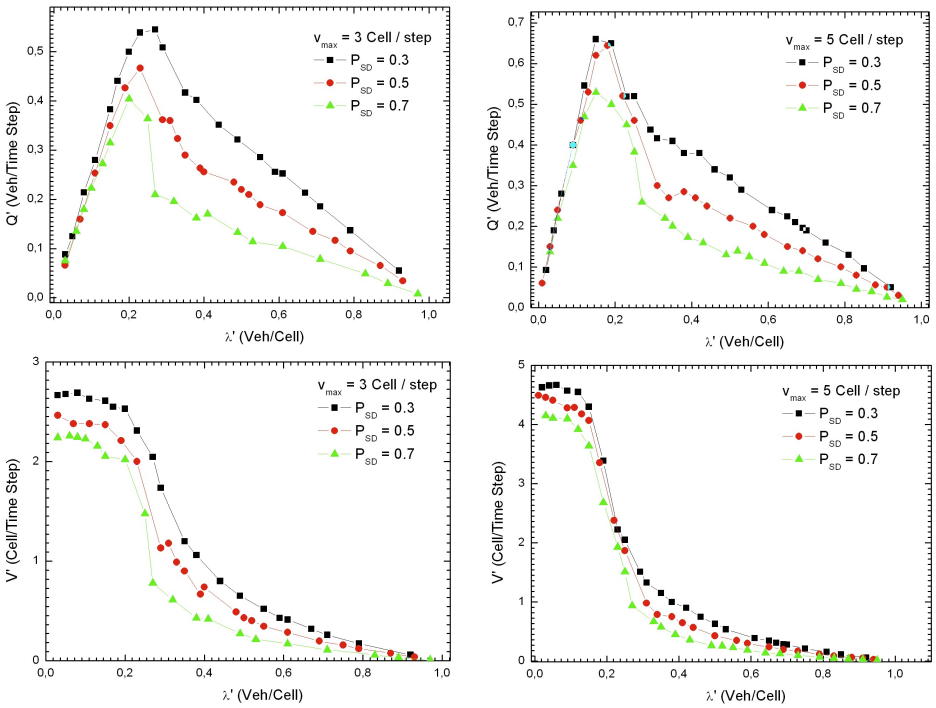

Figure 6.10: Up. Flux-density fundamental diagram for Nagel-Schreckenberg model for differentV_{max} and slow down probability. Bottom: Speed-Density fundamental diagram for Nagel-Schreckenberg model with different V_{max} and slow down probability.

the speed-density diagram is reported. Looking at the graphs it appears clear that the role of slow down probability is greater at density higher than the critical density while for low density the curves perfectly overlap. In particular, in the flux-density graphs at high slow down probability the diagram lose the typical triangular shape.

6.2.5 Stochastic Fukui-Ishibashi SFI-TCA

The non deterministic formulation of Fukui and Ishibashi model [93] introduced a stochasticity, but only for vehicles driving at the highest possible speed. The subsequent transition rules are then preceded by the extra rule R0:

(R0) determine stochastic noise:

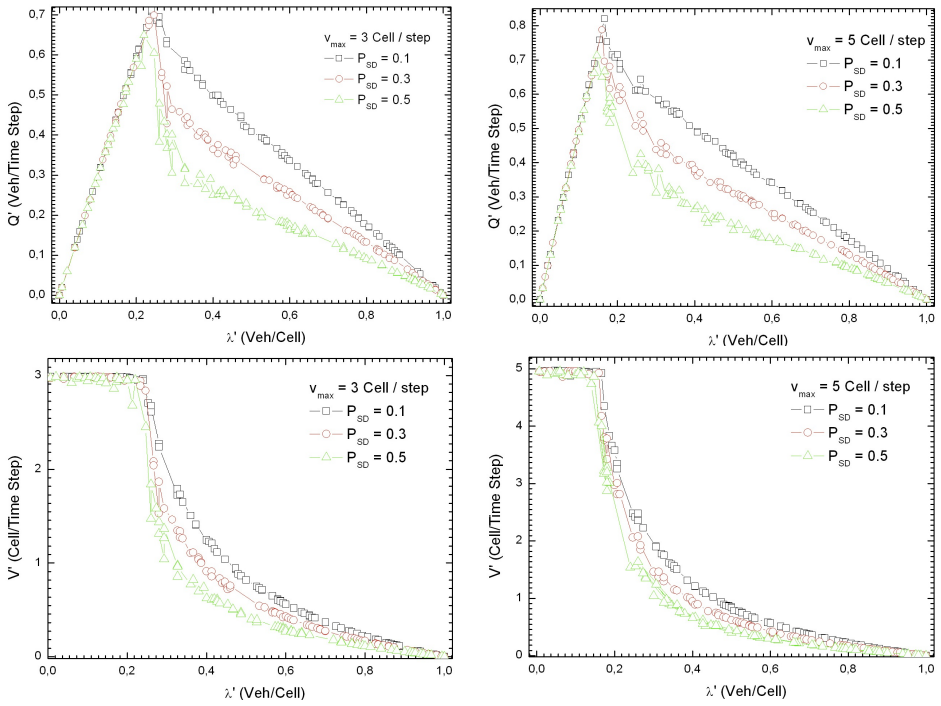

Figure 6.11: Up. Flux-density fundamental diagram for STCA-CC model for differentV_{max} and slow down probability. Bottom: Speed-Density fundamental diagram for STCA-CC model with different V_{max} and slow down probability.

$$v_i(t-1) = v_{max} \Rightarrow p'(t) = p,$$
$$v_i(t-1) < v_{max} \Rightarrow p'(t) = 0.$$

and are similar to the ones of STCA, but with p replaced by *p'(t)* in R2. If $v_{max} = 1$ the SFI-TCA and the STCA models coincide, while for $p = 0$ the stochastic feature is lost and SFI-TCA becomes deterministic.
The rationale behind the specific randomization in the SFI-TCA model, is that drivers who are moving at a high speed, are not able to focus their attention indefinitely. As a consequence, there will be fluctuations at these high speeds. As such, this corresponds to the opposite of a cruise-control limit previously described. In fig. 6.12, the fundamental diagrams have been reported for a lattice of 150 cells over a period of 300 timesteps. In particular, in the upper graphs we report the flux-density diagram for different V_{max} and slow down probability while in the lower graphs the speed-density diagram is reported. Looking at the graphs, it appears clear that the role of slow

down probability is greater at density lower than the critical density while after this point the curves perfectly overlap. This effect is more evident for lower V_{max} clearly because the model applies the slow down probability only to high speed vehicles. This behaviour is completely the opposite of cruise-control model that apply the slow down only to vehicles that drive at speed different from the highest possible speed.

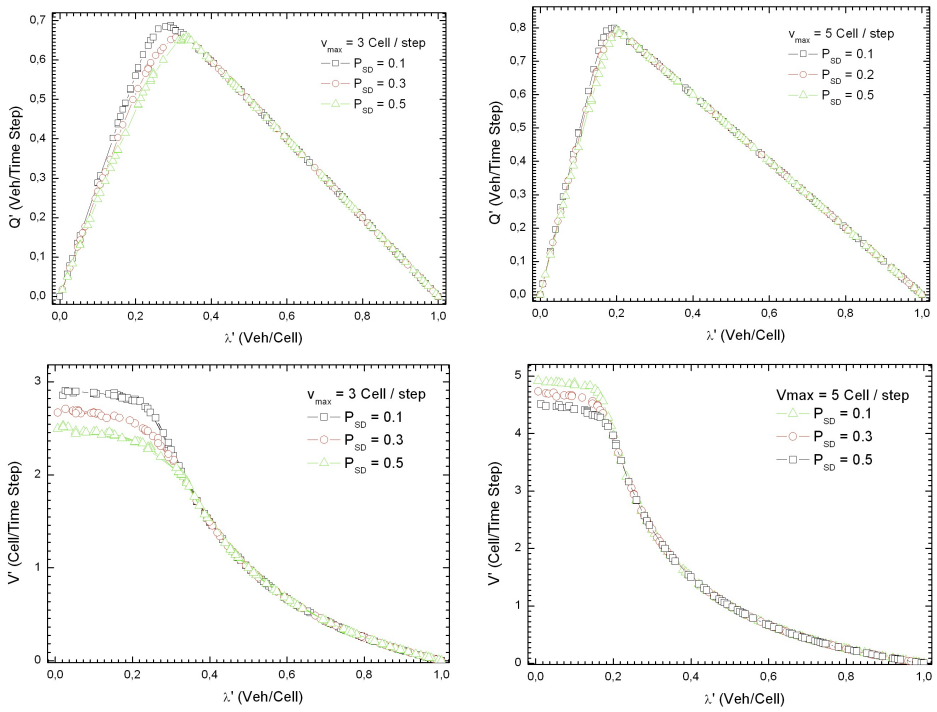

Figure 6.12: Up. Flux-density fundamental diagram for Stochastic Fukui-Ishibashi model for differentV_{max} and slow down probability. Bottom: Speed-Density fundamental diagram for Nagel-Schreckenberg model with different V_{max} and slow down probability.

6.3 Traffic noise prediction with Traffic Cellular Automata

The main purpose of this section is to introduce the noise estimation in the framework of Traffic Cellular Automata models following the same procedure

adopted for noise estimation with car following model. Also in this case we have implemented some numerical algorithms (one for each TCA model) in the framework of Wolfram Mathematica ^{TM}. In particular, the main idea is to evaluate the noise emission directly from the dynamics, recording for each vehicle position $x_i(t)$ and speed $v_i(t)$ for each time step. Thus, by the knowledge of the contextual vehicle speed $v_i(t)$, it is possible to assign to each vehicle a noise power source L_W^i for each time step, following the experimental relations 3.5 already presented in section 3.1. In particular, for light vehicles it reads:

$$L_W^i(v) = 53.6 + 23.8Log[v_i] \tag{6.1}$$

In addition, to take into account the presence of stochastic parameters such as driving conditions and skills, vehicles mechanics and maintenance, different vehicle model etc., we correct the previous expressions with a stochastic additive term. This is obtained choosing a gaussian correction with mean zero and unitary variance, as widely explained in section 3.3.1.. Thus, from geometrical and emission parameters, for each vehicle, at each time step t, the noise level can be propagated to the receiver choosing an appropriate source model, as discussed in chapter 3. Following a procedure similar to what described in paragraph 3.1 we use a point-like source, described by the expression:

$$L_I^i(t) = L_W^i - 20Log[r_i(t)] - 11 \tag{6.2}$$

where $r_i(t)$ is the distance between the i-th vehicle and the receiver, that, according to figure 6.13, is defined as:

$$r_i(t) = \sqrt{d^2 + \left(\frac{S}{2} - v_i(t)\right)^2} \tag{6.3}$$

where S is the road length and d is the distance between road and receiver. In this way, we are able to rebuild, for each vehicles, the noise emission curve $L_I(t)$, i.e. its time-history such as done in section 3.1. Iterating this procedure for all passing vehicles and performing the logarithmical sum we are able to construct the equivalent continuous sound pressure level $L_I(t)$ at the receiver as function time. Now, by the knowledge of the time-history of the entire signal, it is possible to evaluate the equivalent continuous sound pressure level in the simulation period ΔT by the use of expression 3.18. In figures 6.14 we report the equivalent continuous sound pressure level as

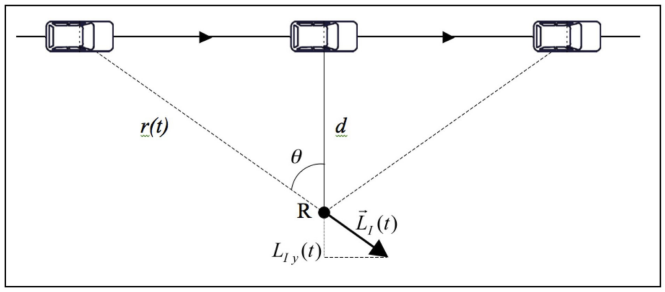

Figure 6.13: Geometry for noise calculation in TCA models.

function of time in two different traffic situations of Nagel-Schreckenberg, for a receiver at the perpendicular distance of 15 m from the road. In particular, in the up panel of figure 6.14 we can see the noise level in a nearly free flow situation ($\lambda = 0.1$), while in down panel a more congested situation is represented ($\lambda = 0.8$). In the first case, we achieve an equivalent continuous sound pressure level $L_{eq} = 72.2$ dBA, while, in the second case we achieve the lower value $L_{eq} = 57.3$ dBA.

6.4 From traffic fundamental diagram to noise fundamental diagram

All the information about noise emission as a function of traffic condition can be well summarized with a construction of a sort of noise fundamental diagram (NFD), where the equivalent continuous sound pressure level (L_{eq}) is reported as a function of road's density. In figure 6.15 and 6.16 these diagrams are reported for all TCA model presented in the previous section. It is also important to notice that, with respect to the noise prediction performed with expression like those described in chapter 2, this type of analysis is capable to carry more information about the noise emission of the road. As pointed out in chapter 2, in fact, many traffic noise models frequently used in pratical application, give the equivalent continuous sound pressure level only as a function of vehicular flux by expression of type $L_{eq}(Q)$. This kinf of approach makes no distiction in function of traffic state on the road, giving a flat response in term of density. From a common empirical point of view, it is evident that this is not real true because we can have the same vehicular flux Q but not necessary the same traffic conditions (i.e. different λ). This is well

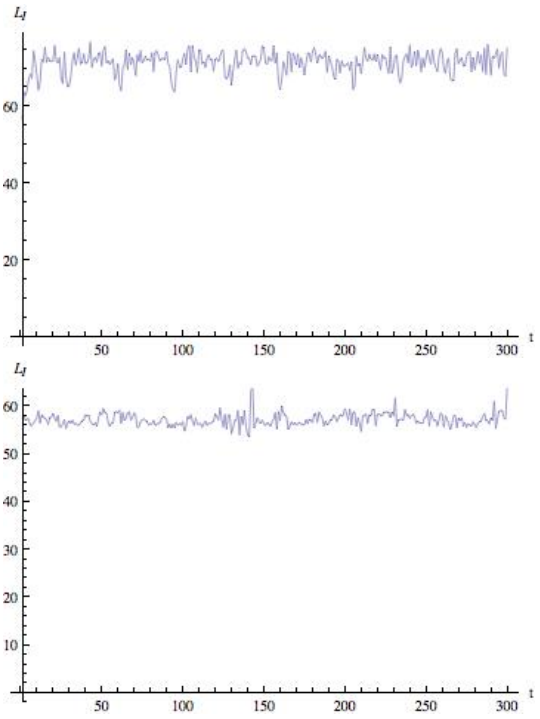

Figure 6.14: Equivalent continuous sound pressure level as function of time for Nagel-Schreckenberg model over a lattice of 150 cells and a period of T=300 timesteps (each timestep correspond to $\Delta t = 1$ s). The slow down probability is fixed to $p = 0.3$ and $V_{max} = 5$. *Up:* Simulation for $\lambda = 0.1$. *Down:* Simulation for $\lambda = 0.8$. In both cases we assume the receiver at the perpendicular distance of 15 m from the road.

evidenced looking at the general shape of fundamental traffic noise diagram reported in figure 6.15 and 6.16. In particular a non monotonic behaviour is achieved. In particular in the free-flow region the noise level curve present a sudden grown up to a well defined noise peak in corrispondence of the critical density λ_c where the flow reaches a maximum, called the capacity flow Q_{cap}. After the critical density we enter in the region of congested traffic and the noise level descreases with a density increasing. Looking specifically at each model we achieve a strong dependence of noise by slow down probability in Nagel-Schreckenberg model, while this dependence is lighter for STCA-CC and stochastic Fukui-Ishibashi. In particular, while for STCA-CC the effect of slow down probability is experienced for higher density, in stochastic Fukui-Ishibashi the effect of P_{SD} can be evidenced at lower density. This effect is clearly due to the different speed range afflicted by the slow down probability. In figure 6.17 a comparison between different NFD is reported. As it appear evident from the graph, the deterministic version of Fukui-Ishibashi model presents the greater noise maximum level. This happens because in this model non random speed suppression are admited, so being the noise power source dependent from speed, the global level increases. It is also useful to notice that for STCA and STCA-CC models, the critical density it's an inflection point for the $L_{eq}(\lambda)$ curve. Before critical density, in fact, the curve it's concave whereas in the congested region is convex. This does not happen instead for stochastic Fukui-Ishibashi model where we always observe a concave curve.

6.5 Noise Mapping with Cellular Automata

In all the previous sections, we mainly focused on acoustical noise level experienced by a receiver in a well defined position of the space. In practical applications a very useful approach results, instead, in the construction of a sort of "noise map", able to quantify the influence of a certain type of road over all the surrounding areas. To perform the noise mapping, in particular, we modify the previous described algoritms in order to calculate the global noise L_{eq} in each cell of lattice space and to represent the value in a contour plot with the color scale reported in figure 6.18. In figures 6.19, 6.20, 6.21, 6.22 and 6.23 the noise mapping corresponding to different geometries of road section are reported. For a gain of simplicity and computational time, we implemented the traffic dynamic in the framework of Wolfram's rule 184 but

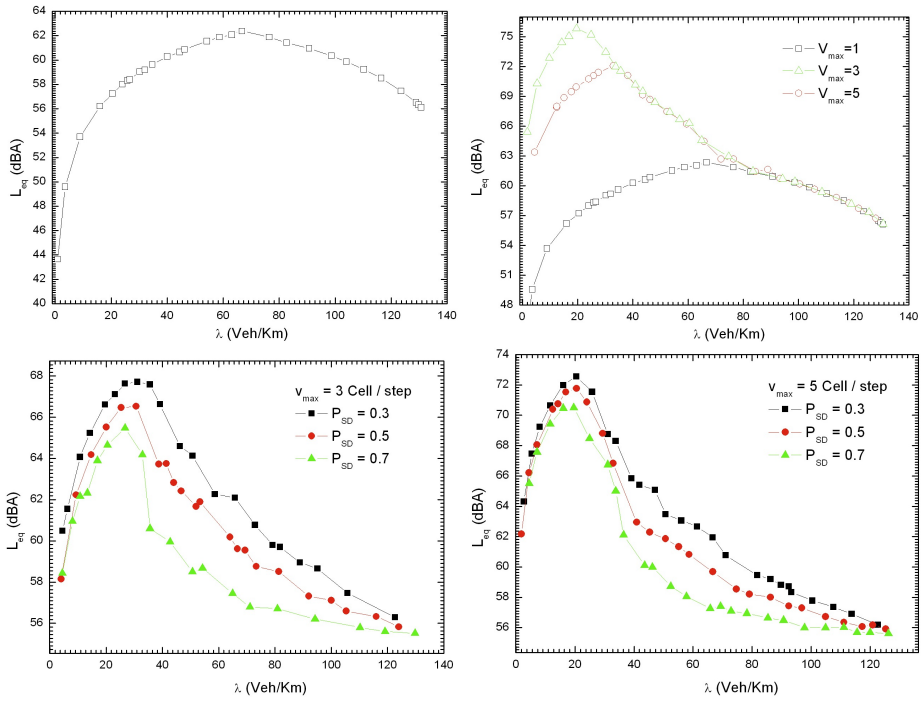

Figure 6.15: Fundamental diagram of noise for a single lane traffic on 150 cells lattice over a period of $T = 300$ timesteps. *Up - left:* NFD for Wolfram Rule 184. *Up - right:* NFD for Deterministic Fukui-Ishibashi model. *Down:* NFDs for Nagel-Schreckenberg model with different V_{max} and slow-down probability.

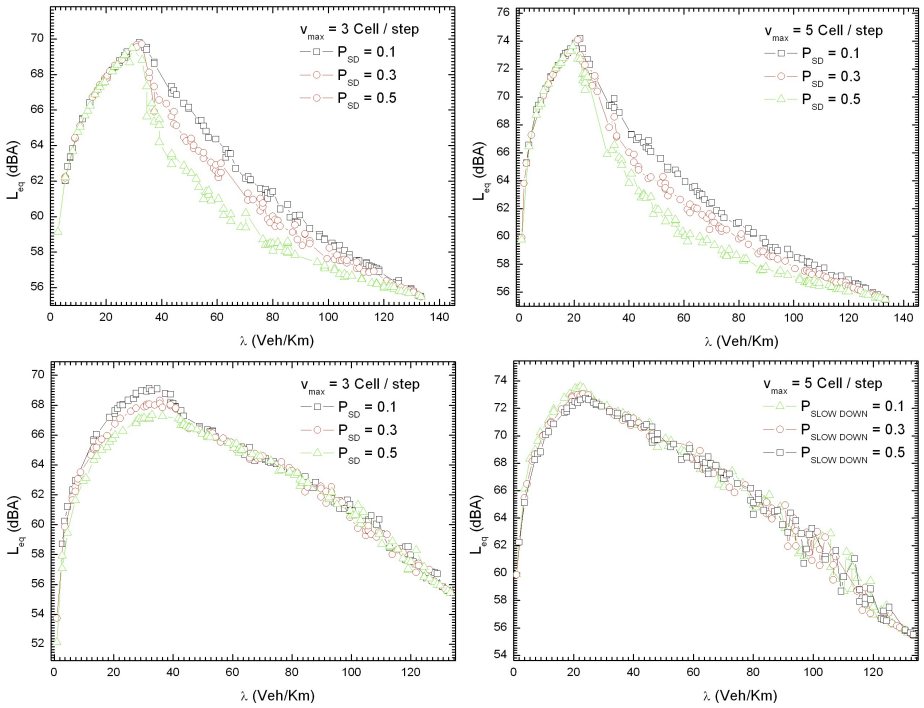

Figure 6.16: Fundamental diagram of noise for a single lane traffic on 150 cells lattice over a period of $T = 300$ timesteps. *Up:* NFD for Nagel-Schreckenberg with cruise control with different V_{max} and slow-down probability. *Down:* NFDs for stochastic Fukui-Ishibashi model with different V_{max} and slow-down probability.

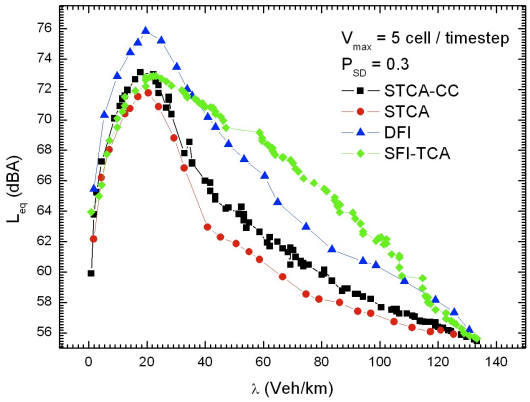

Figure 6.17: Comparison of different NFD of noise for a single lane traffic on 150 cells lattice over a period of $T = 300$ timesteps.

Figure 6.18: Color scale adopted in the noise mapping. Global equivalent noise level L_{eq} increase from left to the right.

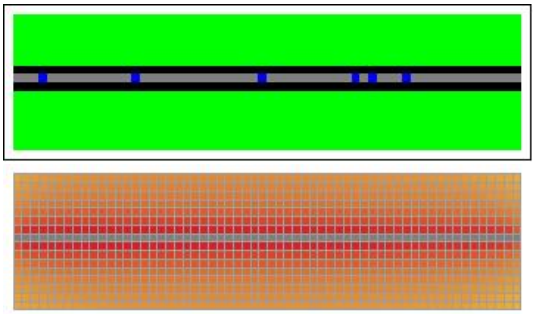

Figure 6.19: Vehicles dynamics (*up*) and noise map (*down*) for a single lane traffic on a straight line. The lattice size is 16x60 cells and the period $T = 200$ timesteps. Spatial discretization is $\Delta x = 7.5$ while time discretization is $\Delta t = 1$ s. The probability that a new car entersin the system is $p = 0.138$, corresponding to a hourly flux of about 500 veh/h. The gray cells correspond to road's area, blue cells correspond to cars, green and black cells correspond to empty areas. The level scale correspond to that reported in figure 6.18.

the extension to other models can be simply performed.
The main idea is that by the combination of these elementary sections, any kind of road pattern can be represented and its noise map can be evaluated. In figure 6.24, for example, we report the noise map related to a more complex road pattern obtained by the combination of elementary sections reported in the previous figures.
In the next chapter a similar procedure for the evaluation of noise maps at road intersection will be presented.

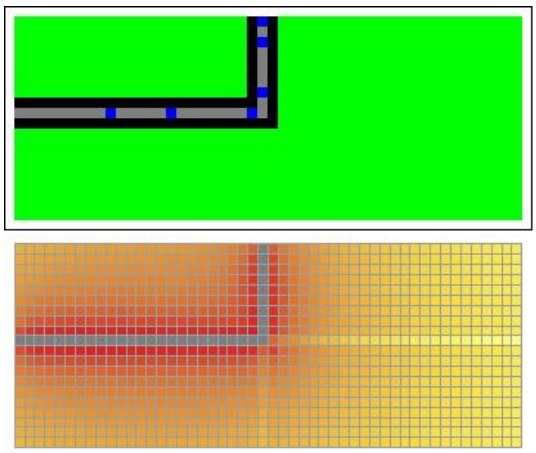

Figure 6.20: Vehicles dynamics (*up*) and noise map (*down*) for a single lane traffic in presence of a road bend. The lattice size is 20x50 cells and the period $T = 200$ timesteps. Spatial discretization is $\Delta x = 7.5$ while time discretization is $\Delta t = 1$ s. The probability that a new car enters in the system is $p = 0.138$, corresponding to a hourly flux of about 500 veh/h. The gray cells correspond to road's area, blue cells correspond to cars, green and black cells correspond to empty areas. The level scale correspond to that reported in figure 6.18.

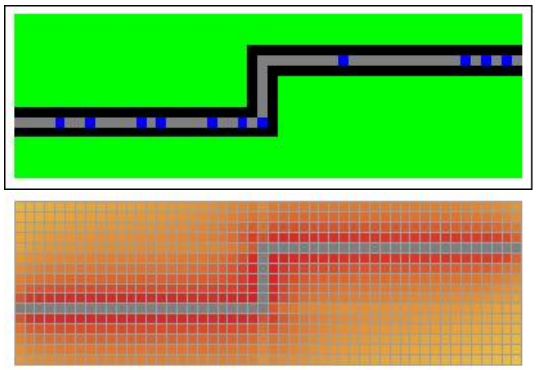

Figure 6.21: Vehicles dynamics (*up*) and noise map (*down*) for a single lane traffic in presence of a "S". The lattice size is 16x50 cells and the period $T = 200$ timesteps. Spatial discretization is $\Delta x = 7.5$ while time discretization is $\Delta t = 1$ s. The probability that a new car entersin the system is $p = 0.138$, corresponding to a hourly flux of about 500 veh/h. The gray cells correspond to road's area, blue cells correspond to cars, green and black cells correspond to empty areas. The level scale correspond to that reported in figure 6.18.

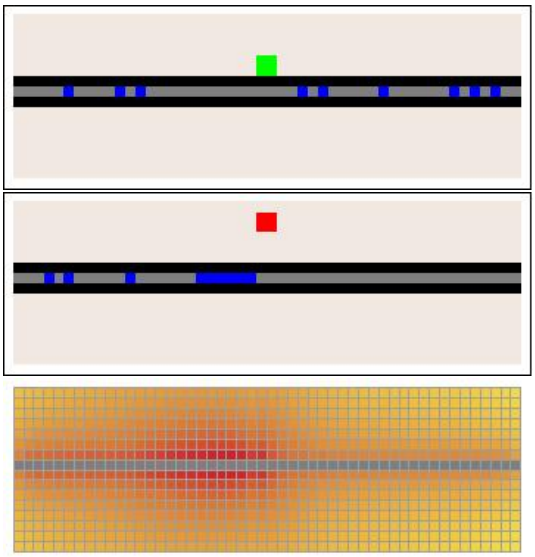

Figure 6.22: Vehicles dynamics and noise map for a single lane traffic in presence of a traffic lights. The lattice size is 16x50 cells and the period $T = 200$ timesteps. Spatial discretization is $\Delta x = 7.5$ while time discretization is $\Delta t = 1$ s. The probability that a new car enters in the system is $p = 0.138$, corresponding to a hourly flux of about 500 veh/h. The traffic light is red from t=100 until t=200 timesteps. The gray cells correspond to road's area, blue cells correspond to car,s green and black cells correspond to empty areas. The level scale correspond to that reported in figure 6.18.

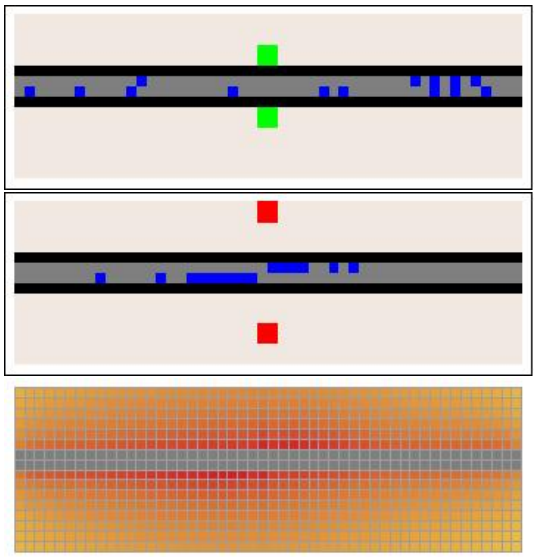

Figure 6.23: Vehicles dynamics and noise map for a double lane traffic in presence of a traffic lights. The lattice size is 16x50 cells and the period $T = 200$ timesteps. Spatial discretization is $\Delta x = 7.5$ while time discretization is $\Delta t = 1$ s. The probability that a new car enters in the system is $p = 0.138$, corresponding to a hourly flux of about 500 veh/h from both directions. The traffic light is red from t=100 until t=200 timesteps. The gray cells correspond to road's area, blue cells correspond to cars, green and black cells correspond to empty areas. The level scale correspond to that reported in figure 6.18.

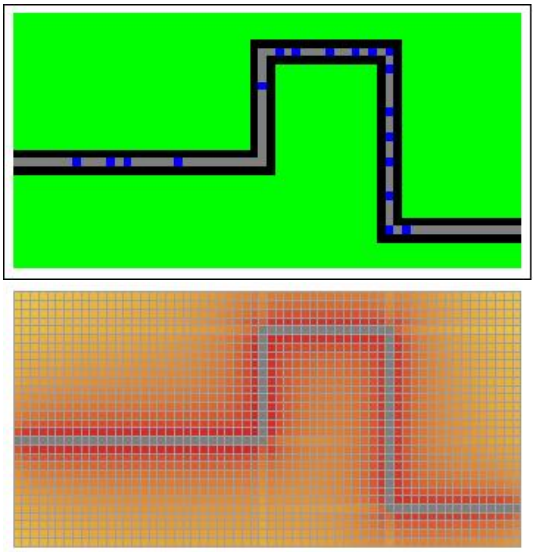

Figure 6.24: Vehicles dynamics (*up*) and noise map (*down*) for a single lane traffic on a particular road pattern. The lattice size is 30x60 cells and the period $T = 200$ timesteps. Spatial discretization is $\Delta x = 7.5$ while time discretization is $\Delta t = 1$ s. The probability that a new car enters in the system is $p = 0.138$, corresponding to a hourly flux of about 500 veh/h. The gray cells correspond to road's area, blue cells correspond to cars, green and black cells correspond to empty areas. The level scale correspond to that reported in figure 6.18.

Chapter 7

Noise prediction at road intersection

The modelling and the prediction of noise coming from vehicular flows is strongly related with the geometry and the general features of the road, including the presence of conflicting points. In an intersection configuration, in fact, noise cannot be predicted in a standard way, since the traffic depends on many factors, such as priority, signals, traffic lights, driving behaviour, etc.. In this chapter, the author focuses on the noise prediction problems related to road intersections by the use of cellular automata traffic models.

7.1 Intersections classification

The road intersection is defined as the area obtained by the convergence in the same point of three or more road branches.
The intersections, wherever they are localized, constitute a critical point for a road network because of the crossing of different traffic flows. They are divided into three main categories:

- *Planar Intersection*, subdivided in linear intersections and roundabouts, where the converging roads are coplanar, with consequent interferences between transiting and curving currents.

- *Traffic Light Controlled Intersections*, which are still coplanar crossings, but there is a periodic and alternate stop of the traffic currents. They are used quite exclusively in urban and suburban ambits.

- *Not Planar Intersections*, in which the separation of the different transit currents is obtained through overpasses, while the connection between the two streets is given by one or more exchanging ramps. In the following, we will briefly report a description of the main planar intersection typologies, including the traffic light controlled ones.

7.1.1 Linear Planar Intersection

To this category belong all the Linear Planar Intersections without traffic lights, with three or four branches, that are the roads converging in the conflict point. If the number of branches is five or more than five, it is preferable to adopt the roundabout solution. These intersections are particularly suitable for secondary or local roads, where, in general, flows and velocities are not extremely high. Depending on reference velocities and on vehicles flows, one could find different configurations for the intersection, from the simplest to the most complex ones. For example, in the local road ambits, one can have the standard simple cross configuration (see 7.1), with smooth borders and a radius ranging from 6 to 8 meters, in order to allow turnings, also in low speed regime.
Moreover, if velocity and traffic volume grow, in order to improve safety and functionality of the intersection, one could insert special lanes of deceleration, acceleration and accumulation (waiting), or one could realize shaped island to favour the regulation of flows. The regulation is made on the basis of national laws, but, in general, is achieved thanks to priority signals for some currents and STOP signals for others, with the additional rule that a STOP on the principal road is predominant to a STOP on the secondary one. In quite all the intersection schemes, the central part of principal road is devoted to waiting (accumulation) for vehicles turning on the left (see 7.1), while acceleration and deceleration lanes, that help exit and enter actions, are present on the principal road only in more complex schemes.
The insertion of these special lanes is decided on the basis of a deep evaluation study, in which one should take into account the interfering flows entity and the frequency of conflicting turning actions by vehicles engaging the intersection. An overview of the criteria that help these evaluations can be found in the next section, while, for a deeper description, one can refer to literature, for example to [104, 105]. in low speed regime.

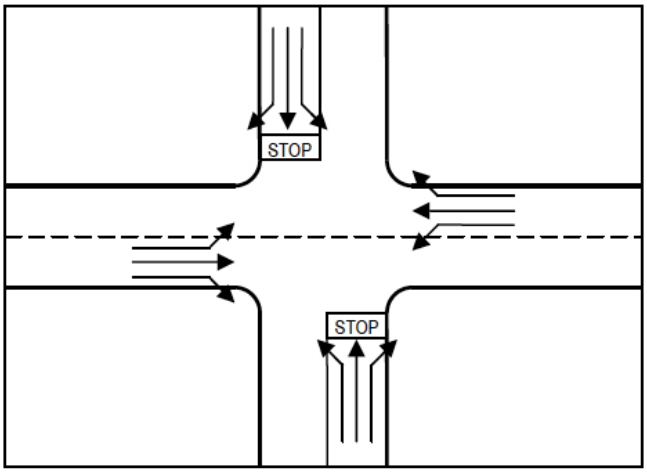

Figure 7.1: Example of simple cross intersection.

7.1.2 Roundabout Intersection

The roundabout is a planar intersection constituted by a ring drivable only in one direction, from vehicles coming from different branches. During last years, roundabouts design has evolved from a starting planning scheme where the priority was assigned to entering flows with respect to vehicles running on the ring. This scenario resulted in the disadvantage that an increase in entering flows could bring to a congestion in the area between two following branches of the roundabout, i.e. the exchange area. Thus, in order to guarantee the functionality of these intersections, too large dimensions where required, especially for ring diameter, with consequent higher building costs. Subsequently, in order to avoid these problems, the design evolved towards a more efficient scheme, giving priority to vehicles running on the ring, respect to the entering ones. This brought to a sensible lowering of the ring diameter and to the introduction of the compact roundabouts instead of the first ones. In the compact roundabouts, the central island is not drivable. Nowadays, in urban ambit, designers are preferring smaller dimensions for the central island, resulting in a kind of "mini roundabouts". In these element, the island is drivable, so that heavy vehicles are not prevented from transiting in that intersection.
Many states are installing roundabouts instead of traditional intersections because of clear evidence that roundabouts dramatically reduce the incidence

Figure 7.2: *Up:* Traffic jam at a linear planar intersection. *Down:* Non-planar road's intersection.

of severe injury and death for vehicle occupants involved in crashes at intersections [106, 107, 108]. It also often occurs that traditional intersections are replaced by roundabouts in some critical situation, where the traffic flow needs to be better reorganized.
In the past, the principal design element of roundabouts was the length of exchange zones, that were calculated according to theoretical models based on the "critical interval" concept, which is the minimal time interval needed to perform an action (entering or exiting the intersection, turning) [104]. Models used nowadays for the calculation of modern roundabouts parameters, are based also on experimental issues [105]. This is due to the need for a rigorous description of users behavior, which is a really difficult issue. From a general point of view, the user approaching the roundabout should wait a suitable gap before entering the ring, but, very often, this does not happen and the driver enter the ring using a lower interval with respect to the critical one. This leads to a slow down in the ring current, with a significant growth of the accident risk.
In general the roundabout design main criterion consists in the assignment of geometrical features able to satisfy the traffic demands and in the verify of the relative level of service and safety. Finally, we can summarize the principal advantages coming from the adoption of a roundabout intersection:

- Easiness in turning and global reduction of waiting times, which become equilibrated between different currents, since it doesnÕt exist a hierarchy between different flows.
- Better managing of traffic fluctuations with respect to traffic light intersections with fixed time.
- Consequent reduction of acoustic and atmospheric pollution.
- Growing, in general, of the safety level [106, 107, 108].
- Efficient connection from non urban fast roads to suburban and local ones.
- Possibility to invert the direction without dangerous actions.
- Easiness of insertion in urban sites, where many squares are already configured in a ring scheme.

Figure 7.3: Different examples of roundabout over the world.

7.1.3 Traffic Light Controlled Intersection

The Traffic Light controlled intersections are probably the most used intersections in the big cities, where the traffic flows need to be carefully organized and merged with the pedestrian ones. In the previous subsections, in fact, it has been explained how one can improve the circulation in proximity of a critical node of the road network, but the pedestrians issue is quite always neglected in a traffic optimization process. The traffic light helps to improve pedestrian safety, especially in urban environment, because it can have a cycle which provides a time interval totally dedicated to pedestrian crossing.
One can distinguish three main classes of traffic lights.

- Fixed cycle traffic light, characterized by constant time intervals of the cycle; they are particularly used where the flows are almost stable during all functioning time.
- Adaptive traffic lights at the node level, which can change their time intervals for each intersections. They are equipped with some sensors, placed along the various branches of the intersection, that allow the traffic light to adapt cycle's phases depending on the traffic demand of each road.
- Adaptive traffic lights at the network level, which are similar to the previous ones, but which adapt their cycles on the basis of data coming from the overall road network. The calculus of traffic lights cycle consists in defining the number of phases in which the cycle itself has to be divided and which currents can have the green light in each phase. One can find a more exhaustive description of these calculations in literature, for example in [105].

7.2 Intersection choice criteria

The design of a new road corresponds, in general, to the insertion of new road branches and nodes in the actual road network. The choice of a given path fixes the choice of the nodes position, i.e. the position and the typology of the intersections.
Once the position has been fixed, the choice between the three different kind of intersections described above comes from the different kind of roads that

Figure 7.4: Example of traffic light controlled intersection.

converge in the node, in particular from the network in which the intersection has to be inserted.
In this section we will refer in particular to the Italian "New Road Regulation" ("Nuovo Codice della Strada") which has been issued in 1992 and updated in 2009 [109]. In this regulation, roads are classified as follows:

- A: Highways (urban or not);
- B: Primary extra urban roads;
- C: Secondary extra urban roads;
- D: Urban road with continuous flow;
- E: Urban road;
- F: Local road (urban or not);
- F-bis: Cycle-pedestrians route.

Starting from these categories, four levels of networks can be introduced:

1. Primary Network:
   It is the network of class A roads, that are supposed to provide national or inter regional connections. This network serves long distance connections and has to be designed with high average speed features; this

network is forbidden to some components of traffic, such as pedestrians, light motorcycles, etc..

2. Principal Network:
   B and D road categories belong to this network and their role is to distribute flows from the Primary Network to the secondary ones, or, eventually to local roads. The average speed of this kind of network is usually lower than the speeds of the Primary Network and also here, some traffic components are excluded.

3. Secondary Network: It includes C and E roads that ensure movements towards the local connections. The average speeds result to be still lower than the previous networks but this time there are not any limitations to traffic components.

4. Local Network: F class roads belong to this network with access function; in this network one finds the lowest average speeds and, also here, there are not any limitations to traffic components.

To these four network levels, four interconnection classes are associated, with the same names: Primary, Principal, Secondary and Local. In order to achieve a suitable functioning of the global network, connections should be realized between roads of the same class of network (homogeneous connection) or between roads belonging to adjacent network classes (non homogeneous connections), as reported in 7.5.

It is important to remark that Homogeneous Connections are always convenient to be realized, while connections between different classes, if allowed, have to be carefully examined, especially on the economic point of view.
In the figure 7.6, the allowed connections and the intersection categories are reported per each couple of roads, according to the ranking done in [109].

At this point, the typology of intersection, inside each categories, is chosen according to the following elements:

- Safety;
- Functionality;
- Environmental Impact;
- Building Costs and Maintenance.

In particular, referring to safety issues, the position of the crossing is very important: it is necessary that it is clearly visible and perceived from users and pedestrians. In order to perform an optimal design, one should also consider the statistics of accidents and injuries corresponding to different typologies of intersections. These statistics, in fact, could be used as indexes of high or low safety.
Functionality is evaluated determining some performing indexes particularly significant, such as: waiting time intervals, average number of queued vehicles, total average delay, level of service, capacity and, in the roundabout configuration, simple or overall capacity. Concerning the effects of traffic on the environment, it must be considered that noise and exhaust gases or fine dust (air pollution) emissions grow especially in correspondence of planar intersections. In fact, in these cases, because of the intrinsic features of circulation (interrupted flow), characterized from the preeminence of accelerating and decelerating phases, one could find significant values for noise levels emissions and exhaust gases and fine dust concentrations. In local urban ambits, a particular care has to be devoted to weak users, such as pedestrians, bicycles and light motorcycles, and it should be preferred to use traffic lights, especially in the major intersections.
Finally, from these considerations, one can affirm that, at least in the most difficult cases, the choice of the typology of intersection cannot be performed only on the basis of regulation issues and/or expertise and knowledge of the designer, but it should be supported by an analytical calculation which compares direct and not direct benefits and costs, considering all the social components, not only the users.

7.3 Intersections noise impact

To perform a traffic noise prediction in a road intersection configuration we use the Cellular Automata method widely explained in chapter 6. In particular, we apply the same methodology presented in section 6.5 to evaluate a global noise map of this type of urban infrastructure.
In particular, we start our analysis with the simplest intersection, i.e. the road bifurcation at a single, as reported in figure of 7.7. In this case, we have cars moving along a straight line that, and when they arrive at the conflict point, they can go left or right. To mime the drivers decision processing, we include a random term: a driver turn left with probability p_{left} or right

Network Classes	Roads			
	Primary (A-B)	Principal (B-D)	Secondary (C-E)	Local (F)
Primary	PR-H	PR-NH		
Principal	PR-NH	PN-H	PN-NH	
Secondary		PN-NH	SC-H	SC-NH
Local			SC-NH	LC

PR-H = Primary Homogeneous connection
PR-NH = Primary Non Homogeneous connection
PN-H = Principal Homogeneous connection
PN-NH = Principal Non Homogeneous connection
SC-H = Secondary Homogeneous connection
SC-NH = Secondary Non Homogeneous connection
LC = Local connection

Figure 7.5: Connections allowed for the network classes.

	A Non urban	A urban	B	C	D	E	F extra	F urban
A Non urban	OE							
A urban	OE	OE						
B	OE	OE	OE					
C	OI	OI	OI	PI/ TL*				
D	OE	OE	OE	OI	OE/ TL*			
E	OI	OI	-	PI/ TL	OI/ TL*	PI/ TL*		
F extra	-	-	-	PI	-	PI	PI	
F urban	-	-	-	PI	-	PI/ TL	PI	PI

OE = Overpasses with exchange lanes
OI = Overpasses with exchange lanes and planar intersection
TL = Traffic Light controlled intersection
PI = Planar intersection
* In some exceptions for particular local configurations

Figure 7.6: Connections allowed for intersections typologies.

with probability $1 - p_{left}$. In this way we are also able to control the relative flows in both directions that clearly strongly affect the global noise level. We simulate this type of dynamics in the framework of Wolfram Rule's 184 with open boundary condition. In particular, at each timestep a new car enter in the system with probability $p = 0.138$ (that corresponds to a hourly flow of about 500 veh/h) and $p_{left} = 0.7$. Results obtained from this analysis are shown in figure 7.7. As it can be noticed from the noise map, the left lane afflict the surrounding area with a noise level greater than the right one. This happens because the fraction of vehicles that turns left is greater than that one that turn right.

The next step we consider is to add another lane to the previous pattern realizing a simple trifurcation. In this case, when a car arrives at the conflict point, it can decide to turn left, right or to proceed straighthead. To mime the drivers processing decision we include three probability terms: a driver turns left with probability p_{left}, right with probability p_{right} and proceeds straighthead with $p_{straight}$. Clearly we have the constrain $\sum_i p_i = 1$. Results obtained from the analysis of this system are shown in figure 7.8.

We can now complicate this system including the presence of traffic lights. In particular, we consider a crossroad between two lanes regulated by traffic lights: when the traffic light is green, vehicles on the corresponding lane can proceed along their direction while vehicles on the other lane are stopped; after a certain time Δt_{TL} the situation is inverted. This system is reported in 7.9 for single lane crossroad and in 7.10 for double lane crossraod.

The next step is to try to include some priority rule in the decision process studying the "T" intersection shown in figure 7.11. In this case a vehicle coming from left can turn right (with probability $p_{conflict}$) or choose to access the other lane (with probability $1 - p_{conflict}$). Moreover, to perform this last action, it must have the necessary distance from vehicles running on this lane. So if the conditions on the distance are satisfied, the car enters in the new lane while on the contrary it wait until these will be satisfied. Results obtained from the analysis of this system are shown in figure 7.11.

Following the same procedure, in general, each type of intersection can be reproduced and so its noise impact on surrounding areas can be evaluated.

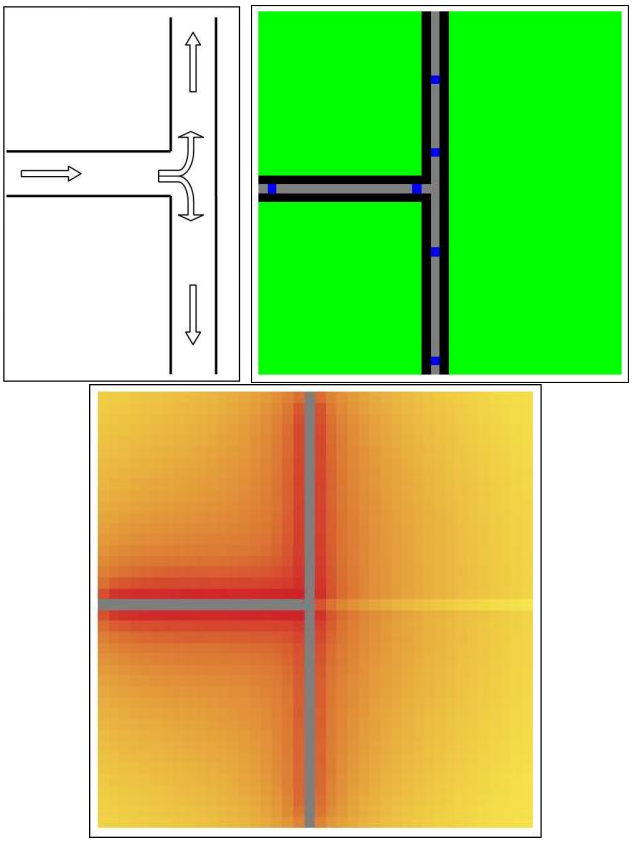

Figure 7.7: Vehicles dynamics (*up*) and noise map (*down*) for a single lane traffic in a bifurcation. The lattice size is 40x40 cells and the period $T = 200$ timesteps. Spatial discretization is $\Delta x = 7.5$, while time discretization is $\Delta t = 1$ s. The probability that a new car enters in the system is $p = 0.138$, corresponding to a hourly flow of about 500 veh/h. A given vehicle turns left with probability 0.7 and right with 0.3. The gray cells correspond to road's area, blue cells correspond to cars, green and black cells correspond to empty areas. The level scale corresponds to that reported in figure 6.18.

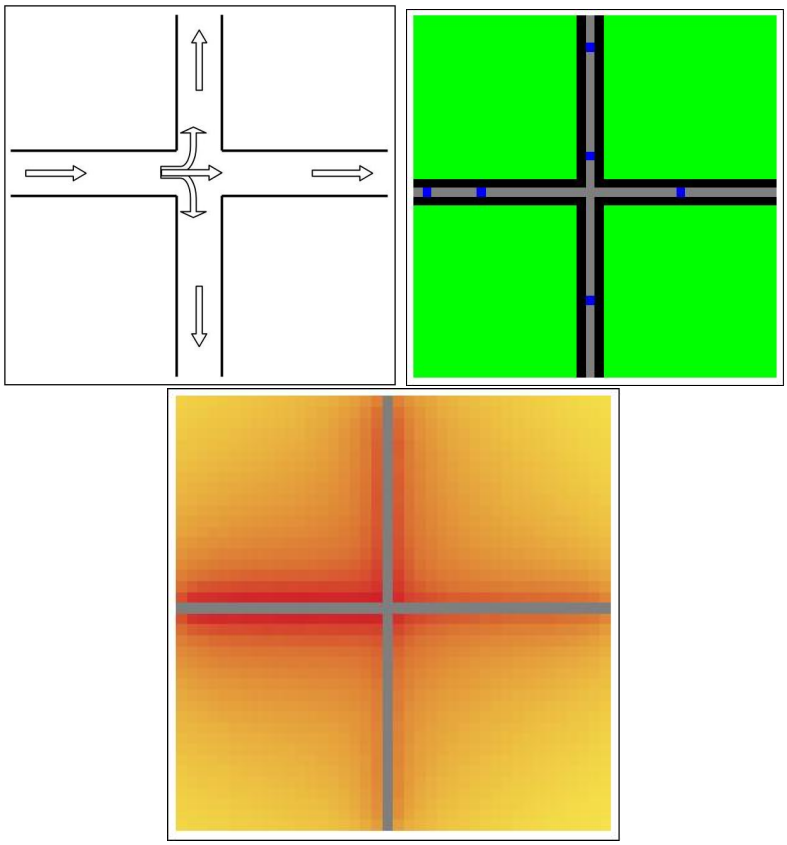

Figure 7.8: Vehicles dynamics (*up*) and noise map (*down*) for a single lane traffic in a crossroad configuration. The lattice size is 40x40 cells and the period $T = 200$ timesteps. Spatial discretization is $\Delta x = 7.5$, while time discretization is $\Delta t = 1$ s. The probability that a new car enters in the system is $p = 0.138$, corresponding to a hourly flow of about 500 veh/h. A given vehicle proceeds along a straight direction, turns left or right with the same probability $p = 1/3$. The gray cells correspond to road's area, blue cells corresponds to cars, green and black cells correspond to empty areas. The level scale correspond to that reported in figure 6.18.

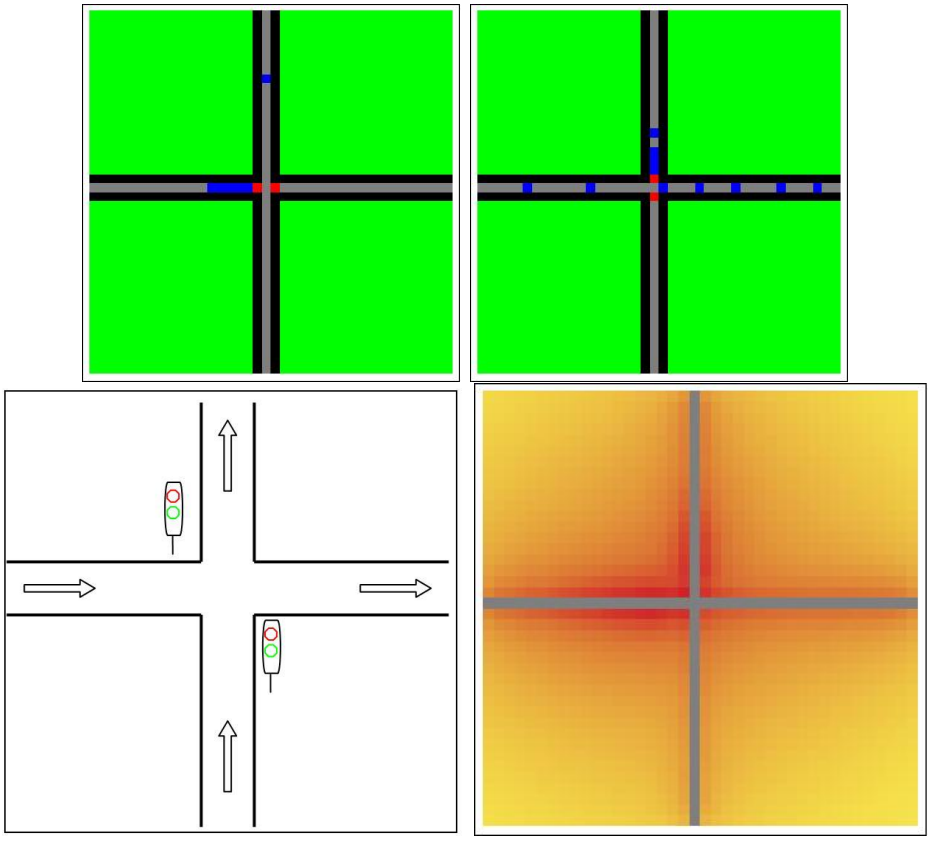

Figure 7.9: Vehicles dynamics (*up*) and noise map (*down*) for a single lane traffic in crossroad configuration with traffic lights. The lattice size is 40x40 cells and the period $T = 200$ timesteps. Spatial discretization is $\Delta x = 7.5$, while time discretization is $\Delta t = 1$ s. The probability that a new car enters in the system from left side is $p = 0.138$, while the probability that enters from down side is $p = 0.138$, both corresponding to a hourly flow of about 500 veh/h. Traffic lights have a temporal duration of $\Delta t_{TL} = 100$ timesteps. The gray cells correspond to road's area, blue cells correspond to cars, green and black cells corresponds to empty areas. The level scale correspond to that reported in figure 6.18.

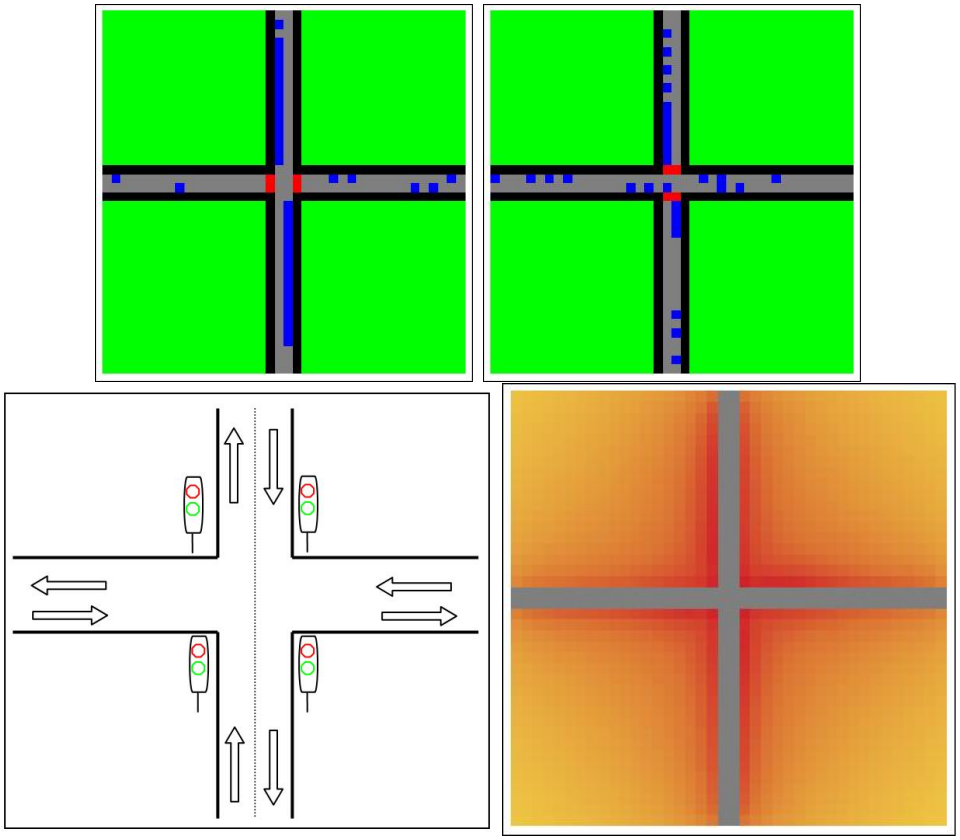

Figure 7.10: Vehicles dynamics (*up*) and noise map (*down*) for a double lane traffic in a crossroad with traffic lights. The lattice size is 40x40 cells and the period $T = 200$ timesteps. Spatial discretization is $\Delta x = 7.5$, while time discretization is $\Delta t = 1$ s. The probability that a new car enters in the system is $p = 0.138$ for all the directions, corresponding to a hourly flux of about 500 veh/h per each branch. Traffic lights have a temporal duration of $\Delta t_{TL} = 100$ timesteps. The gray cells correspond to road's area, blue cells corresponds to cars, green and black cells correspond to empty areas. The level scale correspond to that reported in figure 6.18.

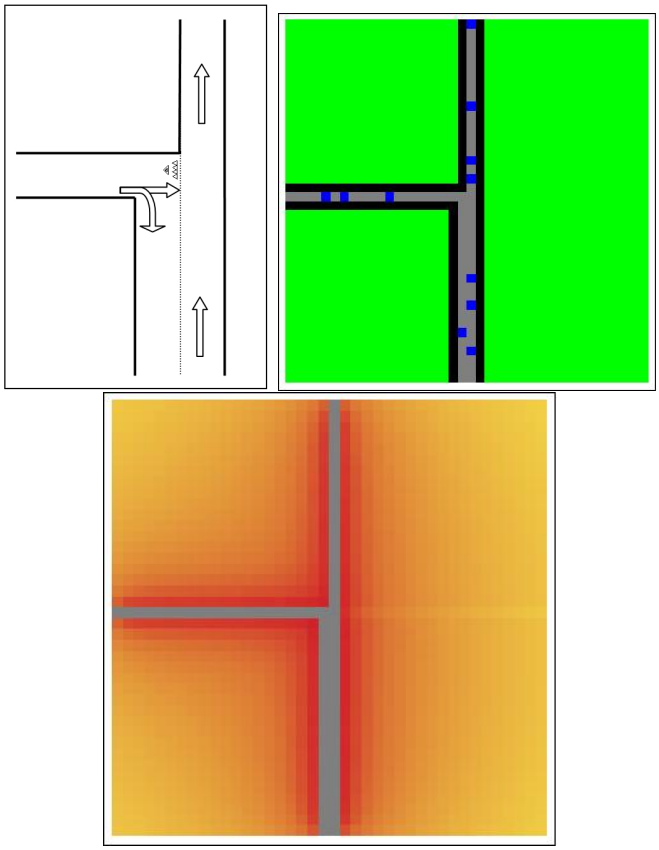

Figure 7.11: Vehicles dynamics (*up*) and noise map (*down*) for a single lane traffic at a cross. The lattice size is 40x40 cells and the period $T = 200$ timesteps. Spatial discretization is $\Delta x = 7.5$ while time discretization is $\Delta t = 1$ s. The probability that a new car enters in the system from left is $p = 0.138$ while the probability that enters from down is $p = 0.138$, both corresponding to a hourly flux of about 500 veh/h. A given vehicle coming from the left goes down with probability $p_{conflict} = 0.5$ or enter in the right lane with probability $1 - p_{conflict}$. The gray cells correspond to road's area, blue cells correspond to cars, green and black cells correspond to empty areas. The level scale correspond to that reported in figure 6.18.

Chapter 8

Conclusions

In this Ph.D. thesis, new tools for traffic noise prediction have been presented. In particular, in the first part the author presented the development of a new vehicular traffic noise model, "Gerian2009", aimed at a more realistic prediction in urban areas and in different conditions. The main idea was to implement in a numerical framework a vehicular noise model able to consider the intrinsic stochastic feature of traffic phenomenon. This feature is embedded in the model thanks to the inclusion of the dependance from speed of the equivalent noise level. Speed of vehicles, in fact, with its typical stochastic behavior, affects the amount of acoustical energy emitted by roads. Moreover, the distribution of speeds of vehicles on a given road can be approximated with a normal distribution. The choice of mean value and standard deviation has to be performed according to the specific situation, either measuring the mean speed on a suitable sample of vehicles, or inferring the value considering traffic flow typology and road geometrical features and working conditions. This type of model is like a "parameter free" approach, since does not require the fit on any measurements in order to estimate the model parameters. Thus, a gain in simpleness and time is evident. This work led to the development of a "micro to macro" energy-based approach to the traffic noise prediction that, starting from theoretical issues, requires no preliminary noise measurements in situ but only, easy to be obtained, general information about the road. Results obtained by the application of this procedure has been also compered with several sets of experimental data, finding a good agreement.
In the second part of this thesis, the author improved the current prediction tools for traffic noise prediction in order to keep into account non standard

situations such as traffic lights, traffic jam, intersections etc.. As evidenced in the work, in fact, standard traffic noise prediction models are currently used to predict average noise descriptors, as required for example in noise mapping or in legislation. Those models usually consider traffic flow as a steady noise source,whose level depends on flow rate and mean speed. Unfortunately, this static representation does not take urban traffic dynamics into account. An accurate description of average noise levels is bounded to dynamic representation of traffic flows. Thus, to perform a more realistic prediction we propose to introduce some aspects of traffic dynamics in noise prediction, by the use of traffic models (TM), that are "following the leader" model and Cellular Automata models.
In particular, by the use of TM, the traffic dynamics has been simulated in different situations and the related global equivalent continuous sound pressure level has been evaluated in different situation, like free-flow, traffic jam, traffic light etc. The main result of this work is the construction of a kind of "fundamental diagram of traffic noise", where the global noise level is related to vehicle density on the road, so that different traffic conditions can be easily implemented and simulated. In addition we used this model to construct a noise map of a generic road patter trough the information obtained directly from the dynamics. In the last part of this dissertation we have studied the problem of noise prediction at urban intersections modelling the dynamics by Cellular Automata models for a "T" intersection, crossroads and traffic light controlled croassroads.

Bibliography

[1] ACI-CENSIS, Rapporto automobile 2008.

[2] Ouis D., Annoyance from road traffic noise: a review, Journal of Environmental Psychology 21, (2001), 101-120.

[3] Kryter K.D., Annoyance from aircraft and ground vehicle noise, Journal of the Acoustical Society of America 72, (1982), 1222-1242.

[4] Langdon F. J., Noise nuisance caused by road traffic in residential areas: Parts I and II. Journal of Sound and Vibration 47 (1976), 243-282.

[5] Italian D.P.C.M. 1 march 1991, Limiti massimi di esposizione al rumore negli ambienti abitativi e nell'ambiente esterno - Gazzetta Ufficiale della Repubblica Italiana, n. 57, 8 march 1991.

[6] Anon, Handbook of acoustic noise control WADC technical report 52-204, Wright Air Development Center, (1952).

[7] Nickson AF, Can community reaction to increased traffic noise be forecast?, Proc. Fifth International Congress on Acoustics, 1965.

[8] Lamure C., Niveaux de bruit au voisinage des autoroutes, Proc. Fifth International Congress on Acoustics, 1965

[9] Johnson D.R., Saunders E.G., The evaluation of noise from freely flowing road traffic, Journal of Sound and Vibration 7, (1968), 287-309.

[10] Galloway WJ, et al., Urban highway noise: measurement, simulation and mixed reactions, NCHRP report, 78, 1969.

[11] Burgess M.A., Noise prediction for urban traffic conditions related to measurements in Sydney Metropolitan Area, Applied Acoustics, vol. 10, (1977), 1-7.

[12] Griffiths I.D., Langdon F.J. , Subjective response to road traffic noise, Journal of Sound and Vibration 8, (1968), 16-32.

[13] C. Fagotti and A. Poggi, Traffic Noise Abatement Strategies. The Analysis of Real Case not Really Effective, in Proc. of 18th International Congress for Noise Abatement, pp. 223-233, Bologna, Italy, 1995

[14] Centre Scientifique et Technique du Batiment, Etude théorique et expérimentale de la propagation acoustique, Revue d'Acoustique n.70, (1991).

[15] Anon, Calculation of Road Traffic Noise, London, United Kingdom Department of Environment and welsh Office Joint Publication, HMSO, (1975).

[16] Department of Transport, Calculation of Road Traffic Noise, HMSO, UK, (1988).

[17] RLS 1990, Richtlinien fur den Larrmschutz an Strassen, BM fur Verkehr, Bonn, (1990).

[18] Der Bunderminister fur Verkehr -"Richtlinien fur den Larmschutz an Strassen" - RLS81 (1981).

[19] Canelli G. B., Gluck K., Santoboni S. A., A mathematical model for evaluation and prediction of mean energy level of traffic noise in Italian towns, Acustica, 53, (1983), 31-53.

[20] Cocchi A., Farina A., Lopes G., Modelli matematici per la previsione del rumore stradale: verifica ed affinazione del modello CNR in base a rilievi sperimentali nella citta' di Bologna, Acta of 19-esimo Convegno Nazionale AIA, Naples 10-12 April, 1991.

[21] Directive 2002/49/EC of the European Parliament and of Council of June 25 2002 relating to the assessment and management of environmental noise, Official Journal of the European Communities, L189/12-25,18.7.2002

[22] NMPB-Routes-96 (SETRA-CERTU-LCPC,CSTB), is the French national computation method, referred to in Arrete' du 5 mai 1995 relatif au bruit des infrastructures routiéres, Journal Officiel du 10 mai 1995, Article 6 and in the French standard XPS 31-133. For input data concerning emission, these documents refer to the Guide du bruit des transports terrestres, fascicule prevision des niveaux sonores, CETUR1980.)

[23] Guide du bruit des transports terrestres, fascicule prévision des niveaux sonores, CETUR,1980.

[24] Anon. FHWA. traffic noise prediction model US. Washington: Department of Transportation, Federal Highway Administration National Technical Information Service, 1978.

[25] Anon. Highway noise - generation and control. National Cooperative Highway Research Program report 173. Washington: Transportation Research Board, 1976.

[26] Anon. Highway noise - a design guide for prediction and control, National Cooperative Highway Research Program Report 174. Washington: Transportation Research Board, 1976.

[27] EMPA. Model le de calcul de bruit du traffic routier pour ordinateur, lére partie: manuel d'utilisation du logiciel STL-86. Berne: version 1.0, 1987.

[28] Balzari, Schudel, Grolimund, Petermann. Modéle le de bruit du traffic routier dans les zones habiteés. Berne, (1988).

[29] Koyasu M. Method of prediction and control of road traffic noise in Japan. Inter-noise 78, San Francisco, 1978.

[30] Tachibana, H, Sasaki M. ASJ prediction methods of road traffic noise. Inter-noise 94, Yokohama, 1994.

[31] Takagi, K, Yamamoto K. Calculation methods for road traffic noise propagation proposed by ASJ. Inter-noise, Yokohama, 1994.

[32] Reken- en Meetvoorschrift Railverkeerslawaai 1996, Ministerie Volkshuisvesting, Ruimtelijke Ordening en Milieubeheer, 20 November 1996.

[33] Quartieri J., Troisi A., Guarnaccia C., Lenza TLL, D'Agostino P., D'Ambrosio S., Iannone G., Application of a Predictive Acoustical Software for Modelling Low Speed Train Noise in an Urban Environment, WSEAS Transactions on Systems, Issue 6 Vol.8 (2009), 673-682.

[34] Quartieri J., Troisi A., Guarnaccia C., Lenza TLL, D'Agostino P., D'Ambrosio S., Iannone G., An Acoustical Study of High Speed Train Transits, WSEAS Transactions on Systems, Issue 4, Vol.8 (2009), 481-490.

[35] Bell L. H., Bell D. H., Industrial noise control: fundamentals and applications, 1994, Marcel Dekker.

[36] Johnson D. L, Field studies: Industrial exposures, J. Acoust. Soc. Am. Volume 90, Issue 1(1991), 170-174.

[37] Glassner Andrew S., An Introduction to Ray Tracing. Academic Press, (1989).

[38] Lelong J., Michelet R., Effect of acceleration on vehicle noise emission, in Proceedings of Forum Acustica (Joint ASA/EAA Meteting), Berlin, Germany (1999).

[39] Lelong J., Vehicle noise emission: evaluation of tyre/road-and motor-noise contributions, Internoise conference, Florida, USA (1999).

[40] Mithra 5.2, technical manual, pag 52.

[41] Castro M, Sanchez JA, Vaquero CM, Iglesias L, Rodriguez-Solano R. Automated GIS-Based System for Speed Estimation and Highway Safety Evaluation, Journal of Computing in Civil Engineering, (2008), 22(5):325-331.

[42] Fitzpatrick K, Carlson PL, Wooldridge MD, Brewer MA. Design factors that affect driver speed on suburban arterials. 2000.

[43] Trozzi C, Vaccaro R, Crocetti S, Speed frequency distribution in air pollutants's emissions estimate from road traffic, The Science of the Total Environment 189/l90 (1996) pp 181 - 185.

[44] Dey P. P., Chandra S., Gangopadhaya S., Speed distribution curves under mixed traffic conditions, Journal of transportation engineering, vol. 132, no. 6, (2006), 475-481.

[45] McLean J. R., Observed speed distributions and rural road traffic operations, in Proceedings of the 9th ARRB Conference, Part 5, Australian Road Research Board, (1978).

[46] Helbing D., Fundamentals of traffic flow, Physical Review E 55, (1997), 3735-3738.

[47] Helbing D., Derivation and empirical validation of a refined traffic flow model, Physica A 223, (1996), 253-282.

[48] Helbing D., Empirical traffic data and their implications for traffic modeling, Phys. Rev. E 55, (1997), R25-R28.

[49] Leong H. J. W., Distribution and trend of free speed on two-lane two way rural highway in New South Wales, in Proceeding of the 4th ARRB Conference, Part 1, Australian Road Research Board, (1968), 791-814.

[50] Peeters B., IMAGINE Work package 2 - Review of data needs for road noise source modelling, IMAGINE Report No. IMA2TR-040615-M+P10, 2004.

[51] Abate D., Analisi del comportamento dell'utente stradale su strade extraurbane a due corsie, a carreggiata unica e a doppio senso di marcia, Universitá degli studi di Napoli, Phd Thesis, (2009).

[52] Haight F. A., Mosher W. W., A practical method of improving the accuracy of vehicular speed distribution measurements, HRR 341, Highway Research Board, Washington, D.C., (1962), 92-116.

[53] Rodriguez R. J., Speed, speed diversion and the highway fatality rate, Southern Economic Journal, Vol. 57, No. 2, (1990), 349-356.

[54] Asensio C., Lopez J.M., Pagan R., Pavon I., Ausejo M., GPS-based speed collection method for road traffic noise mapping, Transportation Research Part D 14, (2009), 360-366.

[55] Fitzpatrick K., Collins J. M., Speed-profile model for two-lane rural highways, Transportation Research Record: Journal of the Transportation Research Board 1737, (2000), 42-49.

[56] International Organization for Standardization ISO 11819 -1, Measurement of influence of road surfaces on traffic noise. Part 1: Statistical Pass-By method, 1997.

[57] Data made available by ABOMA/KEBOMA on http://www.xs4all.nl

[58] Pisani R., Giovinetto R., Fogola J., Previsione del rumore emesso dal traffico veicolare e interventi di riduzione, in Noise Mapping - Determinazione e gestione del rumore ambientale, Proceedings of the Conference on "Noise Mapping, Determinazione e gestione del rumore ambientale", AIA-GAA (2001), 271-304.

[59] Conte A., Stragapede F., Inquinamento Acustico - monitoraggio anni 1996 ÷ 1998, Area 08 - Ambiente, Ufficio Rumore, Provincia di Genova (2005).

[60] Arpa EMILIA-ROMAGNA, Sezione Provinciale di Bologna, Servizio Sistemi Ambientali (2004).

[61] J. Wardrop. Some theoretical aspects of road traffic research. In Proceedings of the Institution of Civil Engineers, volume 1 of 2. 1952.

[62] M.J. Lighthill and G.B. Whitham. On kinematic waves: II. A theory of traffic flow on long crowded roads. In Proceedings of the Royal Society, volume A229, pages 317-345, 1955.

[63] Paul I. Richards. Shockwaves on the highway. Operations Research, 4:42-51, 1956.

[64] R.E. Chandler, R. Herman, and E.W. Montroll. Traffic dynamics: studies in car following. Operations Research, 6:165-184, 1958.

[65] D.C. Gazis, R. Herman, and R.B. Potts. Car-following theory of steady-state traffic flow. Operations Research, 7:499-506, 1959.

[66] R. Herman, E.W.Montroll, R.B. Potts, and R.W. Rothery. Traffic dynamics: analysis of stability in car-following. Operations Research, 7:86-106, 1959.

[67] D. Gazis, R. Herman, and R. Rothery. Nonlinear follow the-leader models of traffic flow. Operations Research, 9:545-567, 1961.

[68] Kai Nagel and Michael Schreckenberg. A cellular automaton model for freeway traffic. Journal de Physique I France, 2:2221-2229, 1992.

[69] Verkeerscentrum Vlaanderen, Departement Leefmilieu en Infrastructuur, Administratie Wegen en Verkeer, Vuurkruisenplein 20, 2020 Antwerpen. MINDAT - Databank ruwe verkeersdata Vlaams snelwegennet - 2001 en 2003, Feb 2003.

[70] C. Yang and T. Lee. Statistical theory of equations of state and phase transitions: I. Theory of condensation. Physical Review, volume 87(3):pages 404-409, Aug 1952.

[71] C. M. Tampére. Human-Kinetic Multiclass Traffic Flow Theory and Modelling. TRAIL Thesis Series nr. T2004/11, TRAIL Research School, P.O. Box 5017, 2600 GA Delft, The Netherlands, Dec 2004.

[72] B. D. Greenshields. A study of traffic capacity. In Highway Research Board Proceedings, volume 14, pages 448-477. 1935.

[73] N. Gartner, H. Mahmassani,C.J.Messer,H.Lieu,R.Cunard,and A. K.Rathi.Traffic Flow Theory: A State-of-the-Art Report. Technical report, Transportation Research Board, Dec 1997.

[74] M. Lighthill and G. Whitham. On kinematic waves: II. A theory of traffic flow on long crowded roads. In Proceedings of the Royal Society, volume A229, pages 317-345. 1955.

[75] A. D. May, Traffic Flow Fundamentals, Prentice Hall, Englewood Cliffs, NewJersey 07632, 1990. ISBN 0-13-926072-2.

[76] A. Messmer and M. Papageorgiou. METANET: A macroscopic simulation program for motorway networks. Traffic Engineering and Control, volume 31:pages 466-470, 1990.

[77] J. A. Acha-Daza and F. L. Hall. The application of catastrophe theory to traffic flow variables. Transportation Research B, volume 28:pages 235-250, 1994.

[78] B. S. Kerner. The Physics of Traffic - Empirical Freeway Pattern Features, Engineering Applications, and Theory. Understanding Complex Systems. Springer, 2004. ISBN 3-540-20716-3.

[79] F Haight, Mathematical Theories of Traffic Flow, Elsevier (1963).

[80] A. Reuschel, Fahrzeugbewegungen in der Kolonne bei gleichfoermig beschleunigtem oder verzoegertem Leifahrzeug, Z Oesterr Ingr Architekt Vereines, volume 95: pages 59-62, 73-77, 1950.

[81] L. Pipes. An operational analysis of traffic dynamics. Journal of Applied Physics, volume 24(3): pages 274-281, 1953.

[82] T. Forbes, H. Zagorski, E. Holshouser, and W. Deterline, Measurement of driver reactions to tunnel conditions, in Proceedings of the Highway Research Board, volume 37, pages 345-357, 1958.

[83] R.Chandler ,R.Herman and E. Montroll, Traffic dynamics: studies in car following, Operations Research, volume 6: pages 165-184, 1958.

[84] D. Gazis, R. Herman, and R. Potts. Car-following theory of steady-state traffic flow. Operations Research, volume 7:pages 499-506, 1959.

[85] L. Edie. Car following and steady-state theory for non-congested traffic. Operations Research, volume 9: pages 66-76, 1961.

[86] D. C. Gazis. The origins of traffic theory. Operations Research, volume 50(1): pages 69-77, Jan 2002.

[87] M. Treiber and D. Helbing. Microsimulations of freeway traffic including control measures. Automatisierungstechnik, volume 49: pages 478-484, 2001.

[88] Helbing D., Traffic and related self-driven many-particle systems, Rev. Mod. Phys. vol 73, 2001.

[89] G. F. Newell. Instability in dense highway traffic, a review, in Proceedings of the 2nd International Symposium on the Theory of Road Traffic Flow, pages 73-83, OECD, London, 1963.

[90] M. Bando, K. Hasebe, A. Nakayama, A. Shibata, and Y. Sugiyama. Dynamic model of traffic congestion and numerical simulation. Physical Review E, volume 51(2): pages 1035-1042, 1995.

[91] von Neumann J., The general and logical theory of automata, L.A. Jeffress (Ed.), Cerebral Mechanisms in Behavior, Wiley, New York, 1948, pp. 1-41, paper presented at the Hixon Symposium.

[92] Wolfram S., Statistical mechanics of cellular automata, Rev. Mod. Phys. 55 (1983) 601-644.

[93] M.Fukui, Y.Ishibashi, Traffic flow in 1D cellular automaton model including cars moving with high speed, J. Phys. Soc. Jpn. 65, 6, 1996.

[94] K.Nagel, M.Schreckenberg, A cellular automaton model for freeway traffic, J. Phys. I France 2, 1992.

[95] K.Nagel, High-speed microsimulations of traffic flow, Ph.D. Thesis, University of Cologne, March 1995.

[96] K. Nagel, M. Paczuski, Emergent traffic jams, Phys. Rev. E 51 (4)(1995), pp 2909-2918.

[97] Wolfram S., A New Kind of Science,Wolfram Media, Inc., 2002.

[98] Aktekin N., The simulation of the Ising model on the Creutz Cellular Automaton, Annual Reviews of Computational Physics VII, 1999.

[99] Lahoz-Beltra R., Molecular automata assembly: principles and simulation of bacterial membrane construction, BioSystems 44, 209-229, 1997.

[100] Mayer B., Kohler G.,Rasmussen S., Simulation and dynamics of entropy-driven, molecular self-assembly processes, Phys. Rev. E, 55, 4 1997.

[101] Vancheri A., Giordano P., Andrey D., Albeverio S., Urban growth processes joining cellular automata and multiagent systems. Part 1: theory and models, Environment and Planning B, 35, 723-739, 2008.

[102] M. Gardner, Mathematical games: the fantastic combinations of John ConwayÕs new solitaire game ÒLifeÓ, Sci. Am. (1970) 120-123.

[103] R. Gosper, Life is universal!, in: E. Berlekamp, J. Conway,R. Guy (Eds.),WinningWays for your Mathematical Plays, vol. 2, 1982, Proceedings of theWinter Simulation Conference,Washington DC, 1974, Academic Press, NewYork, 1974 (Chapter 25).

[104] Highway Capacity Manual, National Research Council, Washington, DC, 2000.

[105] Myer Kurz (editor), Handbook of Transportation Engineering, McGraw-Hill, 2004.

[106] R. Elvik, Effects on road safety of converting intersections to roundabouts-review of evidence from non-US studies, Transp. Res. Rec. 1847, 1-10, 2003.

[107] R.A. Retting, et al., Crash and injury reduction following installation of roundabouts in the United States, Am. J. Public Health 91 (4), 628-631, 2001.

[108] A. Flannery, Geometric design and safety aspects of roundabouts, Transp. Res. Rec. 1751, 76-81, 2001.

[109] D. L. 30 April 1992, n. 285, Nuovo codice della strada, Suppl. ordinario Gazz. Uff., 18 May 1992, n. 114 - Updated with D.L. 15 July 2009, n.94.